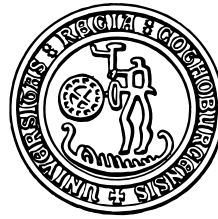


THESIS FOR THE DEGREE OF DOCTOR OF TECHNOLOGY

Non-overlapping Germ-grain Models: Characteristics and Material Modelling

JENNY ANDERSSON

CHALMERS | GÖTEBORG UNIVERSITY



Department of Mathematical Sciences
Division of Mathematical Statistics
Chalmers University of Technology and Göteborg University
SE-412 96 Göteborg, Sweden
Göteborg, Sweden 2005

Non-overlapping Germ-grain Models: Characteristics and Material Modelling
JENNY ANDERSSON

©JENNY ANDERSSON, 2005

ISBN 91-7291-704-0

Doktorsavhandlingar vid Chalmers tekniska högskola. Ny serie nr 2386.

ISSN 0346-718X

Department of Mathematical Sciences

Division of Mathematical Statistics

Chalmers University of Technology and Göteborg University

SE-412 96 Göteborg, Sweden

Telephone +46 (0)31-772 1000

Göteborg, 2005

Abstract

We consider three different non-overlapping germ-grain models, two of which are constructed in a similar fashion. These two models are generalisations of Matérn's hard-core models. In both cases we start with a homogeneous Poisson process and use the points as centres of convex sets, grains, of the same shape. The process is thinned so that no grains overlap. Two different thinning schemes result in the two models. The pair-correlation functions and the mark-correlation functions for both models are derived. The models are fitted to images of inclusions in cast iron.

For one of the models above, if the thinning is performed independently of the grain sizes we show that the volume fraction is at most $1/2^d$ for dimension $d = 1$ or 2 . If the thinning is performed dependently of the grain sizes, it is possible to achieve volume fraction arbitrarily close to one for any dimension.

The third non-overlapping germ-grain model is a Voronoi tessellation. It is used as a model for the grain structure of the surface of a metal. As an example of this approach, we study the influence of grain structure on fatigue life. A crack growth model is applied to simulated grain structures. The conclusion is that the fatigue life increases, compared to a model with grains of equal size.

Keywords: Poisson process; Convex sets; Material fatigue; Voronoi tessellation; Germ-grain process; Pair-correlation function; Mark-correlation function; Short cracks; Volume fraction

Acknowledgements

In the making of this thesis, there are a number of people whom I couldn't have done without. First of all my advisor and co-author Marianne Månsson has been a patient and thorough reader of my manuscripts but above all involved and open for discussions. Without my co-advisor Jacques de Maré I wouldn't even have known that a chemical engineer could convert to a graduate student in mathematical statistics; thank you also for comments on all parts of this work. Thomas Svensson has been a great resource when it comes to fatigue related questions. Moreover I want to thank my co-author Olle Häggström for the cooperation and for giving inspiring courses.

For a not so direct involvement I want to thank my mum, dad and brother for their support. Finally, thank you Johan for sharing my life.

Contents

List of papers	vi
1 Introduction	1
2 Stochastic geometry	2
2.1 Definitions	2
2.2 Second-order measures	3
2.3 Marked point processes and germ-grain models	3
2.4 Convex sets	4
3 Fatigue	6
4 Metal structure	6
5 Summary of Paper A	7
6 Summary of Paper B	8
7 Summary of Paper C	11
8 Future work	12

List of papers

This thesis consists of the following papers

Paper A J. Andersson *The influence of grain size variation on metal fatigue*, International Journal of Fatigue 27 (2005) 847-852.

Paper B J. Andersson *Product densities and mark–correlations of two models of non-overlapping grains*, submitted in a shortened version.

Paper C J. Andersson, O. Häggström, M. Månsson *The volume fraction of a non-overlapping germ–grain model*.

1 Introduction

Non-overlapping germ-grain models are important for modelling structures from a wide range of subjects such as forestry, medicine, astronomy and material science. Properties characterising germ-grain models are the intensity, the volume fraction and second-order information such as the pair-correlation function and the mark-correlation function. In this thesis we will concentrate on finding theoretical characteristics of two closely related models that will also be used for modelling a material. Another material in another scale will be modelled using a Voronoi tessellation, which can also be described as a germ-grain model.

Non-overlapping germ-grain models are described in the literature on stochastic geometry. We will not attempt to make a detailed reference list, but instead give [10] as an excellent starting point. A survey on models of non-overlapping spheres is given in [9] and a survey on the applications of Voronoi tessellations can be found in [8]. Stochastic models suitable for modelling materials are described in [3].

In the first paper, Paper A, appended to this thesis, we use a Voronoi tessellation on Poisson points as the grain structure of a metal without defects. The influence of grain structure on fatigue life is then studied by simulating such grain structures and letting a crack grow according to a deterministic crack growth model.

The second paper, Paper B, is more mathematical. Here two models of non-overlapping convex sets, called grains, are considered. We derive second-order characteristics, more precisely the pair-correlation function and the mark-correlation function. The pair-correlation can be used to compare the models to a Poisson process with the same intensity, in the sense that the frequency of pairs of points a certain distance apart is smaller or greater than in the Poisson process. The mark-correlation function is defined as the expectation of the product of the marks, here the sizes, of two points given their locations divided by the mean mark squared. The models are fitted to data such as in Figure 1, which is an image of inclusions, impurities, in cast iron.

In the third paper, Paper C, we consider the volume fraction of one of the models in Paper B. The model is constructed by thinning a Poisson process with a convex set, grain, and a weight associated to each point. A grain is kept only if it is not intersected by any other grain with equal or higher weight. If the weights are independent of the grain sizes, we give an upper bound for the volume fraction. If the weights depend on the grain sizes, the volume fraction can be made arbitrarily close to one.

The outline of this thesis is as follows. Some background for the appended papers is given in Sections 2, 3 and 4. First, we give an introduction to point processes including second-order measures, marked point processes, germ-grain models and theory on convex sets, followed by a short description of fatigue and finally a section on the structures of metals. In Sections 5, 6 and 7 there are summaries of Papers A, B and C respectively. Note that the word grain has different meanings in the papers. In Paper A a grain is a part of the metal with equal orientation of the atom layers. In Paper B and C the non-overlapping sets are called grains in accordance with such models being called germ-grain models. Finally, some ideas for further work are given in Section 8.

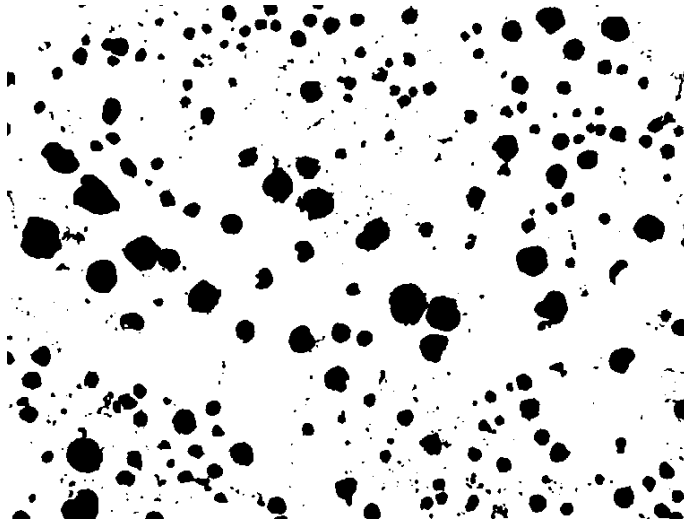


Figure 1: A cut of cast iron with the black shapes being defects. The image was produced by Stefano Beretta.

2 Stochastic geometry

2.1 Definitions

We start with the definition of a point process and continue with some basic definitions to make the notation clear. Let N be the family of all sequences, ϕ , of points in \mathbb{R}^d such that ϕ is locally finite, that is each bounded subset of \mathbb{R}^d contains a finite number of points of ϕ . Usually ϕ is also required to be simple, that is all points of ϕ are distinct. If B is a subset of \mathbb{R}^d , denote the number of points of ϕ in B by $\phi(B)$. Let \mathcal{N} be the smallest σ -algebra on N such that all mappings $\phi \rightarrow \phi(B)$ are measurable for any Borel set B . The formal definition of a *point process* Φ in \mathbb{R}^d is as a measurable mapping of a probability space $(\Omega, \mathcal{F}, \mathbb{P})$ into (N, \mathcal{N}) .

The *distribution*, P , of a point process Φ is defined as

$$P(Y) = \mathbb{P}(\Phi \in Y) = \mathbb{P}(\{\omega \in \Omega : \Phi(\omega) \in Y\}), \quad Y \in \mathcal{N}.$$

The *expectation* of the number of points of Φ in a set B can be written

$$\mathbb{E}[\Phi(B)] = \int_N \phi(B)P(d\phi) = \mathbb{E} \left[\sum_{x \in \Phi} 1_B(x) \right].$$

A point process Φ is *stationary* if its distribution is invariant under translation, that is the processes $\Phi = \{X_n\}$ and $\Phi_x = \{X_n + x\}$ have the same distribution for all $x \in \mathbb{R}^d$. Furthermore it is *isotropic* if its distribution is invariant under rotations about the origin. The *intensity measure* Λ of Φ is defined as

$$\Lambda(B) = \mathbb{E}[\Phi(B)],$$

for B a Borel set. If it has density with respect to Lebesgue measure then Λ can be written in terms of an *intensity function* $\lambda(x)$,

$$\Lambda(B) = \int_B \lambda(x)dx.$$

If the process is stationary, the intensity function is independent of x and it becomes a non-negative real constant, called the *intensity*, λ . Let the Lebesgue measure in \mathbb{R}^d be denoted l_d and then for a stationary process

$$\Lambda(B) = \lambda l_d(B).$$

A useful theorem, which will be applied in more complicated forms in Paper B, is the Campbell theorem. For any non-negative measurable function f ,

$$\mathbb{E} \left[\sum_{x \in \Phi} f(x) \right] = \int \sum_{x \in \phi} f(x) P(d\phi) = \int f(x) \Lambda(dx).$$

In the stationary case the last expression is simplified to

$$\lambda \int f(x) dx.$$

2.2 Second-order measures

The second-order measures of a point process correspond to variances and covariances of stochastic variables. One such measure is the *second-order factorial moment measure* $\alpha^{(2)}$, defined on $\mathbb{R}^d \times \mathbb{R}^d$. If B_1 and B_2 are Borel sets and Φ is a point process on \mathbb{R}^d with distribution P , $\alpha^{(2)}$ is defined as

$$\begin{aligned} \alpha^{(2)}(B_1 \times B_2) &= \mathbb{E}[\#\{(x_1, x_2) : x_1 \in \Phi \cap B_1, x_2 \in \Phi \cap B_2, x_1 \neq x_2\}] \\ &= \int \sum_{\substack{x_1, x_2 \in \phi \\ x_1 \neq x_2}} 1_{B_1}(x_1) 1_{B_2}(x_2) P(d\phi). \end{aligned}$$

For a stationary Poisson process with intensity λ it is equal to $\lambda^2 l_d(B_1) l_d(B_2)$. If the second-order factorial moment measure $\alpha^{(2)}$ has density with respect to the Lebesgue measure, this density is called the *second-order product density* $\varrho^{(2)}$. An interpretation of the second-order product density is that $\varrho^{(2)}(x_1, x_2) dV_1 dV_2$ is the probability of having a point in each of two infinitesimally small disjoint Borel sets, with Lebesgue measures dV_1 and dV_2 , where x_1 and x_2 belong to one set each.

The *variance* of the number of points in a Borel set B can be written in terms of $\alpha^{(2)}$ as

$$\text{Var}(\Phi(B)) = \alpha^{(2)}(B \times B) + \Lambda(B) - \Lambda(B)^2.$$

If B_1 and B_2 are Borel sets, the *covariance* of the number of points in these two sets is,

$$\text{Cov}(\Phi(B_1), \Phi(B_2)) = \alpha^{(2)}(B_1 \times B_2) + \Lambda(B_1 \cap B_2) - \Lambda(B_1)\Lambda(B_2).$$

2.3 Marked point processes and germ-grain models

A *marked point process* in \mathbb{R}^d , $\Psi = \{X_n, M_n\}$, is a point process in \mathbb{R}^d , with points X_n , each having a mark M_n belonging to some space of marks, \mathbb{M} . The marked process can be interpreted as an ordinary point process on the space $\mathbb{R}^d \times \mathbb{M}$. All definitions for ordinary point processes can be repeated analogously for marked processes. The only difference is

that a translation or rotation of a marked process usually only acts on the points and not on the marks.

Having introduced marked point processes we may be interested in the dependence between marks. For that purpose the *mark–correlation function* is defined as

$$k_{mm}(x, y) = \frac{\mathbb{E}_{x,y}[M_x M_y]}{\bar{m}^2},$$

where $\mathbb{E}_{x,y}[M_x M_y]$ is the conditional expectation of the product of two marks given that the locations of the points are x and y and \bar{m} is the mean mark. The mark–correlation function tends to one as $|x - y|$ tends to infinity. If it is above one then the product of the marks of points in x and y are on average larger than the mean mark squared. If it is below one then the product of the marks are on average smaller than the mean mark squared.

From some marked point processes we can construct so–called germ–grain models. Suppose the marks are compact sets in \mathbb{R}^d , that is consider $\{X_n; S_n\}$, where $X_n \in \mathbb{R}^d$ is called a germ and $S_n \subseteq \mathbb{R}^d$ is called a grain. A *germ–grain model* is defined as the union

$$\cup_{n=1}^{\infty} \{X_n + S_n\}.$$

Since grains are affected by rotations, the usual convention for marked point processes that rotations only apply to the points is not reasonable for germ–grain models.

A characteristic of a germ–grain model is the *volume fraction*, i.e. the fraction of space covered by grains. For a stationary germ–grain model of non–overlapping grains it is simply

$$\rho = \lambda \bar{v},$$

where λ is the intensity of the germs and \bar{v} is the mean volume of the grains.

One example of a germ–grain model is the Voronoi tessellation. A *tessellation* partitions a Euclidean space, \mathbb{R}^d , into sets, C_i , with non-overlapping interior, that is $\mathbb{R}^d = \cup_i C_i$. Let $\{p_i\}$ be a set of points. Each point p_i in this set, from now on called nucleus, generates a cell (or grain) C_i . Let one grain C_i consist of all points in \mathbb{R}^d which has p_i as their nearest nucleus,

$$C_i = \{x \in \mathbb{R}^d : |p_i - x| \leq |p_j - x|, \forall p_j\}, \tag{1}$$

where $|\cdot|$ is the Euclidean distance. If the set of points, $\{p_i\}$, is locally finite, i.e. any finite region contains a finite number of points, the C_i 's are called a *Voronoi tessellation* and C_i a Voronoi cell.

See [10] for a general reference on point processes. A general reference on the properties of Voronoi tessellations is [8] and a more mathematical reference is [6].

2.4 Convex sets

In this section we will consider \mathbb{R}^d , mostly for $d = 2$ or 3 . We start with some set theoretic definitions. The multiplication of a set A by scalar is denoted

$$cA = \{cx : x \in A\}.$$

The *reflection* of A is

$$\check{A} = \{-x : x \in A\}$$

and the *translation* of A by x is

$$A_x = \{x + y : y \in A\}.$$

The *Minkowski addition* of two sets A_1 and A_2 is

$$A_1 \oplus A_2 = \{x_1 + x_2 : x_1 \in A_1, x_2 \in A_2\},$$

that can also be written

$$A_1 \oplus A_2 = \{x : A_1 \cap (\check{A}_2)_x \neq \emptyset\}.$$

A set C is *convex* if

$$\alpha x + (1 - \alpha)x \in C \quad \forall x, y \in C, \quad 0 < \alpha < 1.$$

Minkowski addition of convex sets preserves the convexity. In Paper C, we are interested in the addition of sets of the same shape. For two convex sets C_1 and C_2 and scalars x_1 and x_2 the volume of $x_1 C_1 \oplus x_2 C_2$ can be written as a sum in terms of the *mixed volumes*,

$$v_{i,d-i}(C_1, C_2) = v(\underbrace{C_1, \dots, C_1}_i, \underbrace{C_2, \dots, C_2}_{d-i}),$$

as

$$l_d(x_1 C_1 \oplus x_2 C_2) = \sum_{i=1}^d \binom{d}{i} x_1^i x_2^{d-i} v_{i,d-i}(C_1, C_2).$$

For our purposes it is enough to know that $v_{d,0}(C_1, C_2) = l_d(C_1)$, $v_{0,d}(C_1, C_2) = l_d(C_2)$ and that for a convex set C ,

$$l_2(C) \leq v(C, \check{C}) \leq 2l_2(C),$$

and

$$l_3(C) \leq v(C, C, \check{C}) \leq 3l_3(C).$$

The lower bounds are attained by centrally symmetric sets and the upper bounds are attained by triangles if $d = 2$ and tetrahedrons if $d = 3$. For a convex set C_1 with a rotation invariant distribution and an arbitrary convex set C_2 the *generalised Steiner formula* gives

$$\mathbb{E}[l_d(C_1 \oplus C_2)] = \frac{1}{\kappa_d} \sum_{k=0}^d \kappa_{d-k} \mathbb{E}[v_{d-k,k}(C_1, B_d)] v_{k,d-k}(C_2, B_d),$$

where B_d is the unit d -dimensional ball with volume κ_d . In $d = 2$ and $d = 3$ this simplifies to

$$\mathbb{E}[l_2(C_1 \oplus C_2)] = \mathbb{E}[l_2(C_1)] + \frac{\mathbb{E}[S_1(C_1)]S_1(C_2)}{2\pi} + l_2(C_2)$$

and

$$\mathbb{E}[l_3(C_1 \oplus C_2)] = \mathbb{E}[l_3(C_1)] + \frac{\mathbb{E}[\bar{b}(C_1)]S_2(C_2)}{2} + \frac{\mathbb{E}[S_2(C_1)]\bar{b}(C_2)}{2} + l_3(C_2),$$

where $S_{d-1}(C)$ is the $(d - 1)$ -dimensional surface area and $\bar{b}(C)$ is the mean width of a convex set $C \in \mathbb{R}^d$. Let g be a line passing through the origin, then $g(C)$ is the smallest distance between two parallel hyperplanes such that C is between them and that are perpendicular to g . Then $\bar{b}(C)$ is the mean of $g(C)$ for all lines g .

A general reference on convex geometry is [2].

3 Fatigue

Fatigue is the failure in a structure that occurs after the structure has been subjected to a repeated load. The term fatigue is used since the failure often occurs after a long period of repeated stress, at a level considerably lower than the stress needed to break the structure if it was applied only once. The standard example of fatigue is to take a paperclip and notice that it breaks after repeatedly bending it back and forth at the same spot, although it is virtually impossible to break it in one bending. When a metal is subjected to a load, it is possible that small cracks start to form in the metal grains, most often at the surface. Cracks can also start growing in some defect already present within the metal. The cracks then continue to grow, as more load cycles are applied, until a crack spans the entire object and it breaks. Possibly cracks can stop or close, but that is not our concern here.

Laboratory tests can be performed to assess the fatigue properties of materials. Identical test specimens are subjected to a cyclic load until the specimens break or to a maximum number of load cycles. The procedure is repeated for different load amplitudes. Data are plotted in a Wöhler curve, where the logarithm of the load amplitude is plotted against the logarithm of the number of cycles to failure. Often there is a linear relation between the load level and the fatigue life, the number of cycles to failure, for high loads. For some materials there may be a fatigue limit, which is a stress level below which failure will never occur. In [1] there is a section on fatigue.

4 Metal structure

Metals are crystalline materials, that is the atoms are ordered in a three-dimensional pattern. Common atomic arrangements in metals are the body-centred cubic (BCC), the face-centred cubic (FCC) and the hexagonal closed-packed (HCP) structures. The last two arrangements are the most efficient ways, in terms of occupied space, of stacking equally sized spheres and because of this they are called close-packed structures. One way of illustrating the atomic structure is in terms of a unit cell, which is the smallest repetitive unit within the crystal, see Figure 2.

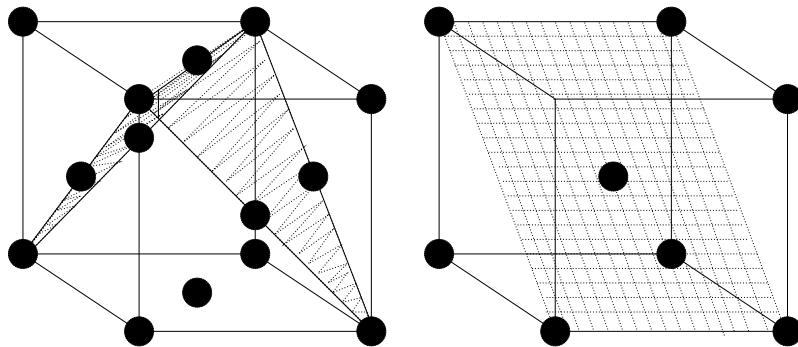


Figure 2: Unit cells of the face-centred cubic (to the left) and the body-centred cubic atomic structures. Two slip planes are shaded in the FCC cell and one in the BCC cell.

A slip plane, such as those shown in Figure 2, is a preferred plane of atoms that will move when a stress is applied. The number of unique non-parallel slip planes depends on

the crystal structure. The FCC crystal has four slip planes, the BCC has six and the HCP has one. Each plane can slip in three directions in the FCC and HCP crystals and in two directions in the BCC crystal.

A crystalline material is usually composed of many crystals. In the cooling process of a melt of a crystalline material, small crystals, or grains, start to form at many locations. As the melt cools each of the grains grows by incorporating atoms from the liquid surroundings. In the area where two grains meet, called the grain boundary, the atoms are not ordered since the two grains do not generally have the same direction of their atomic planes. If all grains have the same chemical composition, the metal is said to have one phase. More on metal structures can be found in textbooks in material science, for example [1].

5 Summary of Paper A

Supposedly identical components made of metal often show substantial differences in fatigue lives. The differences are apparent even during controlled tests with identical stress levels. One source of variation could be differences in the structure of the metal. The idea in Paper A is to use a simulated grain structure and apply the existing theory of crack propagation to study the influence of grain structure on fatigue life. A short crack growth model is used since the main part of the fatigue life occurs during the crack initiation phase.

The crack growth model is adapted from Navarro-de los Rios model for short crack growth under uniaxial loading [7]. The crack is modelled on the surface of the metal and consequently the three-dimensional structure is disregarded. Since the point here is to use a grain structure with grains of different sizes, the Navarro-de los Rios model, which is described for grains of equal size, has to be modified to the current situation.

In the simulations the metal grain structure is a Voronoi tessellation in two dimensions of points generated from a Poisson process. The crack path was determined and the crack was allowed to grow to a maximum length of ten times the mean grain size, with possibility to stop before that. The crack growth rate as a function of crack length and the number of cycles to failure were calculated for fifteen stress levels, the latter resulting in a Wöhler curve for the short crack growth. Compared with the fatigue life of a metal with all grains equal in size, that is the original Navarro-de los Rios model, the fatigue lives in the simulations were longer. The fatigue life decreased with increasing number of grains, probably reflecting the fact that with increasing number of grains there is a greater probability of finding a large grain, where the crack is assumed to start. The standard deviation of the logarithm of the life lengths conditional on finite life is in the order of 0.2-0.4.

As expected grain size variation gives rise to fatigue life dependent on component size. However, only a part of the observed fatigue life variation is explained by the varying grain size according to the simulations.

6 Summary of Paper B

We consider two models of non-overlapping convex grains, which are generalisations of Matérn's two hard-core processes, see [5]. These models were described in [4] and are constructed as follows. Convex sets, called grains, are placed at points of a homogeneous Poisson process and the process is thinned by two different procedures. The first thinning scheme, called pairwise, gives independent weights to both points in a pair with overlapping grains and the point with strictly higher weight wins. New weights are assigned in every comparison. A point is kept only if it wins in all pairwise comparisons. The second scheme, called global, gives each point a weight once and for all, and the point with strictly higher weight is kept when comparing with weights of overlapping grains. The weight may depend on the size of the grain in both cases.

The second-order product densities, defined in Section 2, of the above models are derived when the grains have equal orientation. In the derivation of the product densities, the thinning procedure can be thought of as a process giving marks to the original Poisson process. A point gets mark 0 if it is removed and mark 1 if it is retained. The second-order product density can then be written in terms of the intensity, λ , of the Poisson process and the two-point mark distribution \mathcal{M}_{x_1, x_2} as

$$\varrho^{(2)}(x_1, x_2) = \lambda^2 \mathcal{M}_{x_1, x_2}((1, 1)). \quad (2)$$

The two-point mark distribution is the distribution of the marks in x_1 and x_2 under the condition that there are points in x_1 and x_2 . The main idea, when calculating the product density, is then to find the probability that two points in x_1 and x_2 both have marks 1. It is equal to the probability that no points of the original point process win over them. The number of points that win over x_1 or x_2 is Poisson distributed and the essential step, when deriving the product density, is to calculate the expectation of this distribution.

As spheres are an important special case, the product densities for the models are stated both for spheres of equal radii in Theorems 2 and 3 and for spheres having a certain radius distribution in Theorems 4 and 5. When the grains are convex sets with the same orientation, the product densities are stated in Theorems 6 and 7. Except for some special cases, the product densities must be calculated by means of a numerical integration.

In the case of spheres of equal size the pair-correlation g , which is the product density divided by the squared intensity, is compared to a Poisson process with the same intensity, see Figure 3 below and also Figure 5 in Paper B. The comparisons is made in terms of the frequency of pairs of points with certain interpoint distances. For short distances, less than two times the radius, the pair-correlation is 0, meaning that two points cannot exist at that distance. For a slightly larger distance, between two times and four times the radius, pairs of points occur more frequently than in a Poisson process. For even larger distances, larger than four times the radius, the frequency of point pairs is the same as in a Poisson process. As the intensity of the original Poisson process tends to infinity the frequency of point pairs, at a distance between two and four times the radius, in the global model gets smaller, but is still slightly larger than for a Poisson process. In the pairwise model on the other hand the pair-correlation at this distance tends to infinity as the intensity of the original Poisson process tends to infinity.

Next we consider the mark-correlation function for the radii. Observe that we now consider our processes to have two marks. One of the marks is as above the 0–1 mark and

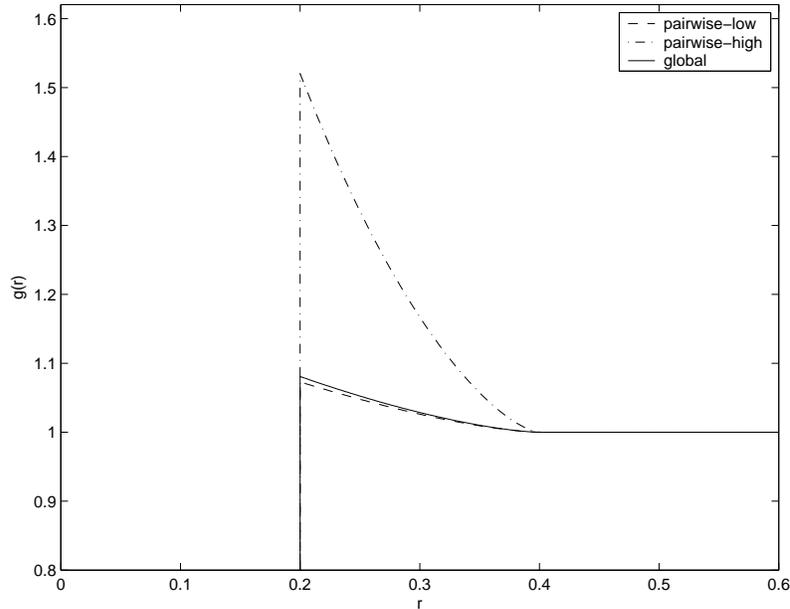


Figure 3: Pair-correlation function for the pairwise and the global model in two dimensions with the same intensity after thinning, $\lambda_{th} = 4$, and radius of the spheres $r_0 = 0.1$. The intensity before thinning was 5.74 and 34.11 for the two pairwise models giving the same λ_{th} , labelled low and high respectively in the plot, and 5.56 for the global.

the other is the radius. Let the radius distribution before thinning be denoted F_R and let the intensity before thinning be denoted λ . The conditional distribution of the 0–1 mark of two points given their locations x_1 and x_2 and their radii k_1 and k_2 is denoted $\mathcal{M}_{x_1, k_1, x_2, k_2}$. A new second-order measure is introduced for the radii marks, which in the current setting can be written,

$$\varrho_S^{(2)}(x_1, x_2) = \lambda^2 \int_0^\infty \int_0^\infty \mathcal{M}_{x_1, k_1, x_2, k_2}((1, 1)) F_R(dk_1) F_R(dk_2).$$

We show that the mark-correlation function, defined in Section 2, can be expressed in terms of this measure,

$$k_{mm}(x_1, x_2) = \frac{\varrho_S^{(2)}(x_1, x_2)}{\varrho^{(2)}(x_1, x_2)}.$$

From examples, for instance with Rayleigh distributed radii, see Figure 4, we can see that the mark-correlation behaves qualitatively like the pair-correlation in the sense that the curves have similar shapes. If the mark-correlation is below one for some distance between the two points then the product of the marks, radii, at those points are lower than the mean radius squared. If the mark-correlation is above one the product of the marks for points that distance apart are larger than the mean mark squared. Observe that in Figure 4 the correlation functions are shown for two pairwise models and one global model, all having the same intensity. One of the pairwise models and the global model have pair-correlation and mark-correlation that coincide, because when at most two spheres overlap, the result of global and pairwise thinning is similar.

The models were constructed to describe inclusions in cast iron, see Figure 1. They were fitted to such data in the case when the weight distribution was independent of the

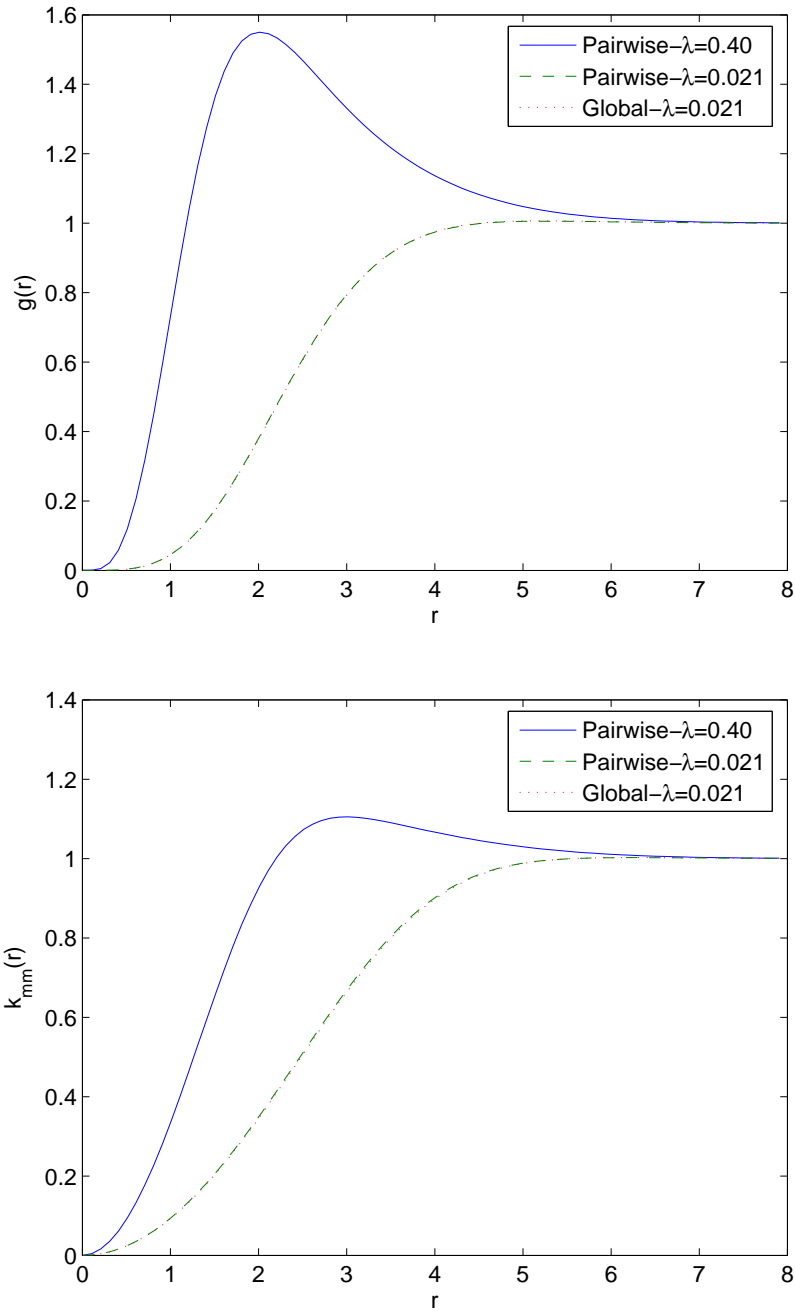


Figure 4: Pair-correlation function, above, and mark-correlation function, below, for models starting with Rayleigh distributed radii with parameter 1 and weights independent of the radii. Both the pair-correlation and the mark-correlation coincides for the global model and one of the pairwise models.

radius. The fit was made by estimating the intensity and the radius distribution. The pair–correlation function was used as a measure of the quality of the fit. Two images of the same material were used. The fit to one of the images for both models seemed reasonable and the other one was not. The problem was that the pair–correlation of the images seemed higher than achievable with either of the models. Possibly the fit could be better either by letting the weights depend on the radius or by thinning an inhomogeneous Poisson process. In the later case some theoretical work is needed.

7 Summary of Paper C

The purpose of this paper is to study the volume fraction of the global model in Paper B. The model is defined as follows. Grains in the form of convex sets are placed at points of a homogeneous Poisson process. The points are given weights that may depend on the grain sizes. The process is thinned by only keeping those grains that do not overlap with any other grain with equal or higher weight.

By a coupling argument we can show that the process is increasing in the intensity of the Poisson process if the weights are continuous and independent of the radii. This is not necessarily the case if the weights are allowed to depend on the radii or if they are not continuous.

If the intensity of the Poisson process tends to infinity and the weight distribution is independent of the grain sizes, then the volume fraction is at most $1/2^d$ if $d = 1$ or $d = 2$, with equality for centrally symmetric grains of equal size. In this case our model is identical to considering the intact grains of the dead leaves model. For simplicity we consider spherical grains in the following. If $d = 1$ we can show the result by Jensen’s inequality. Let R be the radius before thinning and let μ be the mean radius before thinning. Then the volume fraction can be written

$$v = \mathbb{E}\left[\frac{R}{R + \mu}\right].$$

If $d = 2$ the volume fraction can be written

$$v = \mathbb{E}\left[\frac{R^2}{R^2 + 2\mu R + \gamma}\right],$$

where $\gamma = \mathbb{E}R^2$, which can be shown to be less than or equal to $1/4$. This is proved by observing that the argument of the expectation of is below a line which in turn has expectation less than or equal to $1/4$. We can show that for a two point radius distribution the volume fraction is at most $1/2^d$ for any d by straightforward calculations. This makes it natural to conjecture that the volume fraction is at most $1/2^d$ for all d .

If the weights are allowed to depend on the radii the volume fraction can be made arbitrarily close to one. The idea is most easily described in two dimensions. The model can be thought of as dropping discs on a plane. The discs are dropped in reversed weight order. When all discs have been dropped the ones that can be seen whole from below are the ones remaining after thinning. The achieved volume fraction can be made close to one by dropping large discs first and then smaller and smaller in the right way.

8 Future work

Common for all three papers appended to the thesis is that we have worked with non-overlapping germ–grain models. The models have been used to describe materials.

In the future, the ideas from Paper A could be applied to a material for which there is real life data available. Then we could compare the variance in the theoretical results to the variance of the data and draw conclusions about the importance of the variability of grain sizes. Since the large grains in a grain structure seem to be of importance it would also be interesting to find the extreme value distribution of the largest grain in a Voronoi tessellation and compare to real data.

The models in Paper B were inspired by images of inclusions in cast iron, see Figure 1. The fit was not satisfactorily and one idea is to use weights depending on the radius. Another idea is to have an inhomogeneous Poisson process as starting process. The last approach would need some theoretical work before application. Other models could be explored.

In Paper C we conjecture that the upper bound $1/2^d$ holds for any dimension d , but it remains to be proved for $d \geq 3$. To show this would probably involve some other technique than the one used in the paper.

References

- [1] Callister Jr, W.D. (1997), *Materials, Science and Engineering: An Introduction*. Wiley.
- [2] *Handbook of Convex Geometry* Editors Gruber, P.M, Wills, J.M., Elsevier Science Publishers B.V. Amsterdam, 1993.
- [3] Hermann, H. (1991), *Stochastic Models of Heterogeneous Materials*. Material Science Forum, Vol. 78. Trans Tech Publications.
- [4] Månsson, M., Rudemo, M. (2002), *Random patterns of nonoverlapping convex grains*. Adv. Appl. Prob. 34, 718-738.
- [5] Matérn, B. (1960), *Spatial Variation*. Meddelanden Statens Skogsforskningsinst. 49. Statens Skogsforskningsinstitut, Stockholm, Second edition: Springer, Berlin, 1986.
- [6] Möller, J. (1994), *Lecture Notes on Random Voronoi Tessellations*. Springer-Verlag.
- [7] Navarro, A., de los Rios, E.R. (1988), *A microstructurally-short fatigue crack growth equation*. Fatigue Fract. Eng. Mater. Struct. Vol. 11, pp 383-396.
- [8] Okabe, A., Boots, B., Sugihara, K. (1992), *Spatial Tessellations: Concepts and Applications of Voronoi Diagrams*. Wiley, 1992.
- [9] Stoyan, D. (1998), *Models of random systems of non-intersecting spheres*. Prague Statistics '98, 543-547.
- [10] Stoyan, D., Kendall, S.K., Mecke, J. (1995), *Stochastic Geometry and its Applications*. 2nd edition. Wiley.

Paper A

The influence of grain size variation on metal fatigue

Jenny Andersson*

Department of Mathematical Statistics, Chalmers University of Technology, SE-412 96 Göteborg, Sweden

Received 21 July 2004; received in revised form 13 October 2004; accepted 18 November 2004

Abstract

The aim of the present study is to investigate the influence of the variation of metal grain sizes on fatigue lives. The grain structure is simulated from a Poisson–Voronoi model and the short crack growth model of Navarro and de los Rios is applied. The resulting fatigue life decreased with increasing component size, probably reflecting the fact that with increasing number of grains there is a larger probability of finding a large grain where the crack starts. The standard deviation of the logarithm of the lives was in the order of 0.2–0.4, i.e. the variation in grain size explains only part of the observed variance in real fatigue data.

© 2005 Elsevier Ltd. All rights reserved.

Keywords: Short crack; Grain structure; Voronoi tessellation

1. Introduction

Supposedly identical components made of metal often show substantial differences in fatigue lives. The differences are apparent even during controlled tests with identical stress levels. Miller writes in [3] that the scatter in fatigue data needs to be put in a perspective by for example detailed studies of the effect of material structure on early crack growth. One model of early (short) crack growth has been developed by Navarro and de los Rios in [5–10]. The purpose of this study is to investigate the effect of grain size variation on fatigue life. Since the main part of the fatigue life is explained by the crack initiation, the model of Navarro–de los Rios will be used, as in [12], but modified to handle grains of varying sizes. A stochastic grain structure will be obtained by simulation. Similar ideas have been used by Ahmadi and Zenner [1] in a study of the growth of microcracks under the influence of cyclic loading. They compared simulations of cracks in a two-dimensional hexagonal lattice with experiments and the distribution of cracks was claimed to be in quantitatively good agreement between simulations and experiments. The main differences in the ideas from the present paper is the deterministic grain

structure and our focus on scatter. A stochastic grain structure, a Voronoi tessellation, is used by Meyer, Brückner-Foit and Möslang [2] but focusing more on the crack patterns when several cracks are allowed to grow. Here also the results were found to be in good agreement with experiments.

The grain model is introduced in Section 2.1 and the Navarro–de los Rios model with modifications is described in Section 2.2 along with some computational details. The results are presented in Section 3 and analysed in Section 4.

2. Model

2.1. Grain structure

In the proposed model the metal grain structure is a Voronoi tessellation in two or three dimensions of points generated from a Poisson process (see Fig. 1). The reason for using a Voronoi tessellation can be argued as follows. If, in the crystallisation process of a one phase metal, all grains begin to grow simultaneously and at the same rate the resulting grain structure would be a Voronoi tessellation. The tessellation could be modified by allowing the grains to begin their growth at different times and by using a different point process with more or less clustering of the points.

A tessellation partitions an Euclidean space (\mathbb{R}^n) into sets, (C_i), with non-overlapping interior, that is $\mathbb{R}^n = \cup_i C_i$. Let $\{p_i\}$ be a set of points. Each point p_i in this set, from now

* Tel.: +41 772 82 94; fax: +31 772 35 08.

E-mail address: jennya@math.chalmers.se.

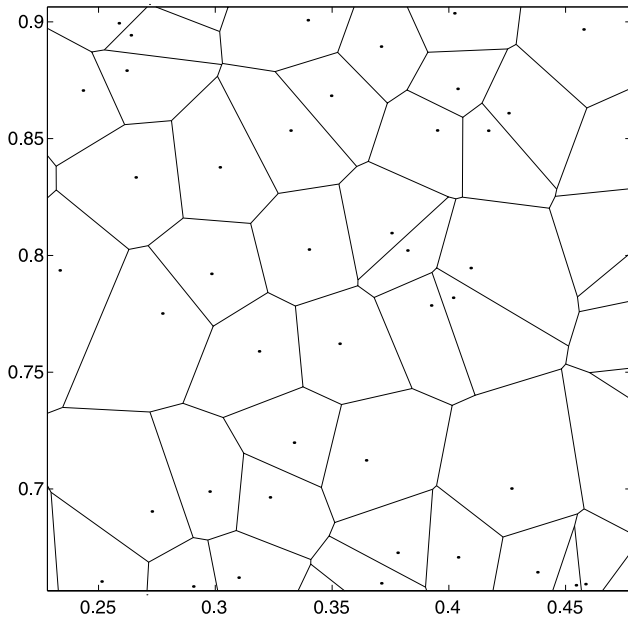


Fig. 1. A Voronoi tessellation of points generated from a Poisson process.

on called nuclei, generates a cell (or grain) C_i . One grain C_i consists of all points in \mathbb{R}^n which has p_i as their nearest nuclei

$$C_i = \{x \in \mathbb{R}^n : \|p_i - x\| \leq \|p_j - x\|, \forall p_j\}, \quad (1)$$

where $\|\cdot\|$ is the Euclidean distance. If the set of points $\{p_i\}$ is locally finite (any finite region contains a finite number of points) the C_i s are called a Voronoi tessellation and C_i a Voronoi cell. A general reference on the properties of Voronoi tessellations is [11] and a more mathematical one is [4].

The realisations of Voronoi tessellations were accomplished using MATLAB version 6.5.1. First points were generated according to a Poisson process in two dimensions. Secondly, the function ‘voronoin’ were used on these points giving the Voronoi tessellation. To handle the effect of edges, points were generated in a slightly larger area than the one needed.

The metal simulated here is assumed to have a face-centred cubic (FCC) atomic structure and one phase (homogeneous in terms of chemical composition). In the model each grain is given a random (uniformly distributed) slip plane direction which determines the directions for the other slip planes (Fig. 2).

2.2. Crack growth model

The crack growth model is adapted from Navarro–de los Rios model for short crack growth under uniaxial loading [5–10]. The crack is modelled on the surface of the metal and consequently the three dimensional structure is disregarded. Since the point here is to use a grain structure with grains of different sizes, the Navarro–de los Rios

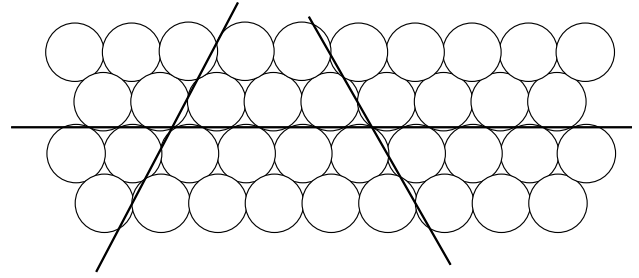


Fig. 2. Slip planes in a closed packed metal seen in two dimensions.

model, which is described for grains of equal size (as in [12]), has to be modified to the current situation. In short, the Navarro–de los Rios model considers the plastic slip produced ahead of a crack to be represented by a continuous distribution of dislocations. It is assumed that when slip is initiated in a grain the entire grain undergoes slip and is only blocked by the grain boundary, i.e. the front of the plastic zone coincides with the grain boundary. Slip is initiated in the next grain when the stress ahead of the plastic zone is enough to move new dislocations. This stress only depends on the position of the crack tip relative to the grain boundary.

The crack is initiated in the centre of a large grain with a slip plane close to the plane of maximum shear stress, that is the angle between the slip plane and the load direction is close to 45° . In making a decision in which grain to start, a compromise is made between size and direction of slip planes. If l is the length of the grain along a slip plain going through the centre of the grain and θ is the angle between the slip plane and the plane of maximum shear stress, a new length is calculated by $l_c = l \cos 2\theta$ (this is repeated for the three slip planes through the centre of the grain). This calculation reflects the fact that the shear is zero both perpendicular and parallel to the main load direction. The grain selected for the crack to start in is the one with maximal l_c . The crack is supposed to grow along a slip plane at all times.

The crack growth rate is determined by

$$\frac{da}{dN} = f\phi, \quad (2)$$

where a is half the surface crack length, N the number of load cycles, f represents the fraction of dislocations ahead of the crack that participates in the crack growth process and depends on the applied stress and the material and ϕ is the plastic displacement of the crack-tip given by

$$\phi = \frac{2(1-\nu)\sqrt{1-n^2}}{\mu n} \sigma a, \quad (3)$$

where σ is the applied load, μ the shear modulus and ν Poisson’s ratio. Here, $n = a/c$ is a dimensionless parameter, c the length of half the crack and half the plastic zone (see Fig. 3).

The slip band is blocked by the grain boundary and the crack will grow at a decreasing rate as it approaches

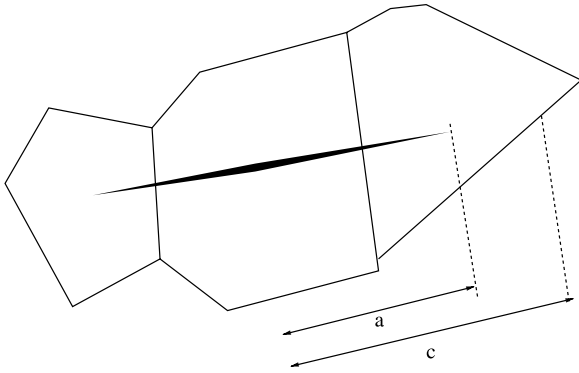


Fig. 3. Illustration of the parameters c and a .

the boundary until slip can be transferred to the next grain. This happens at a critical value of n equal to

$$n_c^i = \cos\left(\frac{\pi}{2} \frac{\sigma - \sigma_{Li}}{\sigma_{comp}}\right), \quad (4)$$

where σ_{comp} is the resistance to plastic deformation of the crack tip. Consecutive grains are numbered $i=1,2,3,\dots$. When σ is smaller than σ_{Li} the stress is not enough to overcome the boundary and the crack stops. The minimum stress required for slip propagation is given by

$$\sigma_{Li} = \sigma_{FL} \frac{m_i}{m_1} \sqrt{\frac{\bar{d}_i}{2c_i}} \quad (5)$$

where c_i is the length of half the crack plus half the plastic zone when the crack grows in grain i , \bar{d}_i is the mean of the length the crack has grown in each grain, σ_{FL} is the fatigue stress and

$$\frac{m_i}{m_1} = 1 + 2.07 \left(\frac{2}{\pi} \arctan(0.522(i-1)2)\right)^{1.86} \quad (6)$$

is the ratio of grain orientations.

When a new slip band is initiated in the next grain and the plastic zone is supposed to span the entire new grain, and therefore, n decreases to

$$n_s^{i+1} = \frac{c_i}{c_{i+1}} n_c^i, \quad (7)$$

which is a rescaling of the old value of n by the new value of c . According to the model, the crack will grow along that slip plane in the new grain that is closest to the plane of maximum shear stress (the angle between this plane and the loading direction is 45°), regardless of which direction the slip plane takes in the third dimension under the surface.

The growth rate Eq. (2) can be integrated over a grain (or over parts of a grain) to give the number of cycles spent in that grain

$$\Delta N_i = \frac{\mu}{f(1-\nu)2\sigma} (\arcsin n_c^i - \arcsin n_s^i). \quad (8)$$

Table 1
Parameter values for commercially pure aluminium

Parameter	Value
μ	25.0 GPa
σ_{comp}	50.0 MPa
σ_{FL}	42.5 MPa
ν	0.33

The total number of cycles is then obtained by summing over all grains.

In the Navarro–de los Rios model all the grains are assumed to be equal in size and because of the symmetry in that case it is enough to do calculations on half the crack. Here, however, the crack may not grow at the same rate at both directions after the first grain. Practically, this is solved by considering the two growth directions separately. As an approximation of the total cracklength after, say, N cycles, we can calculate how long the crack is in both directions separately, by using Eq. (8). The total cracklength after N cycles is then obtained by adding the cracklengths in the two directions. The growth rate at N cycles is approximated by adding the growth rates for the two directions at N cycles.

The values of the parameters used in the calculations are the same as in [12] for commercially pure aluminium. These are shown in Table 1. They used $f=6.16 \times 10^{-5} (2(\sigma-\sigma_{FL}))^{2.696}$.

3. Results

Simulations were made of two-dimensional Voronoi tessellations where the number of nuclei were taken from a Poisson distribution with expectation (denoted λA) 2000, 4000 and 9000, which corresponds to looking at

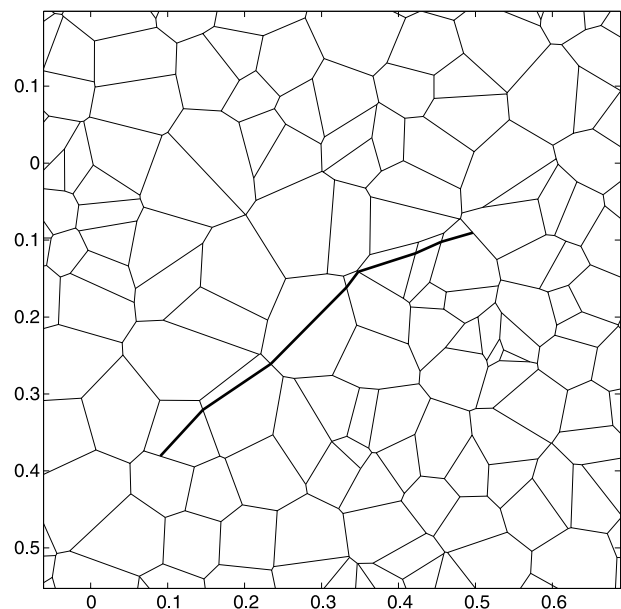


Fig. 4. A simulated crack and grain structure.

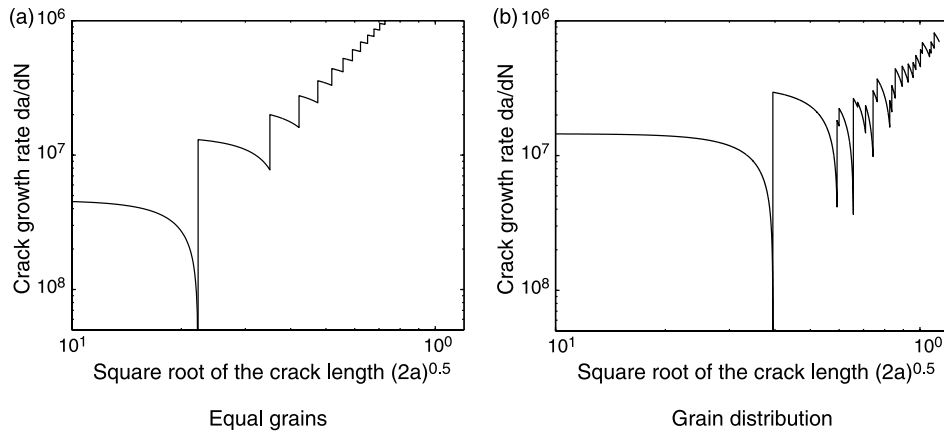


Fig. 5. Logarithmic crack growth rate plots for the original Navarro–de los Rios model to the left and for the Voronoi tessellation model to the right.

components of increasing size. More specifically, squares of sides 2, 4 and 6 giving the area A to be 4, 16 and 36, respectively, were used with an intensity, λ , of points per unit area as 250. The unit of the area is not important since the grain size is only included implicitly in the Navarro–de los Rios models, i.e. in the material constants. These choices gave a mean intercept length of the grains in the tessellations as approximately 0.050 calculated from the simulations. The crack path was determined as described in Section 2.2 and the crack was allowed to grow to a maximum (it could stop before, if $\sigma < \sigma_{Li}$ in Eq. (4)) length of 10 times the mean grain size. The crack growth rate as a function of crack length and the number of cycles to failure were calculated, the latter resulting in a Wöhler curve for the short crack growth. For each value of the expectation the simulation was repeated 1000 times.

Fig. 4 shows an example of a simulated crack, not showing the entire simulated square, and Fig. 5 the crack growth rate as a function of crack length for this crack. In the latter figure, there is also the corresponding plot for a grain structure with equal grain sizes. The growth rate decreases when the crack get close to a boundary, then increases sharply as the crack resumes its growth in the next grain. Fig. 6 shows a Wöhler curve for the initial crack growth for expectation in the Poisson distribution equal to 9000. As a comparison the results from using a model without grain size variation is plotted in the same figure. A regression was made on the lives for $\Delta\sigma$ ranging from 94 to 100 MPa to $N = a(\Delta\sigma)^b$ with the values of the coefficients in Table 2 as the result, i.e. the life decreases with λA or equivalently component size.

The observations at $N = 10^8$ are of cracks that have stopped before they were 10 times the mean grain size long. The variation conditional on finite fatigue life of the number of cycles to failure first increases with the applied load and then decreases (plot in Fig. 7). Fig. 8 shows the percentage of cracks that stopped, i.e. the fatigue life is infinite.

It is often claimed that the intercept lengths of the grains in metals with unimodal distribution of grains is

approximately lognormal. In Fig. 9 is a quantile plot of the logarithm of the intercept lengths in a simulation. The points are supposed to follow a straight line if the lognormal distribution is appropriate.

4. Discussion

The discussion following is purely qualitative because of lack of real data. There is no evaluation of the Voronoi model as a grain structure apart from the comparison of

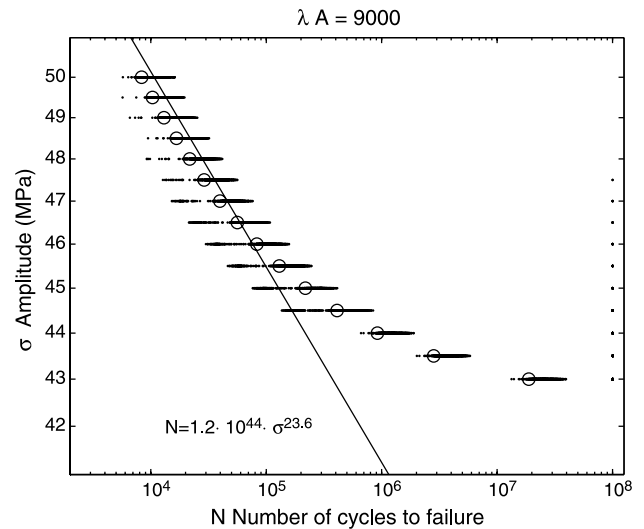


Fig. 6. Wöhler curve for the initial crack growth. The unfilled rings corresponds to life lengths calculated from the model with equal grain sizes.

Table 2
Coefficients in $N = a(\Delta\sigma)^b$, when $\Delta\sigma$ is in MPa

Expectation (λA)	$a \times 10^{44}$	b
1000	1.91	-23.7
4000	1.75	-23.7
9000	1.24	-23.6

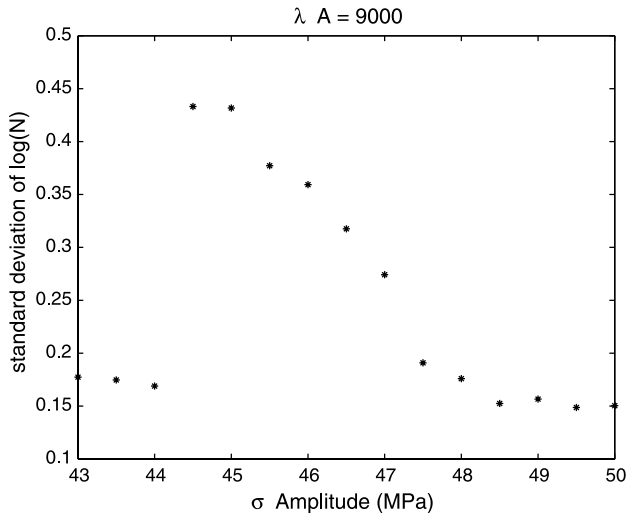


Fig. 7. The standard deviation conditional on finite fatigue life of the number of cycles in Fig. 6 as a function of the load.

the intercepts with the lognormal distribution. The agreement is not very good since the observations are not on a straight line. In this context, however, this is not the crucial thing to compare but rather the distribution of large grains which is more important for the crack growth. Probably the common knowledge of the intercept lengths being lognormal is not always accurate so the best way to do a good comparison would be to use a real material.

The calculated fatigue lives should be seen as an example of what is possible to do with this modelling approach. The crack growth model of Navarro–de los Rios is used only in the form of grains of equal sizes as a first approximation. For future simulations the results for unequal grain sizes in Vallellano, Navarro and Domínguez [13] can be used instead. The reason for not using it here was

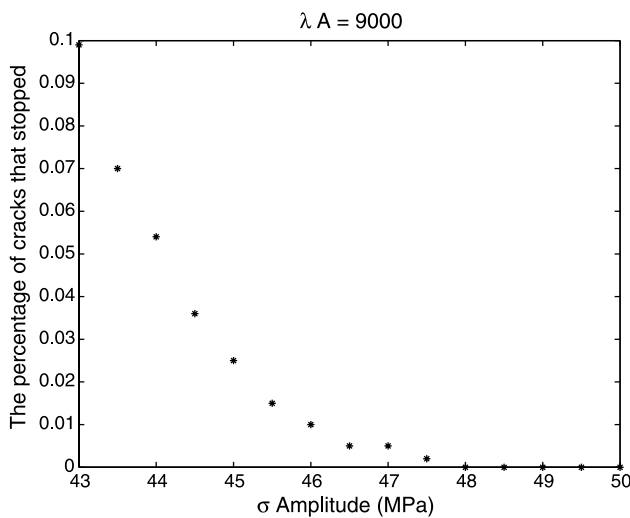


Fig. 8. The percentage of cracks that stopped in Fig. 6, i.e. the number of observations at $N = 10^8$ cycles.

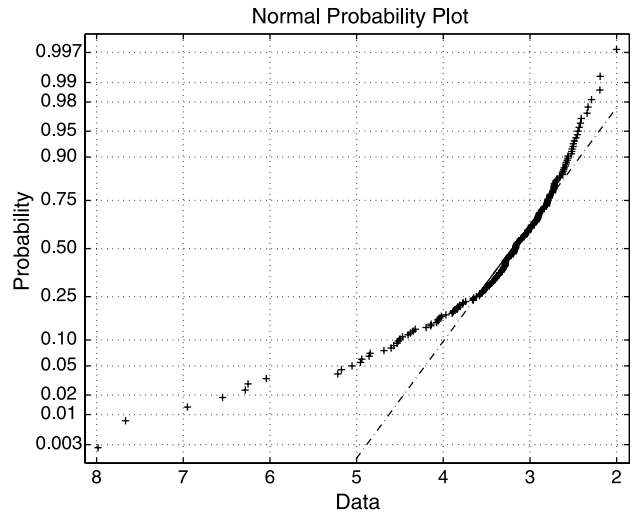


Fig. 9. A normal quantile plot of the logarithm of 110 intercept lengths in a two-dimensional Voronoi tessellation.

the extra complexity in programming. Our belief is that the approximation does not change the results qualitatively and other approximations made have probably a larger impact.

Comparing the simulations to a computation with equal grain sizes show that the crack growth rate curve is more irregular. The advantage of using a grain structure with varying grain sizes as opposed to one with equal grains is that the crack can stop and that it is possible to calculate the variance of the fatigue lives.

There are many simulations with infinite life even for higher loads which is not observed in real data. The explanation is that if a crack stops in a real material there may be a crack that can continue somewhere else in the structure. If a crack stops here there is no other crack that starts at another location. In principle it is possible to simulate that situation, however, then a decision have to be made when to stop creating new cracks.

The standard deviation of the lives conditional on finite life first increases with the load and then decreases as expected from observations. The increase in the beginning is due to the censored data which really have large fatigue lives and hence would increase the standard deviation if they were accounted for.

The fatigue life decreased with increasing number of grains, probably reflecting the fact that with increasing number of grains there is a larger probability of finding a large grain (where the crack is assumed to start). The standard deviation of the logarithm of the lives conditional on finite life is in the order of 0.2–0.4 depending on the load.

Grain size variation gives rise to a longer fatigue life compared with a structure with equal grains. One possible explanation is that even if the crack starts in a large grain and grows fast there, the next grains is probably smaller than in a structure of equally sized grains, and therefore, it grows slower in the second grain. The fatigue life decreases, as

expected with component size, i.e. the size of the area simulated. However, only a part of fatigue life variation observed in doing experiments is explained by the varying grain size according to the simulations.

Acknowledgements

I am grateful to my supervisors Jacques de Maré and Thomas Svensson for starting me on this project and helpful discussions.

References

- [1] Ahmadi A, Zenner H. Simulation of microcrack propagation for different load sequences. In: Blom AF, editor. *Fatigue 2002: Proceedings of the eight international fatigue congress*, vol. 3; 2002. p. 1997–2004.
- [2] Meyer S, Brückner-Foit A, Möslang A. A stochastic simulation model for microcrack initiation in martensitic steel. *Comput Mater Sci* 2003; 26:102–10.
- [3] Miller KJ. A historical perspective of the important parameters of metal fatigue; and problems for the next century. In: Wu XR, Wang ZG, editors. *Fatigue '99: Proceedings of the seventh international fatigue congress*, vol. 1–4. Beijing: China Higher Education Press; 1999. p. 15–39.
- [4] Miller J. *Lecture notes on random Voronoi tessellations*. Berlin: Springer; 1994.
- [5] Navarro A, de los Rios ER. A model for short fatigue crack propagation with an interpretation of the short–long transition. *Fatigue Fract Eng Mater Struct* 1987;10:169–86.
- [6] Navarro A, de los Rios ER. A microstructurally-short fatigue crack growth equation. *Fatigue Fract Eng Mater Struct* 1988;11:383–96.
- [7] Navarro A, de los Rios ER. Short and long fatigue crack growth: a unified model. *Philos Mag A* 1988;57:15–36.
- [8] Navarro A, de los Rios ER. An alternative model of the blocking of dislocations at grain boundaries. *Philos Mag A* 1988;57:37–42.
- [9] Navarro A, de los Rios ER. Compact solution for a multizone BCS crack model with bounded or unbounded end conditions. *Philos Mag A* 1988;57:43–50.
- [10] Navarro A, de los Rios ER. Considerations of grain orientation and work hardening on short-fatigue-crack modelling. *Philos Mag A* 1990;61:435–49.
- [11] Okabe A, Boots B, Sugihara K. *Spatial tessellations: concepts and applications of Voronoi diagrams*. New York: Wiley; 1992.
- [12] Turnbull A, de los Rios ER. Predicting fatigue life in commercially pure aluminium using a short crack growth model. *Fatigue Fract Eng Mater Struct* 1995;18:1469–81.
- [13] Vallellano C, Navarro A, Domínguez J. Compact formulation for modelling cracks in infinite solids using distributed dislocations. *Philos Mag A* 2002;82:81–92.

Paper B

Product densities and mark–correlations of two models of non-overlapping grains

Jenny Andersson

Abstract

We consider two models of non-overlapping convex grains, which are generalisations of Matérn’s two hard-core processes. Grains are placed at points of a homogeneous Poisson process and the process is thinned by two different procedures. The second-order product density and the mark–correlation function is derived for the point process with convex grains of equal orientation. As spheres are an important special case, the product densities for the models are stated both for spheres of equal radii and for spheres having a certain radius distribution. The models are fitted to data of inclusions in cast iron.

Keywords: Second-order product density, Poisson process, Pair-correlation, Marked point process, Convex set

AMS 2000 Subject Classification: Primary 60D05, Secondary 60G55

1 Introduction

A point process where the points cannot be closer than a fixed minimal distance is called a hard-core point process. Matérn [5] introduced two such processes. In the first one he considers a Poisson process and excludes every point with a distance to its nearest neighbour less than a fixed number $R > 0$. In the second model each point is given a weight, uniformly distributed on $(0, 1)$ and independent of the weights of other points. Points are then retained if there are no other points within distance R with lower weight and removed otherwise. These models can be thought of as systems of non-overlapping spheres with radii $R/2$. A survey of random systems of non-intersecting spheres is found in [11]. Hard-core models are used, for example in forestry applications, see [13].

Another example of hard-core models is the simple sequential inhibition model, SSI, which is also called the random sequential adsorption model, RSA, used in physical and biological sciences. Spheres are placed randomly and sequentially in a bounded region. A sphere is rejected if it intersects a previously placed sphere. Other items than spheres could be used. For a survey on RSA models, see for example [17].

The Stienen model and a generalisation, the lily-pond model, describe sets of spheres with random radii. Points are generated according to a stationary Poisson process. In the Stienen model, each Poisson point is the centre of a sphere with a diameter equal to the distance to its nearest neighbour. See [10] and pages 218 and 380 in [12] for more on the Stienen model, for example the pair-correlation function. In the lily-pond model spheres are grown radially, at the same time and at the same rate, from the Poisson points. Each

sphere grows until it meets another sphere. In [1] there are some recent results and an overview of previous results for the lily-pond model.

Some hard-core models are examples of Gibbs processes, which are also studied in the literature on physics. An accessible mathematical treatment can be found in [6].

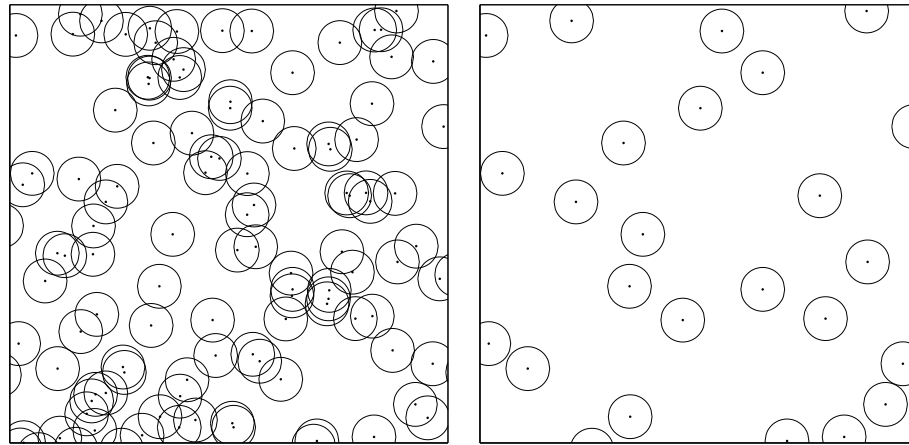
A model which is closely related to Matérn's second model is Matheron's dead leaves model, see [3] and [14]. In two dimensions, discs are dropped sequentially according to a Poisson process on the plane. Parts of a new disc that intersects an old disc are invisible, that is we watch the discs from below. In a finite area, the process can be stopped once all the surface is covered by discs, since new discs dropped do not influence the distribution of the intact discs. The centres of the intact discs correspond to the points that are not removed in Matérn's second model when the intensity of the Poisson process tends to infinity, according to [14].

Månsson and Rudemo [4] describe two models of non-overlapping grains, which are generalisations of Matérn's models. The processes are obtained by thinning a stationary Poisson process. A convex compact set, called grain, is associated with each point. In the simplest case the grains are spheres with equal radii. Points with overlapping grains are either removed or kept, according to two different procedures, in a way that leaves points with non-overlapping grains. The first thinning scheme, called pairwise, gives independent weights to both points in a pair with overlapping grains, and the point with strictly higher weight wins. New weights are assigned in every comparison. A point is kept only if it wins in all pairwise comparisons. The second scheme, called global, gives each point a weight once and for all and the point with strictly higher weight is kept when comparing with weights of overlapping grains. The weight may depend on the size of the grain in both cases. Figure 1 shows realisations of these models for spheres of equal sizes. The models in [4] were originally inspired by inclusions in steel and nodular cast iron, which are important for the fatigue strength of these materials.

Similar to the models in [4] are the generalisations of Matérn's second model in [15]. In the first generalisation the weights may have some distribution that is not uniform and which is independent of the radius. As in Matérn's model, a point in x is removed if there is another point in the ball of radius R , centred in x with lower weight than x . This gives exactly the same point process after thinning as the global model above with the same weight distribution and all radii equal to $R/2$. In the second generalisation, the radii of the points are not constant but follow some distribution, that is a point x gets radius r_x . A point in x is now removed if there is no other point with lower weight in the sphere with radius r_x centred at x . This is not a model of non-overlapping spheres as the global model of [4]. For example, it is possible to have one sphere completely inside another. In [15] thinning intensities, product-densities and mark-correlations for both models are derived.

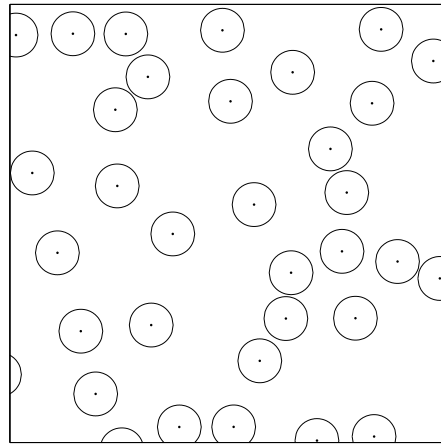
In [4], the thinning probabilities, the relation between the point processes before and after thinning, the volume fraction and the size distributions after thinning are considered. To further characterise these models we are interested in studying second-order characteristics. Once a second-order measure and the first moment measure are known, variances and covariances can be calculated. Furthermore, the second-order properties can be used to compare the models, for example to a stationary Poisson process. For studying the dependence of the sizes of spheres we are also interested in the mark-correlation function.

In Section 2, we give a description of the pairwise and global models. We define the product density and derive an expression for calculating the product density in terms of a



(a) Before thinning

(b) Pairwise thinning



(c) Global thinning

Figure 1: Realisation of pairwise and global thinning of a Poisson process in the unit square of \mathbb{R}^2 with intensity $\lambda = 100$, where all the spheres have an equal radius 0.05.

two-point mark probability in Section 3. This expression has previously been used in [8] and [9]. In Section 4 we calculate the second-order product density for spherical grains with fixed radii for the two thinning procedures. This may seem somewhat superfluous as the same calculations for general radius distribution are carried out in Section 5, but we think it is worthwhile to present the ideas of the proofs in an easier setting. Section 6 states the product densities for convex, compact grains with the same orientation. A general discussion of conditional mark distributions for point processes with two types of marks is given in Section 7. This material is needed in Section 8 where the mark-correlation functions for the pairwise and the global model are stated. As the models were inspired by inclusions in cast iron, we fit them to such data in Section 9. Comments and indications of future work are given in Section 10.

2 Description of the models

Consider a Poisson point process with constant intensity λ in \mathbb{R}^d . On each point a sphere, or some other convex set, in general called grain, is centred. The radius of the sphere associated with a point has distribution F_R , which is independent of the point process and of the radii of other points. The process is thinned so that there are no intersecting spheres, according to two different schemes:

- (P) Pairwise assignment of weights. For each pair of points with intersecting spheres both points get weights independent of each other and the point with the lower weight is removed. In the case of equal weights both are removed. A point will only be retained if it wins in each of the pairwise comparisons. For example, if three points have intersecting spheres it is possible that all three points will be removed.
- (G) Global assignment of weights. The points get i.i.d. weights once and for all. As before, points with intersecting spheres compete and the one with strictly higher weight is retained.

Both in the global and pairwise case the weight may depend on the radius, but not on the point process. Denote the weight distribution for a sphere with radius r by $F_{W|r}$.

The thinning procedure can be thought of as giving marks to the original Poisson process. A point gets mark 1 if it is kept and 0 if it is removed. Now we have a marked process $\Phi = \{[X_n; M_n]\}$ with points $\{X_n\}$ constituting a stationary Poisson process with intensity λ in \mathbb{R}^d and to each X_n an associated mark M_n taking values in $M = \{0, 1\}$.

The intensity is an important characteristic of a point process. For the current models it can be expressed in terms of $h(r)$, the retention probability, i.e. the probability that a point with radius r will be retained, see [4], as

$$\lambda_{th} = \lambda \int_0^\infty h(r) F_R(dr). \quad (2.1)$$

Let $W_1(r)$ and $W_2(y)$ be two independent weights with distribution functions $F_{W|r}$ and $F_{W|y}$, and κ_d the volume of the unit sphere in d dimensions. The retention probability for the pairwise case is

$$h_P(r) = \exp \left\{ -\lambda \kappa_d \int_0^\infty \mathbb{P}(W_1(r) \leq W_2(y)) (r+y)^d F_R(dy) \right\}. \quad (2.2)$$

For a random variable X with distribution function F let $\bar{F}(x) = \mathbb{P}(X \geq x)$. The retention probability for the global case is

$$h_G(r) = \int_0^\infty \exp \left\{ -\lambda \kappa_d \int_0^\infty \bar{F}_{W|y}(w) (r+y)^d F_R(dy) \right\} F_{W|r}(dw). \quad (2.3)$$

A further characteristic of these models is the radius distribution after thinning. In general it is not the same as the distribution before thinning, but the right tail of the distribution can be preserved, if large spheres are kept in the thinning. See [4] for a discussion of the radius distribution.

3 The second–order product density

As mentioned in the Introduction, we want to study functions that describe the second-order behaviour of these models. One such function is the second-order product density $\varrho^{(2)}$. It is the density with respect to the Lebesgue measure of the second-order factorial moment measure $\alpha_P^{(2)}$ on $\mathbb{R}^d \times \mathbb{R}^d$. If B_1 and B_2 are Borel sets and Ψ is a point process on \mathbb{R}^d with distribution P_Ψ , $\alpha^{(2)}$ is defined as

$$\begin{aligned} \alpha_P^{(2)}(B_1 \times B_2) &= \mathbb{E}[\#\{(x_1, x_2) : x_1 \in \Psi \cap B_1, x_2 \in \Psi \cap B_2, x_1 \neq x_2\}] \\ &= \int \sum_{\substack{x_1, x_2 \in \psi \\ x_1 \neq x_2}} 1_{B_1}(x_1) 1_{B_2}(x_2) P_\Psi(d\psi). \end{aligned} \quad (3.1)$$

An interpretation of the second-order product density is that

$$\varrho_P^{(2)}(x_1, x_2) dV_1 dV_2$$

is the probability of having a point in each of two infinitesimally small disjoint Borel sets, with Lebesgue measures dV_1 and dV_2 , where x and y belong to one set each. The following result will be used in the calculation of the second-order product density for the thinned processes defined above.

Lemma 3.1 *Let $\Phi = \{[X_n; M_n]\}$ be a simple marked point process in \mathbb{R}^d with marks in $\mathbb{M} = \{0, 1\}$, where the associated point process $\{X_n\}$ is a stationary Poisson process with intensity λ . Then the second-order product density $\varrho_{th}^{(2)}$ for the process consisting of points with marks 1 can be written as*

$$\varrho_{th}^{(2)}(x_1, x_2) = \lambda^2 \mathcal{M}_{x_1, x_2}((1, 1)), \quad (3.2)$$

where \mathcal{M}_{x_1, x_2} is the two-point mark distribution, defined on $\mathbb{M} \times \mathbb{M}$. If the process consisting of points with marks 1 is stationary and isotropic the product density will only depend on the distance $|x_1 - x_2|$ between the two points, and $\varrho_{th}^{(2)}(x_1, x_2)$ is simplified to

$$\varrho_{th}^{(2)}(r) = \lambda^2 \mathcal{M}_{o, r}((1, 1)), \quad (3.3)$$

for one point at the origin and one point in location \mathbf{r} at distance r from the origin.

The two-point mark distribution \mathcal{M}_{x_1, x_2} describes the marks in x_1 and x_2 under the condition that there are points in x_1 and x_2 , see [7]. It can be thought of as a two-fold Palm distribution.

The proof of Lemma 3.1, which is given below, is rather technical and may be skipped without affecting the reading of further sections. We need a modification of Theorem 2.3 from [7] with the assumption of the stationarity and isotropy of the marked process removed. The proof of this modification can essentially be found in [7], but is not stated in a theorem. The theorem below, which states the modification, can be called the ‘‘two-point Campbell theorem’’.

Theorem 3.2 Let $\Phi = \{[X_n; M_n]\}$ be a simple marked point process in \mathbb{R}^d with marks in $\mathbb{M} = \{0, 1\}$ and distribution P . The set of all outcomes of Φ is denoted by N . Let $\{\mathcal{M}_{x_1, x_2} : x_1, x_2 \in \mathbb{R}^d\}$ be the family of corresponding two-point mark distributions and let $\alpha_{(2)}$ be the second-order factorial moment measure of $\{X_n\}$. For every measurable $f : \mathbb{R}^d \times \mathbb{M} \times \mathbb{R}^d \times \mathbb{M} \rightarrow \mathbb{R}^+$,

$$\begin{aligned} & \int_N \sum_{\substack{[x_1; m_1] \in \varphi \\ [x_2; m_2] \in \varphi \\ x_1 \neq x_2}} f(x_1, m_1, x_2, m_2) P(d\varphi) \\ &= \int_{\mathbb{R}^d \times \mathbb{R}^d} \int_{\mathbb{M} \times \mathbb{M}} f(x_1, m_1, x_2, m_2) \mathcal{M}_{x_1, x_2}(d(m_1, m_2)) \alpha_{(2)}(d(x_1, x_2)). \end{aligned}$$

Now we are ready to prove Lemma 3.1 with the aid of Theorem 3.2.

Proof of Lemma 3.1. For a thinned process with distribution P_{th} the second-order factorial moment measure is

$$\alpha_{th}^{(2)}(B_1 \times B_2) = \int \sum_{\substack{x_1 \in \varphi, x_2 \in \varphi \\ x_1 \neq x_2}} 1_{B_1}(x_1) 1_{B_2}(x_2) P_{th}(d\varphi).$$

This expression can be rewritten in terms of the original marked process Φ with distribution P . Let $1_{\{1\} \times \{1\}}(m_1, m_2)$ be the indicator function of the event that both x_1 and x_2 are retained when thinning. By summing over all points in Φ that are retained in the thinning procedure we get

$$\alpha_{th}^{(2)}(B_1 \times B_2) = \int_N \sum_{\substack{[x_1; m_1] \in \varphi \\ [x_2; m_2] \in \varphi \\ x_1 \neq x_2}} 1_{B_1}(x_1) 1_{B_2}(x_2) 1_{\{1\} \times \{1\}}(m_1, m_2) P(d\varphi).$$

By Theorem 3.2,

$$\begin{aligned} & \alpha_{th}^{(2)}(B_1 \times B_2) \\ &= \int_{B_1 \times B_2} \int_{\mathbb{M} \times \mathbb{M}} 1_{\{1\} \times \{1\}}(m_1, m_2) \mathcal{M}_{x_1, x_2}(d(m_1, m_2)) \alpha^{(2)}(d(x_1, x_2)) \\ &= \int_{B_1 \times B_2} \sum_{m_1=0}^1 \sum_{m_2=0}^1 1_{\{1\} \times \{1\}}(m_1, m_2) \mathcal{M}_{x_1, x_2}(d(m_1, m_2)) \alpha^{(2)}(d(x_1, x_2)) \\ &= \int_{B_1 \times B_2} \mathcal{M}_{x_1, x_2}((1, 1)) \alpha^{(2)}(d(x_1, x_2)). \end{aligned}$$

For a homogeneous Poisson process with intensity λ , the second-order factorial moment measure $\alpha^{(2)}(B_1 \times B_2) = \lambda^2 l_d(B_1) l_d(B_2)$, see for example [12]. Since the product density of the thinned process is the density of $\alpha_{th}^{(2)}$ with respect to Lebesgue measure we get (3.2). ■

4 Spheres with fixed radii

4.1 Second-order product densities

In this section we derive the second-order product density for the two point processes with spheres of radius r_0 and continuous weight distribution. The following notation is used. Let $B_d(x, r) = \{y \in \mathbb{R}^d : |x - y| \leq r\}$ be the d -dimensional sphere centred in x with radius r and let l_d be the Lebesgue measure in \mathbb{R}^d . Moreover, let $\kappa_d = l_d(B(x, 1))$, the volume of the unit d -dimensional sphere, so that $l_d(B(x, r)) = \kappa_d r^d$. Quantities in the pairwise case and the global case are indexed by P and G, respectively.

From equations (2.1), (2.2) and (2.3), the intensities of the thinned processes are

$$\lambda_{thP} = \lambda \exp \left\{ -\frac{1}{2} \lambda \kappa_d (2r_0)^d \right\}$$

for the pairwise model and

$$\lambda_{thG} = \frac{1 - \exp \left\{ -\lambda \kappa_d (2r_0)^d \right\}}{\kappa_d (2r_0)^d},$$

for the global model, when the intensity of the Poisson process before thinning is λ .

Theorem 4.1 *Let $V = \kappa_d (2r_0)^d$ and $q(r) = l_d(B_d(o, 2r_0) \cap B_d(r, 2r_0))^1$, with $|o - r| = r$. For the pairwise model with spherical grains of fixed size, the second-order product density is*

$$\varrho^{(2)}(r) = \begin{cases} 0 & \text{if } r \leq 2r_0 \\ \lambda^2 \exp \left\{ -\lambda(V - \frac{1}{4}q(r)) \right\} & \text{if } 2r_0 < r \leq 4r_0 \\ \lambda^2 \exp \{-\lambda V\} & \text{if } r > 4r_0. \end{cases} \quad (4.1)$$

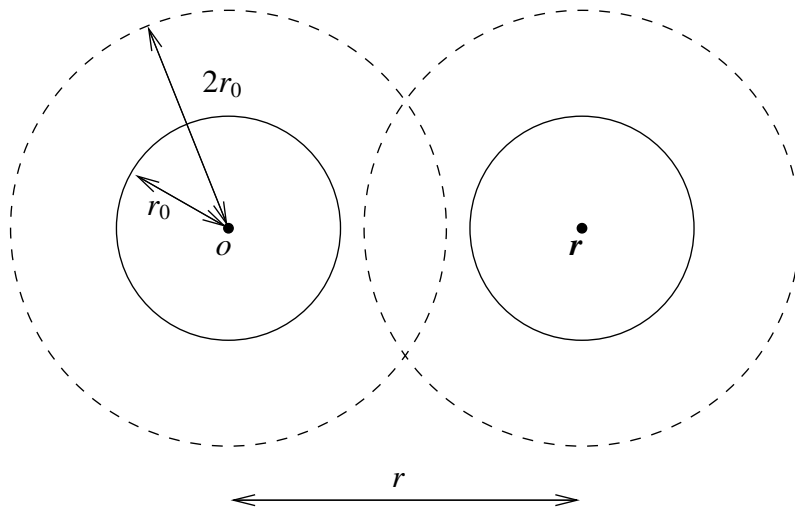


Figure 2: Two spheres at distance r in 2-d.

¹See Appendix A for calculations in two and three dimensions.

Proof. We use (3.3) to calculate the product density, i.e. we need $\mathcal{M}_{o,r}((1, 1))$, the two-point mark probability that two points at distance r both have marks 1, that is the probability of retaining two points at distance r . Given one point at the origin, o , and one point at distance r from the origin located in \mathbf{r} , see Figure 2, the probability that both points are retained is zero if $r \leq 2r_0$, since then their spheres intersect and at least one of them must be removed and hence $\mathcal{M}_{o,r}((1, 1)) = 0$. For $r > 2r_0$ the two-point mark probability can be rewritten as

$$\mathcal{M}_{o,r}((1, 1)) = \mathbb{P}(\{\# \text{ of points that win over } o \text{ or } \mathbf{r}\} = 0). \quad (4.2)$$

The points that win over o or \mathbf{r} constitute an inhomogeneous Poisson process with intensity function $\lambda_b(x)$. When λ is the intensity of the Poisson process before thinning, the mean number of points in \mathbb{R}^d of this inhomogeneous process can be written

$$\int_{\mathbb{R}^d} \lambda_b(x) dx = \int_{\mathbb{R}^d} \lambda \mathbb{P}(\text{A point in } x \text{ wins over } o \text{ or } \mathbf{r}) dx.$$

For $r > 2r_0$ points that belongs to the union of $B_d(o, 2r_0)$ and $B_d(\mathbf{r}, 2r_0)$ are possible candidates for winning over either o or \mathbf{r} or both. More precisely points in $B_d(o, 2r_0) \setminus B_d(\mathbf{r}, 2r_0)$ can beat o , but not \mathbf{r} , points in $B_d(\mathbf{r}, 2r_0) \setminus B_d(o, 2r_0)$ can beat \mathbf{r} , but not o and points in $B_d(o, 2r_0) \cap B_d(\mathbf{r}, 2r_0)$ can beat o or \mathbf{r} . If W_o is the weight of o , W_r is the weight of \mathbf{r} , W_{x1} is the weight of x when competing with o and W_{x2} is the weight of x when competing with \mathbf{r} , then

$$\begin{aligned} \int_{\mathbb{R}^d} \lambda_b(x) dx &= \lambda \int_{\mathbb{R}^d} \left[\mathbb{1}_{\{B_d(o, 2r_0) \setminus B_d(\mathbf{r}, 2r_0)\}}(x) \mathbb{P}(W_{x1} \geq W_o) \right. \\ &\quad + \mathbb{1}_{\{B_d(\mathbf{r}, 2r_0) \setminus B_d(o, 2r_0)\}}(x) \mathbb{P}(W_{x2} \geq W_r) \\ &\quad \left. + \mathbb{1}_{\{B_d(\mathbf{r}, 2r_0) \cap B_d(o, 2r_0)\}}(x) \mathbb{P}(W_{x1} \geq W_o \cup W_{x2} \geq W_r) \right] dx \end{aligned} \quad (4.3)$$

since the sets are disjoint. Further simplification gives,

$$\begin{aligned} \int_{\mathbb{R}^d} \lambda_b(x) dx &= \lambda \int_{\mathbb{R}^d} \left[\mathbb{1}_{\{B_d(o, 2r_0) \setminus B_d(\mathbf{r}, 2r_0)\}}(x) \frac{1}{2} \right. \\ &\quad \left. + \mathbb{1}_{\{B_d(\mathbf{r}, 2r_0) \setminus B_d(o, 2r_0)\}}(x) \frac{1}{2} + \mathbb{1}_{\{B_d(\mathbf{r}, 2r_0) \cap B_d(o, 2r_0)\}}(x) \frac{3}{4} \right] dx \\ &= \lambda \left[\frac{1}{2} l_d(B_d(o, 2r_0) \setminus B_d(\mathbf{r}, 2r_0)) + \frac{1}{2} l_d(B_d(\mathbf{r}, 2r_0) \setminus B_d(o, 2r_0)) \right. \\ &\quad \left. + \frac{3}{4} l_d(B_d(\mathbf{r}, 2r_0) \cap B_d(o, 2r_0)) \right]. \end{aligned} \quad (4.4)$$

Recalling (4.2) we get

$$\mathcal{M}_{o,r}((1, 1)) = \exp \left\{ - \int_{\mathbb{R}^d} \lambda_b(x) dx \right\}. \quad (4.5)$$

Equations (4.4) and (4.5) combined with (3.3), using

$$\begin{aligned} l_d(B_d(o, 2r_0) \setminus B_d(\mathbf{r}, 2r_0)) &= l_d(B_d(\mathbf{r}, 2r_0) \setminus B_d(o, 2r_0)) \\ &= \kappa_d (2r_0)^d - l_d(B_d(o, 2r_0) \cap B_d(\mathbf{r}, 2r_0)) \end{aligned}$$

concludes the proof. Observe that $q(r) = \gamma_d(r, 2r_0) = l_d(B_d(o, 2r_0) \cap B_d(\mathbf{r}, 2r_0)) = 0$ for $r > 4r_0$. \blacksquare

Theorem 4.2 Let $V = \kappa_d(2r_0)^d$ and $q(r) = l_d(B_d(o, 2r_0) \cap B_d(\mathbf{r}, 2r_0))^2$, with $|o - \mathbf{r}| = r$. For the global model with spherical grains of fixed radii, the second-order product density is

$$\varrho^{(2)}(r) = \begin{cases} 0 & \text{if } r \leq 2r_0 \\ 2 \left\{ \frac{1}{V(2V - q(r))} - \frac{e^{-\lambda V}}{V(V - q(r))} \right. \\ \quad \left. + \frac{e^{-\lambda(2V - q(r))}}{(V - q(r))(2V - q(r))} \right\} & \text{if } 2r_0 < r \leq 4r_0 \\ \left(\frac{1 - e^{-\lambda V}}{V} \right)^2 & \text{if } r > 4r_0. \end{cases} \quad (4.6)$$

Remark: This formula can be found on page 164 in [12]. The proof given here is very similar to that of Theorem 4.1.

Proof. Conditioning on the probability that a point in o has weight w_o and a point in \mathbf{r} , at distance r from the origin, has weight w_r , the probability that both points are retained can be found as in the proof of Theorem 4.1 above. Denote a point in x having radius r_x by $[x; r_x]$. For simplicity's sake we take the weight distribution to be uniform, but it could be any continuous distribution. Instead of (4.2) we get

$$\begin{aligned} & \mathcal{M}_{o,r}((1, 1)) \\ &= \int_0^1 \int_0^1 \mathbb{P}(\{\# \text{ of points that win over } [o; w_o] \text{ or } [\mathbf{r}; w_r]\} = 0) dw_o dw_r. \end{aligned}$$

Another difference from the proof of Theorem 4.1 is that in (4.3)

$$\mathbb{P}(W_{x1} \geq W_o) \text{ is replaced by } \mathbb{P}(W_x \geq w_o) = \int_{w_o}^1 dw = 1 - w_o,$$

$$\mathbb{P}(W_{x2} \geq W_r) \text{ is replaced by } \mathbb{P}(W_x \geq w_r) = \int_{w_r}^1 dw = 1 - w_r$$

and similarly

$\mathbb{P}(W_{x1} \geq W_o \cup W_{x2} \geq W_r)$ is replaced by

$$\mathbb{P}(W_x \geq \min(w_o, w_r)) = \int_{\min(w_o, w_r)}^1 dw = 1 - \min(w_o, w_r).$$

This leads to

$$\begin{aligned} & \mathcal{M}_{o,r}((1, 1)) \\ &= \int_0^1 \int_0^1 \exp \left\{ -\lambda \left[(1 - w_o)(\kappa_d(2r_0)^d - l_d(B_d(o, 2r_0) \cap B_d(\mathbf{r}, 2r_0))) \right. \right. \\ & \quad \left. \left. + (1 - w_r)(\kappa_d(2r_0)^d - l_d(B_d(o, 2r_0) \cap B_d(\mathbf{r}, 2r_0))) \right. \right. \\ & \quad \left. \left. + (1 - \min(w_r, w_o))l_d(B_d(o, 2r_0) \cap B_d(\mathbf{r}, 2r_0)) \right] \right\} dw_o dw_r. \end{aligned} \quad (4.7)$$

Evaluating (4.7) and multiplying by λ^2 gives (4.6). ■

²See Appendix A for calculations in two and three dimensions.

4.2 Behaviour of the models

According to [4] the intensities after thinning behave quite differently for the two models, see Figure 3. For the pairwise case $\lambda_{th} \rightarrow 0$ as $\lambda \rightarrow \infty$ and it has a maximum in $\lambda_{th} = 2/(\kappa_d(2r_0)^d e)$ for $\lambda = 2/(\kappa_d(2r_0)^d)$. On the other hand, for the global case, λ_{th} is increasing in λ and as $\lambda \rightarrow \infty$, $\lambda_{th} \rightarrow 1/(\kappa_d(2r_0)^d)$.

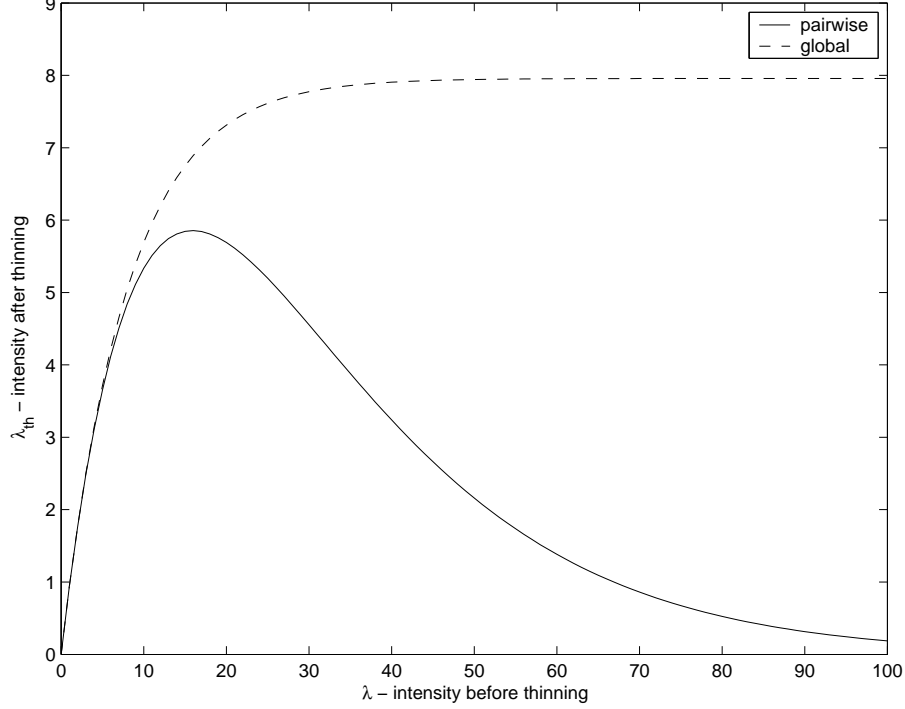


Figure 3: The intensity after thinning for the pairwise and the global models in two dimensions for spheres of equal radii=0.1.

When comparing product densities of the global model and the pairwise model it is clearer to consider the pair-correlation function instead. It is defined as

$$g(r) = \varrho^{(2)}(r)/\lambda_{th}^2,$$

giving

$$g_P(r) = \begin{cases} 0 & \text{if } r \leq 2r_0 \\ \exp\left\{\lambda \frac{1}{4} \gamma_d(r, 2r_0)\right\} & \text{if } 2r_0 < r \leq 4r_0 \\ 1 & \text{if } r > 4r_0 \end{cases}$$

and

$$g_G(r) = \begin{cases} 0 & \text{if } r \leq 2r_0 \\ \frac{2}{\lambda_{thG}^2} \left\{ \frac{1}{V(2V - q(r))} - \frac{e^{-\lambda V}}{V(V - q(r))} + \frac{e^{-\lambda(2V - q(r))}}{(V - q(r))(2V - q(r))} \right\} & \text{if } 2r_0 < r \leq 4r_0 \\ 1 & \text{if } r > 4r_0, \end{cases}$$

for the two models. For a Poisson process $g(r) = 1$, $r > 0$, see [12]. When $r \leq 2r_0$, the pair-correlation is 0 and there can be no pair of points separated by such distances. The pair-correlation is 1 for both models when $r > 4r_0$, meaning that the frequency of point pairs at distances larger than $4r_0$ is the same as in a Poisson process.

For the pairwise model and $2r_0 < r \leq 4r_0$, the pair-correlation is increasing in λ , that is when $\lambda \rightarrow \infty$ the process has a higher frequency of pairs of points at distances between $2r_0$ and $4r_0$ than a homogeneous Poisson process even though the intensity after thinning tends to zero at the same time. On the other hand, when λ goes to infinity for the global model, g_G tends to $(2V)/(2V - q(r))$, for $2r_0 < r \leq 4r_0$, which is between 1 and 1.1 in \mathbb{R}^2 , since $0 \leq q(r)/V < 2/3 - \sqrt{3}/\pi$. In \mathbb{R}^d an upper bound for $q(2r_0)$ is $1/2$, implying that $(2V)/(2V - q(r))$ is never greater than $4/3$. This means that the global process has almost the same pair-correlation as a Poisson process except for the hard cores.

If we compare the pair-correlation functions for the same value of the intensity after thinning we get three different behaviours since the pairwise model can have the same λ_{th} for two different λ , as can be seen in Figure 3. Figure 4 and Figure 5 show a plot of the pairwise and the global pair-correlation function in two dimensions.

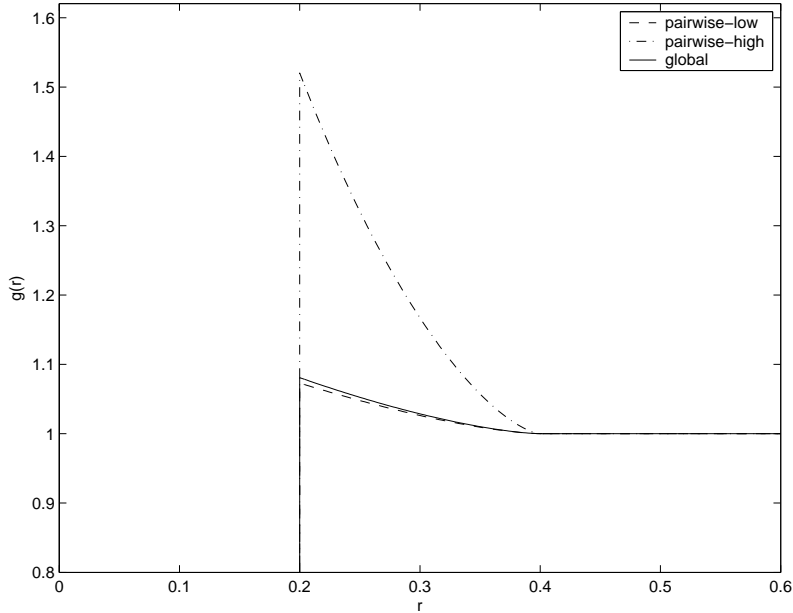


Figure 4: Pair-correlation function for the pairwise and the global model in two dimensions with the same intensity after thinning, $\lambda_{th} = 4$, and radius of the spheres $r_0 = 0.1$. The intensity before thinning was 5.74 and 34.11 for the two pairwise models giving the same λ_{th} , labelled low and high respectively in the plot, and 5.56 for the global.

5 Spheres with general radius and weight distributions

Now we turn to a more general case than above, where the spheres radii have some non-degenerate distribution. Let the spheres have radius distribution F_R and the weights have distribution $F_{W|r}$ which may depend on the radius.

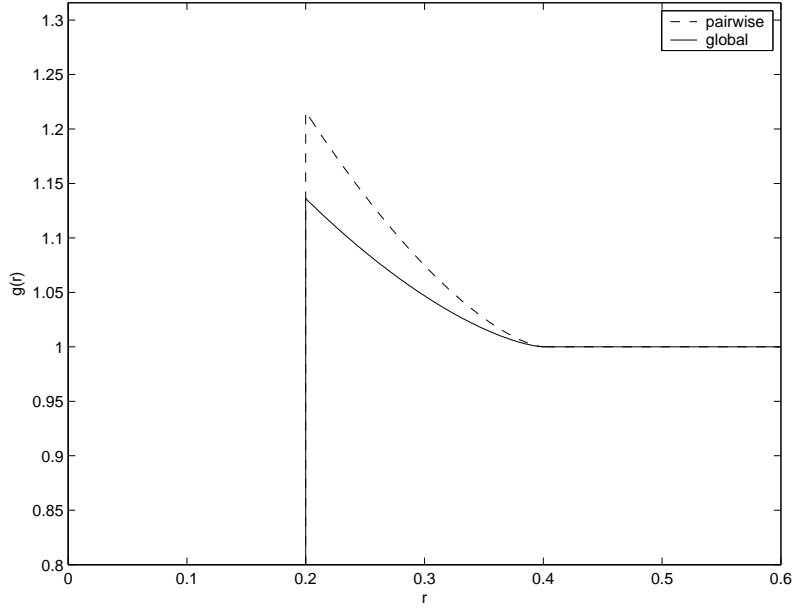


Figure 5: Pair-correlation function for the pairwise and the global model in two dimensions with the same intensity after thinning, $\lambda_{th} = 2/(\kappa_d(2r_0)^d e) = 5.86$, and radius of the spheres $r_0 = 0.1$. The intensity before thinning was 15.92 for the pairwise model and 10.59 for the global. Compared with Figure 4 there is only one pairwise model since λ_{th} is chosen as the maximum in Figure 3.

Theorem 5.1 Let $\delta_d(r, r_1, r_2) = l_d(B_d(o, r_1) \cap B_d(\mathbf{r}, r_2))$ with $|o - \mathbf{r}| = r$ and let $W_i(x)$ have distribution $F_{W|x}$. For the pairwise model with spherical grains, the second-order product density is

$$\begin{aligned}
\varrho^{(2)}(r) = & \lambda^2 \int_0^r \int_0^{r-r_0} \exp\left\{-\lambda \int_0^\infty \right. \\
& \left[(\kappa_d(r_0 + r_w)^d - \delta_d(r, r_0 + r_w, r_r + r_w)) \mathbb{P}(W_1(r_0) \leq W_2(r_w)) \right. \\
& + (\kappa_d(r_r + r_w)^d - \delta_d(r, r_0 + r_w, r_r + r_w)) \mathbb{P}(W_3(r_r) \leq W_4(r_w)) \\
& \left. \left. + \delta_d(r, r_0 + r_w, r_r + r_w) \mathbb{P}(W_1(r_0) \leq W_2(r_w) \cup W_3(r_r) \leq W_4(r_w)) \right] \right. \\
& \left. F_R(dr_w) \right\} F_R(dr_r) F_R(dr_0).
\end{aligned} \tag{5.1}$$

Proof. Consider two points, one at the origin, o , and the other at a distance r from the origin, in location \mathbf{r} . As before, use $\mathcal{M}_{o,r}((1, 1))$ in (3.3) and condition on the sphere at o having radius r_0 and the sphere at \mathbf{r} having radius r_r . Denote a point in x having radius r_x by $[x; r_x]$. If the distance between o and \mathbf{r} is less than the sum of their radii, both of the points cannot be retained, hence we integrate over all radii such that $r > r_0 + r_r$

$$\begin{aligned}
\mathcal{M}_{o,r}((1, 1)) = & \int_0^\infty \int_0^\infty 1_{\{r > r_0 + r_r\}} \\
& \mathbb{P}(\{\# \text{ points that win over } [o; r_0] \text{ or } [\mathbf{r}; r_r]\} = 0) F_R(dr_0) F_R(dr_r).
\end{aligned} \tag{5.2}$$

As before, the points that win over $[o; r_0]$ or $[\mathbf{r}; r_r]$ constitute an inhomogeneous Poisson process with intensity function $\lambda_b(x)$. When λ is the intensity of the stationary Poisson

process, the mean number of points in \mathbb{R}^d of this inhomogeneous process can be written

$$\begin{aligned} \int_{\mathbb{R}^d} \lambda_b(x) dx &= \int_{\mathbb{R}^d} \lambda \mathbb{P}(\text{A point in } x \text{ wins over } [o; r_o] \text{ or } [r; r_r]) dx \\ &= \lambda \int_{\mathbb{R}^d} \int_0^\infty \mathbb{P}(\text{A point in } [x; r_w] \text{ wins over } [o; r_o] \text{ or } [r; r_r]) F_R(dr_w) dx. \end{aligned} \quad (5.3)$$

A point with radius r_w is a possible candidate for winning over o if it belongs to the set

$$\{x \in \mathbb{R}^d : B_d(o, r_o) \cap B_d(x, r_w) \neq \emptyset\} = B_d(o, r_o + r_w),$$

and similarly it is a candidate for winning over r if it belongs to $B_d(r, r_r + r_w)$. Points in $B_d(o, r_o + r_w) \cap B_d(r, r_r + r_w)$ can win over both o and r . These three sets can be made into three disjoint sets, and letting $W_i(x)$ have distribution $F_{W|x}$, we get

$$\begin{aligned} \int_{\mathbb{R}^d} \lambda_b(x) dx &= \lambda \int_{\mathbb{R}^d} \int_0^\infty \left[\mathbb{1}_{\{B_d(o, r_o + r_w) \setminus B_d(r, r_r + r_w)\}}(x) \mathbb{P}(W_{x1}(r_w) \geq W_o(r_o)) \right. \\ &\quad + \mathbb{1}_{\{B_d(r, r_r + r_w) \setminus B_d(o, r_o + r_w)\}}(x) \mathbb{P}(W_{x2}(r_w) \geq W_r(r_r)) \\ &\quad \left. + \mathbb{1}_{\{B_d(r, r_r + r_w) \cap B_d(o, r_o + r_w)\}}(x) \mathbb{P}(W_{x1}(r_w) \geq W_o(r_o) \cup W_{x2}(r_w) \geq W_r(r_r)) \right] \\ &\quad F_R(dr_w) dx. \end{aligned}$$

The weights do not depend on x , thus giving,

$$\begin{aligned} \int_{\mathbb{R}^d} \lambda_b(x) dx &= \lambda \int \left[l_d(B_d(o, r_o + r_w) \setminus B_d(r, r_r + r_w)) \mathbb{P}(W_{x1}(r_w) \geq W_o(r_o)) \right. \\ &\quad + l_d(B_d(r, r_r + r_w) \setminus B_d(o, r_o + r_w)) \mathbb{P}(W_{x2}(r_w) \geq W_r(r_r)) \\ &\quad + l_d(B_d(r, r_r + r_w) \cap B_d(o, r_o + r_w)) \\ &\quad \left. \mathbb{P}(W_{x1}(r_w) \geq W_o(r_o) \cup W_{x2}(r_w) \geq W_r(r_r)) \right] F_R(dr_w). \end{aligned} \quad (5.4)$$

The probability in (5.2) is

$$\begin{aligned} &\mathbb{P}(\{\# \text{ of points that win over } [o; r_o] \text{ or } [r; r_r]\} = 0) \\ &= \exp \left\{ - \int_{\mathbb{R}^d} \lambda_b(x) dx \right\}. \end{aligned} \quad (5.5)$$

Insert (5.4) and (5.5) in (5.2), multiply by λ^2 and the proof is complete. ■

Theorem 5.2 Let $\delta_d(r, r_1, r_2) = l_d(B_d(o, r_1) \cap B_d(\mathbf{r}, r_2))$ with $|o - \mathbf{r}| = r$. For the global model with spherical grains, the second-order product density is

$$\begin{aligned}
\varrho^{(2)}(r) = & \lambda^2 \int_0^r \int_0^{r-r_o} \iint \exp\{-\lambda \int \\
& \left[\int_{w_o}^{\infty} (\kappa_d(r_o + r_w)^d - \delta_d(r, r_o + r_w, r_r + r_w)) F_{W|r_w}(dw) \right. \\
& + \int_{w_r}^{\infty} (\kappa_d(r_r + r_w)^d - \delta_d(r, r_o + r_w, r_r + r_w)) F_{W|r_w}(dw) \\
& \left. + \int_{\min(w_o, w_r)}^{\infty} \delta_d(r, r_o + r_w, r_r + r_w) F_{W|r_w}(dw) \right] \\
& F_R(dr_w) \} F_{W|r_o}(dw_o) F_{W|r_r}(dw_r) F_R(dr_r) F_R(dr_o).
\end{aligned} \tag{5.6}$$

Proof. A point in x with its associated radius and weight is denoted by $[x; r_x; w_x]$. The ideas of the proof are the same as for the proof of Theorem 5.1, but condition also on the weights of the two typical points in o and r being w_o and w_r respectively, i.e. (5.2) becomes

$$\begin{aligned}
\mathcal{M}_{o,r}((1, 1)) = & \int_0^{\infty} \int_0^{\infty} \iint \mathbf{1}_{\{r > r_o + r_r\}} \\
& \mathbb{P}(\{\# \text{ of points that win over } [o; r_o; w_o] \text{ or } [r; r_r; w_r]\} = 0) \\
& F_{W|r_o}(dw_o) F_{W|r_r}(dw_r) F_R(dr_o) F_R(dr_r).
\end{aligned} \tag{5.7}$$

Furthermore, to calculate the expectation of the number of points that beat o or r , we must also condition on the radius and the weight of x

$$\begin{aligned}
& \int_{\mathbb{R}^d} \lambda_b(x) dx \\
& = \int_{\mathbb{R}^d} \lambda \mathbb{P}(\text{A point in } x \text{ wins over } [o; r_o; w_o] \text{ or } [r; r_r; w_r]) dx \\
& = \lambda \int_{\mathbb{R}^d} \iint \left[\mathbf{1}_{\{B_d(o, r_o + r_w) \setminus B_d(r, r_r + r_w)\}}(x) \mathbf{1}_{\{w_x \geq w_o\}} \right. \\
& \quad + \mathbf{1}_{\{B_d(r, r_r + r_w) \setminus B_d(o, r_o + r_w)\}}(x) \mathbf{1}_{\{w_x \geq w_r\}} \\
& \quad \left. + \mathbf{1}_{\{B_d(r, r_r + r_w) \cap B_d(o, r_o + r_w)\}}(x) \mathbf{1}_{\{w_x \geq \min(w_r, w_o)\}} \right] \\
& \quad F_{W|r_w}(dw_x) F_R(dr_w) dx.
\end{aligned}$$

The last steps are the same as those in the proof of Theorem 5.1. ■

Remark: If the weight distribution is continuous and independent of the radius it does not matter which form it has.

To evaluate the product density for special cases it is usually necessary to do the integration numerically. Below there is one simple example when it is possible to calculate the product density exactly and another example when numerical integration is necessary.

Example 5.1. Consider a model in \mathbb{R}^2 with two spheres of radius r_1 and r_2 and let p_i be the probability of a sphere having radius r_i , before thinning. Let the weight distribution be uniform and independent of the radius. An expression for $\delta_2(r, r_i + r_k, r_j + r_k)$, the area of the intersection of two discs with radii $r_i + r_k$ and $r_j + r_k$ at distance r , can be found in Appendix A. Then, for the pairwise model, the intensity after thinning is

$$\lambda_{thP} = \lambda \sum_{i=1}^2 p_i \exp \left\{ -\lambda \frac{1}{2} \pi ((r_i + r_1)^2 p_1 + (r_i + r_2)^2 p_2) \right\},$$

by (2.1) and (2.2). By (5.1), the product density is

$$\begin{aligned} \varrho_P^{(2)}(r) = & \lambda^2 \sum_{i=1}^2 \sum_{j=1}^2 1_{\{r_i+r_j<r\}} \exp \left\{ -\lambda \sum_{k=1}^2 \left[\frac{\pi}{2} ((r_i + r_k)^2 + (r_j + r_k)^2) \right. \right. \\ & \left. \left. - \frac{1}{4} \delta_2(r, r_i + r_k, r_j + r_k) \right] p_k \right\} p_j p_i. \end{aligned}$$

Let $V_i = \sum_{k=1}^2 p_k \pi (r_i + r_k)^2$ and $q_{i,j}(r) = \sum_{k=1}^2 p_k \delta_2(r, r_i + r_k, r_j + r_k)$. From (2.1), (2.3) and (5.6), the corresponding quantities for the global model are

$$\lambda_{thG} = \sum_{i=1}^2 \frac{1 - \exp \left\{ -\lambda \pi \sum_{j=1}^2 (r_i + r_j)^2 p_j \right\}}{\pi \sum_{j=1}^2 (r_i + r_j)^2 p_j} p_i$$

and

$$\begin{aligned} \varrho_G^{(2)}(r) = & \sum_{i=1}^2 \sum_{j=1}^2 1_{\{r_i+r_j<r\}} \left\{ (V_i - q_{i,j}(r))(V_j - q_{i,j}(r))(V_i + V_j) \right. \\ & + V_i V_j (V_i + V_j - 2q_{i,j}(r)) \exp[-\lambda(V_i + V_j - q_{i,j}(r))] \\ & - V_i (V_i + V_j - q_{i,j}(r))(V_j - q_{i,j}(r)) \exp[-\lambda V_j] \\ & \left. - V_j (V_i + V_j - q_{i,j}(r))(V_i - q_{i,j}(r)) \exp[-\lambda V_i] \right\} \\ & / \left\{ V_i V_j (V_i - q_{i,j}(r))(V_j - q_{i,j}(r))(V_i + V_j - q_{i,j}(r)) \right\} p_i p_j. \end{aligned}$$

The pair-correlation functions, $\varrho^{(2)}/\lambda_{th}^2$, for both models with parameters $r_1 = 0.2$, $r_2 = 0.1$, $p_1 = 0.5$ and $p_2 = 0.5$, are shown in Figure 6. The intensities before thinning were 10 in the pairwise case and 4.4 in the global case, giving intensity 2.5 for both models after thinning. In the global model after thinning, the probability that a sphere has radius r_1 is approximately 0.42. In the pairwise model after thinning, the probability that a sphere has radius r_1 is approximately 0.28. The calculations of these probabilities can be done using Theorem 3.2 in [4]. The jump at $r = 0.2$ occurs because the spheres must have a radius which is at least 0.1 and consequently the points must be separated by at least 0.2. The next jump at $r = 0.3$ occurs because two spheres with radii which are 0.1 and 0.2, respectively, cannot be closer than 0.3. The final jump at $r = 0.4$ is explained in the same way. □

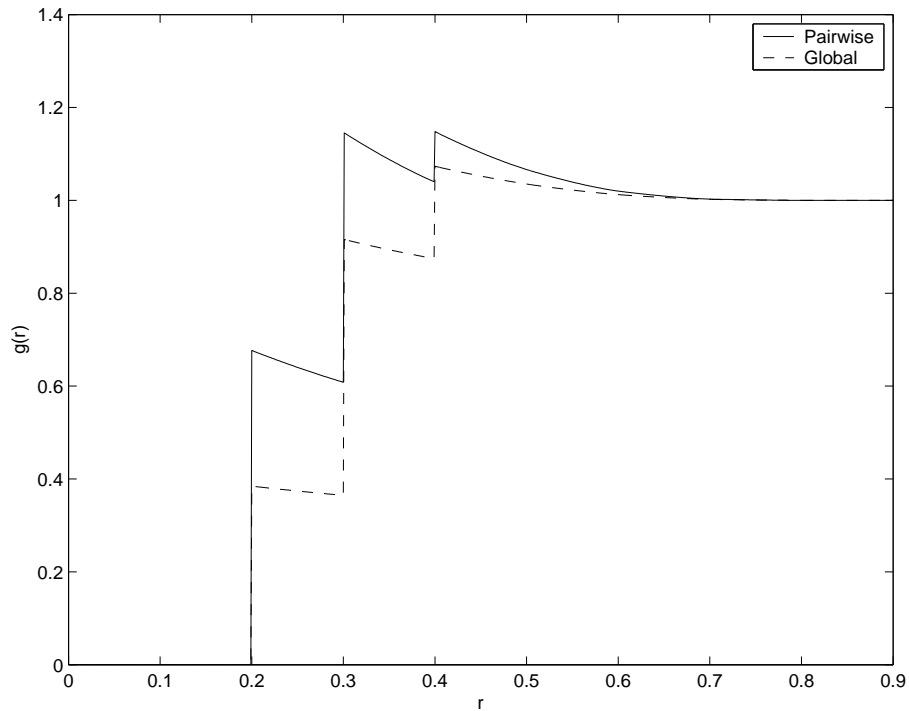


Figure 6: Pair-correlation function for the pairwise and the global model for spheres of two sizes with the same intensity after thinning, $\lambda_{th} = 2.5$.

Example 5.2. Consider the pairwise and global models in \mathbb{R}^2 . Let the radii be Rayleigh distributed with parameter 1, that is mean radius is about 1.25, and take the weight distribution independent of the radii. In Figure 7 there is a plot of the pair-correlations for two versions of the pairwise model and one version of the global model, all with the same intensity after thinning, 0.017. The intensities before thinning were 0.021 for one of the pairwise models and the global model while it was 0.4 for the other pairwise model. The mean radius after thinning was 1.18 for the pairwise model starting with low intensity, for the other pairwise model it was 0.593 and finally for the global model it was 1.19. Pairwise and global models starting with $\lambda = 0.021$ behave almost identically in terms of pair-correlation. When only two spheres overlap, there is no difference between the global model and the pairwise model, hence the similarity of pair-correlations for low starting intensity. In Figure 8 there are simulations of these models in a square of side 50 together with the simulation before thinning.

As we have seen before, the intensity after thinning as a function of the intensity before thinning has a maximum for the pairwise model. In this example it occurs for $\lambda = 0.115$ giving $\lambda_{th} = 0.0373$. In that case the pair-correlation can be found in Figure 9 along with a realisation.

The intensity after thinning of the global model tends to 0.0560 as λ tends to infinity. Taking $\lambda = 0.5$ gives $\lambda_{th} = 0.0558$ and the resulting pair-correlation and a simulation is found in Figure 10.

□

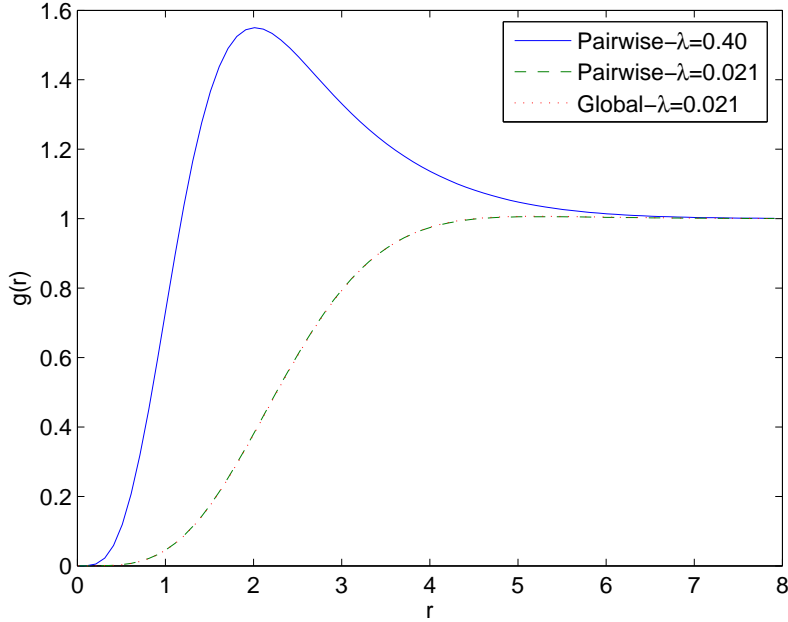


Figure 7: Pair-correlation function for models starting with Rayleigh distributed radii with parameter 1 and weights independent of the radii. See Example 5.2 for further details.

6 Convex, compact grains

Let us instead of spherical grains consider grains with the same shape and orientation as a convex, compact set in \mathbb{R}^d . To describe such a set some notation is needed. For a set $A \subseteq \mathbb{R}^d$, the translation of A by $x \in \mathbb{R}^d$ is defined as

$$A_x = \{x + y : y \in A\},$$

the reflection of A is defined as

$$\check{A} = \{-x : x \in A\}$$

and the Minkowski-addition of A and $B \subseteq \mathbb{R}^d$ is defined as

$$A \oplus B = \{x + y : x \in A, y \in B\}.$$

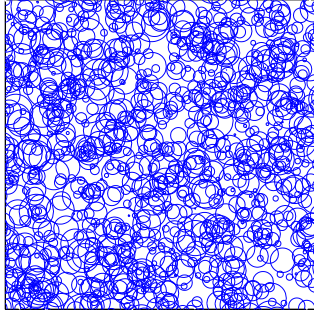
Another useful way to write the Minkowski-addition is

$$A \oplus B = \{x : A \cap (\check{B})_x \neq \emptyset\}. \quad (6.1)$$

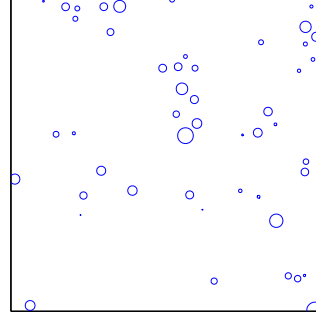
Define the size of a set $A \in \mathbb{R}^d$ as half its diameter, to have the size of a sphere equal to its radius, i.e. the size is defined as,

$$\frac{1}{2} \sup_{x,y \in A} |x - y|.$$

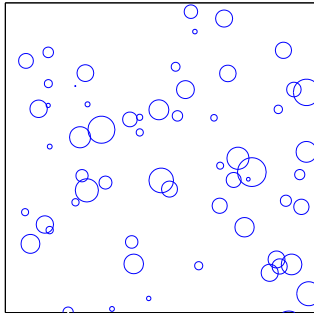
The family of convex, compact sets C in \mathbb{R}^d having size 1 and containing the origin is denoted by C^d . For $C \in C^d$, let $C(r) = \{ry : y \in C\}$, that is a set of the same shape and orientation as C but of size $r > 0$. By Theorem 4.1 in [4], (2.2) and (2.3) are valid if



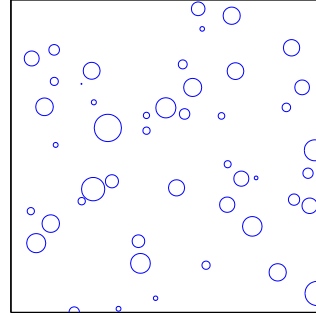
(a) Before thinning, $\lambda = 0.4$



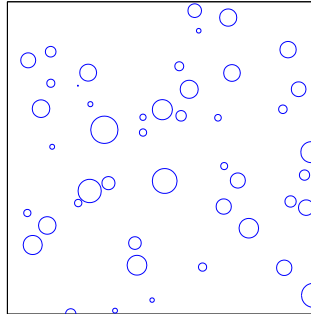
(b) Pairwise, $\lambda = 0.4$, $\lambda_{th} = 0.017$, mean radius = 0.593



(c) Before thinning $\lambda = 0.021$

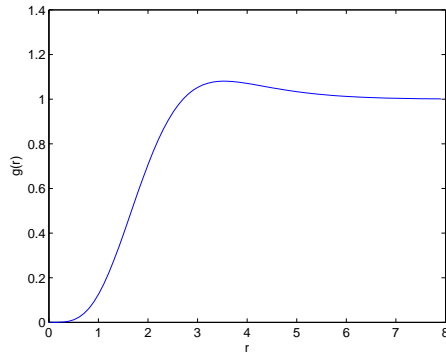


(d) Pairwise $\lambda = 0.021$, $\lambda_{th} = 0.017$, mean radius = 1.18

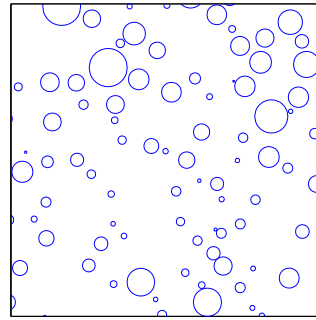


(e) Global $\lambda = 0.021$, $\lambda_{th} = 0.017$, mean radius = 1.19

Figure 8: Realisations of pairwise and global models with the same intensity after thinning, 0.017, see Example 5.2, starting with Rayleigh(1) distributed radii. The squares have side 50. The pairwise realisation in (b) was obtained by thinning (a) and the pairwise and global realisations in (d) and (e) respectively were obtained by thinning (c).

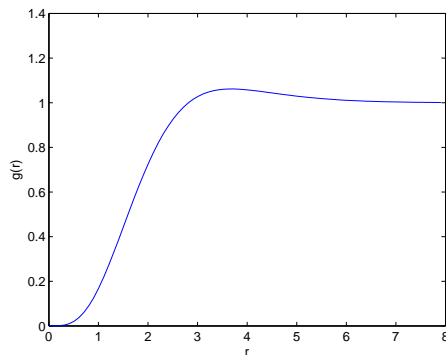


(a) Pair-correlation

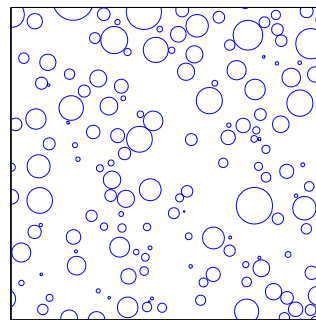


(b) Realisation

Figure 9: Pair-correlation and a simulation for the pairwise model with Rayleigh(1) distributed radii and intensity before thinning 0.115, giving maximal intensity after thinning 0.0373. See Example 5.2.



(a) Pair-correlation



(b) Realisation

Figure 10: Pair-correlation and a simulation for the global model with Rayleigh(1) distributed radii and intensity before thinning 0.5, giving close to maximal intensity after thinning, 0.0558. See Example 5.2.

$\kappa_d(r+y)^d$ is replaced by $\{x : l_d\{C(r) \cap C(y)_x \neq \emptyset\}$, or equivalently $l_d(C(r) \oplus \check{C}(y))$. Take the example where all grains have the same size r_0 , the intensity of the Poisson process before thinning is λ and the weight distribution is independent of size. In that case the intensities for the thinned processes are for the pairwise model,

$$\lambda_{thP} = \lambda \exp \left\{ -\frac{1}{2} \lambda l_d \left(C(r_0) \oplus \check{C}(r_0) \right) \right\}$$

and for the global model,

$$\lambda_{thG} = \frac{1 - \exp \left\{ -\lambda l_d \left(C(r_0) \oplus \check{C}(r_0) \right) \right\}}{l_d \left(C(r_0) \oplus \check{C}(r_0) \right)}.$$

The main difference from spheres is that the second-order product density cannot be written in terms of a distance anymore since the thinned process is not isotropic. However, the process is stationary, meaning that it is enough to consider $\varrho^{(2)}(o, y)$. The following notation is used in the theorems below. Let $Q_d(u, r_u, r) = l_d(C(r_u)_u \oplus \check{C}(r))$ and $S_d(o, r_o, y, r_y, r) = l_d((C(r_o) \oplus \check{C}(r)) \cap (C(r_y)_y \oplus \check{C}(r)))$.

Theorem 6.1 *For the pairwise model with convex grains of the same shape and orientation as $C \in \mathcal{C}^d$, the second-order product density is*

$$\begin{aligned} \varrho^{(2)}(o, y) &= \lambda^2 \int_0^\infty \int_0^\infty \mathbf{1}_{\{r_o, r_y : C(r_o) \cap C(r_y)_y = \emptyset\}} \exp \left\{ -\lambda \int_0^\infty \right. \\ &\quad \left[(Q_d(o, r_o, r) - S_d(o, r_o, y, r_y, r)) \mathbb{P}(W_1(r_o) \leq W_2(r)) \right. \\ &\quad + (Q_d(y, r_y, r) - S_d(o, r_o, y, r_y, r)) \mathbb{P}(W_3(r_y) \leq W_4(r)) \\ &\quad \left. \left. + S_d(o, r_o, y, r_y, r) \mathbb{P}(W_1(r_o) \leq W_2(r) \cup W_3(r_y) \leq W_4(r)) \right] \right. \\ &\quad \left. F_R(dr) \right\} F_R(dr_o) F_R(dr_y). \end{aligned} \tag{6.2}$$

Proof. The proof is similar to that of Theorem 5.1. We consider one point at the origin and one point in y and want to find $\mathcal{M}_{o,y}((1, 1))$. The integration corresponding to (5.2) is only performed for sizes of the grains of o and y such that these grains are not overlapping, hence the indicator function in (5.2) is changed to $\mathbf{1}_{\{r_o, r_y : C(r_o) \cap C(r_y)_y = \emptyset\}}$.

The only other difference compared with spherical grains is the sets where points can win over o or y . A point with a grain of size r is a possible candidate for winning over o if it belongs to the set

$$\{x \in \mathbb{R}^d : C(r_o) \cap C(r)_x \neq \emptyset\} = C(r_o) \oplus \check{C}(r),$$

where the equality comes from (6.1). Similarly a point in $C(r_y)_y \oplus \check{C}(r)$ can win over y . Points common to both these sets can win over either point, that is points in $(C(r_o) \oplus \check{C}(r)) \cap (C(r_y)_y \oplus \check{C}(r))$.

The remaining steps are the same as those in Theorem 5.1. ■

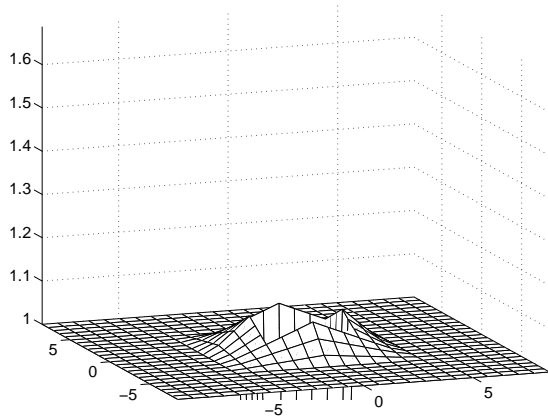
Theorem 6.2 For the global model with convex grains of the same shape and orientation as $C \in \mathcal{C}^d$, the second-order product density is

$$\begin{aligned} \varrho^{(2)}(o, y) = & \lambda^2 \iiint \int 1_{\{r_o, r_y: C(r_o) \cap C(r_y) = \emptyset\}} \exp\left\{-\lambda \int \right. \\ & \left. \int_{w_o}^{\infty} (Q_d(o, r_o, r) - S_d(o, r_o, y, r_y, r)) F_{W|r}(\mathrm{d}w) \right. \\ & + \int_{w_y}^{\infty} (Q_d(y, r_y, r) - S_d(o, r_o, y, r_y, r)) F_{W|r}(\mathrm{d}w) \\ & \left. + \int_{\min(w_o, w_r)}^{\infty} S_d(o, r_o, y, r_y, r) F_{W|r}(\mathrm{d}w) \right] \\ & F_R(\mathrm{d}r) \} F_{W|r_o}(\mathrm{d}w_o) F_{W|r_y}(\mathrm{d}w_y) F_R(\mathrm{d}r_o) F_R(\mathrm{d}r_y). \end{aligned}$$

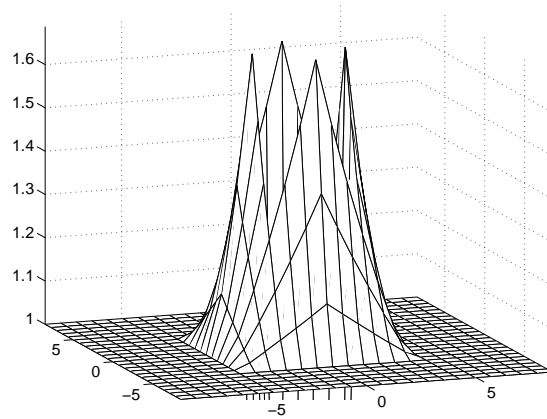
Proof. Apply exactly the same modifications as in the proof above to the proof of Theorem 5.2. ■

For ellipses and squares of equal sizes in \mathbb{R}^d , expressions for the Lebesgue measures needed in this section are stated in Appendix A.

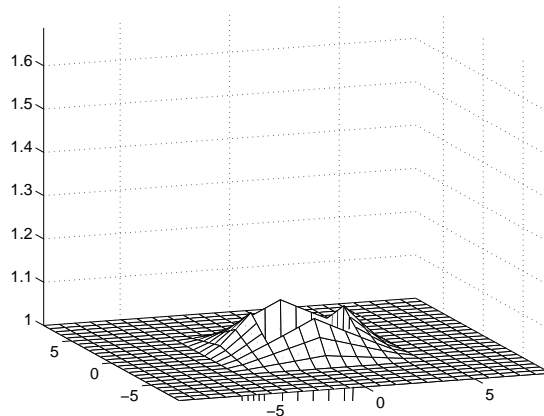
Example 6.3. For squares of equal size, in \mathbb{R}^2 , the pair-correlation function is shown in Figure 11. As in Section 4.2 there are two pairwise models for one intensity after thinning. A discussion of the behaviour of the two models can be carried out in the same manner as in Section 4.2. □



(a) Pairwise - low intensity before thinning



(b) Pairwise - high intensity before thinning



(c) Global

Figure 11: The pair-correlation function for squares of size $\sqrt{2}$, that is side of length 2, in two dimensions. The intensity after thinning is 0.03 for all three models. There are two pairwise models for one intensity after thinning, since the intensity after thinning behaves as in Figure 3. The pair-correlation is 0 for $-2 < x < 2$ and $-2 < y < 2$.

7 Second-order measures of a point process with two types of marks

This section is a preparation for Section 8, where the mark–correlations for the two thinned processes are obtained. We will consider a point process with two types of marks, later to be thought of as a radius and a 0–1 variable telling whether a point is kept or not when thinning. The global and the pairwise models can be described in this setting. Several second–order factorial moment measures and their relations will be discussed with the objective to find relations such as (7.7) and to state Theorem 7.1. This section follows [7] rather closely, the difference being that we treat the two marks as being separate instead of possibly having a mark vector. Since one type of marks will be used to distinguish between kept and deleted points it is impractical to have the marks in vector form.

Consider $\Phi = \{X_n; K_n; M_n\}$, a simple stationary point process in \mathbb{R}^d with two types of marks in the measurable mark spaces $[\mathbb{K}, \mathfrak{K}]$ and $[\mathbb{M}, \mathfrak{M}]$ respectively. Let

$$N_M = \{\phi = \{x_n; k_n; m_n\} : x_n \in \mathbb{R}^d, k_n \in \mathbb{K}, m_n \in \mathbb{M}, \phi(B) < \infty \text{ for bounded } B \subseteq \mathbb{R}^d\}$$

be the set of all locally finite point configurations and let \mathcal{N}_M be the corresponding σ –algebra. Denote the distribution of Φ on $[N_M, \mathcal{N}_M]$ by P . In the following, B, B_1 and B_2 are Borel sets on \mathbb{R}^d , $K_1, K_2 \in \mathfrak{K}$, and $M_1, M_2 \in \mathfrak{M}$.

The second–order factorial moment measure for a point process without marks is defined in (3.1). With the setting of a marked point process several second–order factorial moment measure can be defined either in terms of points or marks or points and marks. The second–order factorial moment measure for the points and both sorts of marks is defined as

$$\begin{aligned} & \alpha^{(2)}(B_1 \times K_1 \times M_1 \times B_2 \times K_2 \times M_2) \\ &= \int_{N_M} \sum_{\substack{[x_1; k_1; m_1] \in \phi \\ [x_2; k_2; m_2] \in \phi \\ x_1 \neq x_2}} 1_{B_1}(x_1) 1_{B_2}(x_2) 1_{K_1}(k_1) 1_{K_2}(k_2) 1_{M_1}(m_1) 1_{M_2}(m_2) P(d\phi). \end{aligned} \quad (7.1)$$

Expressed in words this is the expectation of the number of pairs of distinct points where one is in B_1 having marks belonging to the sets K_1 and M_1 and the other one is in B_2 having marks belonging to K_2 and M_2 .

We will go on to introduce more factorial moment measures that will be used later on. Exploiting the relations between these measures, distributions will arise that can be interpreted as conditional distributions given for example points at certain locations. The next second–order factorial moment measure to be introduced is already defined in (3.1). This factorial moment measure concerns the points and disregards the marks of the process, and we can restate it here as

$$\begin{aligned} \alpha_p^{(2)}(B_1 \times B_2) &= \alpha^{(2)}(B_1 \times \mathbb{K} \times \mathbb{M} \times B_2 \times \mathbb{K} \times \mathbb{M}) \\ &= \int_{N_M} \sum_{\substack{[x_1; k_1; m_1] \in \phi \\ [x_2; k_2; m_2] \in \phi \\ x_1 \neq x_2}} 1_{B_1}(x_1) 1_{B_2}(x_2) P(d\phi). \end{aligned} \quad (7.2)$$

For all K_1, K_2, M_1 and M_2 , $\alpha^{(2)}(\cdot \times K_1 \times M_1 \times \cdot \times K_2 \times M_2)$ is absolutely continuous with respect to $\alpha_p^{(2)}$, since $\alpha^{(2)}(\cdot \times K_1 \times M_1 \times \cdot \times K_2 \times M_2)$ is zero whenever $\alpha_p^{(2)}$ is zero. Hence by the Radon–Nikodym theorem

$$\begin{aligned} & \alpha^{(2)}(B_1 \times K_1 \times M_1 \times B_2 \times K_2 \times M_2) \\ &= \int_{B_1} \int_{B_2} \mathcal{KM}_{x_1, x_2}(K_1 \times M_1 \times K_2 \times M_2) \alpha_p^{(2)}(d(x_1, x_2)), \end{aligned} \quad (7.3)$$

where for fixed K_1, K_2, M_1 and M_2 , $\mathcal{KM}_{x_1, x_2}(K_1 \times M_1 \times K_2 \times M_2)$ is a density. If we instead consider fixed $x_1, x_2 \in \mathbb{R}^d$, $x_1 \neq x_2$, it turns out that \mathcal{KM}_{x_1, x_2} is a distribution on $[\mathbb{K}^2 \times \mathbb{M}^2, \mathfrak{R}^2 \times \mathfrak{M}^2]$ and it can be interpreted as the conditional distribution of the marks given points at x_1 and x_2 . The last result can for example be found in [2].

Another second–order factorial moment measure is obtained by considering the points and one type of marks, that is,

$$\begin{aligned} & \alpha_M^{(2)}(B_1 \times K_1 \times B_2 \times K_2) = \alpha^{(2)}(B_1 \times K_1 \times \mathbb{M} \times B_2 \times K_2 \times \mathbb{M}) \\ &= \int_{N_M} \sum_{\substack{[x_1; k_1; m_1] \in \phi \\ [x_2; k_2; m_2] \in \phi \\ x_1 \neq x_2}} 1_{B_1}(x_1) 1_{B_2}(x_2) 1_{K_1}(k_1) 1_{K_2}(k_2) P(d\phi). \end{aligned} \quad (7.4)$$

Similarly as before, for all M_1 and M_2 , $\alpha^{(2)}(\cdot \times \cdot \times M_1 \times \cdot \times \cdot \times M_2)$ is absolutely continuous with respect to $\alpha_M^{(2)}$ and we get

$$\begin{aligned} & \alpha^{(2)}(B_1 \times K_1 \times M_1 \times B_2 \times K_2 \times M_2) \\ &= \int_{B_1} \int_{B_2} \int_{K_1} \int_{K_2} \mathcal{M}_{x_1, k_1, x_2, k_2}(M_1 \times M_2) \alpha_M^{(2)}(d(x_1, k_1, x_2, k_2)), \end{aligned} \quad (7.5)$$

where $\mathcal{M}_{x_1, k_1, x_2, k_2}$ is a distribution on $[\mathbb{M}^2, \mathfrak{M}^2]$ for fixed $x_1, x_2 \in \mathbb{R}^d$, $x_1 \neq x_2$ and $k_1, k_2 \in \mathbb{K}$. The interpretation is as above as the distribution of the second type of marks given points at x_1 and x_2 with marks k_1 and k_2 respectively.

By the definitions given in (7.2) and (7.4) we can see that $\alpha_M^{(2)}$ is absolutely continuous with respect to $\alpha_p^{(2)}$. Via the Radon–Nikodym theorem another conditional distribution, \mathcal{K}_{x_1, x_2} , arises. For fixed $x_1, x_2 \in \mathbb{R}^d$, $x_1 \neq x_2$, it is a distribution on $[\mathbb{K}^2, \mathfrak{R}^2]$ with the interpretation as the conditional distribution of the \mathbb{K} –marks given points in x_1 and x_2 , that is,

$$\alpha_M^{(2)}(B_1 \times K_1 \times B_2 \times K_2) = \int_{B_1} \int_{B_2} \mathcal{K}_{x_1, x_2}(K_1 \times K_2) \alpha_p^{(2)}(d(x_1, x_2)). \quad (7.6)$$

Rewriting (7.5) and (7.6) in form of densities and combining we get

$$\begin{aligned} & \alpha^{(2)}(d(x_1, k_1, m_1, x_2, k_2, m_2)) \\ &= \mathcal{M}_{x_1, k_1, x_2, k_2}(d(m_1, m_2)) \mathcal{K}_{x_1, x_2}(d(k_1, k_2)) \alpha_p^{(2)}(d(x_1, x_2)). \end{aligned} \quad (7.7)$$

It is now possible to state the following theorem, which is a Campbell type theorem, as in [7] with the notation given above. The theorem can be shown by first showing that it holds for indicator functions, using (7.1) and (7.7), then that it holds for simple functions and finally that it holds for positive functions.

Theorem 7.1 For every measurable $f : \mathbb{R}^d \times \mathbb{K} \times \mathbb{M} \times \mathbb{R}^d \times \mathbb{K} \times \mathbb{M} \rightarrow \mathbb{R}^+$,

$$\begin{aligned} & \int_{N_M} \sum_{\substack{[x_1; k_1; m_1] \in \phi \\ [x_2; k_2; m_2] \in \phi \\ x_1 \neq x_2}} f(x_1, k_1, m_1, x_2, k_2, m_2) P(d\phi) \\ &= \int_{\mathbb{R}^d \times \mathbb{R}^d} \int_{\mathbb{K} \times \mathbb{K}} \int_{\mathbb{M} \times \mathbb{M}} f(x_1, k_1, m_1, x_2, k_2, m_2) \mathcal{M}_{x_1, k_1, x_2, k_2}(d(m_1, m_2)) \\ & \quad \cdot \mathcal{K}_{x_1, x_2}(d(k_1, k_2)) \alpha_p^{(2)}(d(x_1, x_2)). \end{aligned}$$

The following simplifications will be useful later. If the underlying point process is Poisson distributed with constant intensity λ and the \mathbb{K} -marks has distribution F which is independent of the point process and also independent for different points we get $\alpha_p^{(2)}(d(x_1, x_2)) = \lambda^2 dx_1 dx_2$, $\mathcal{K}_{x_1, x_2}(d(k_1, k_2)) = F(dk_1)F(dk_2)$ and hence

$$\begin{aligned} & \int_{N_M} \sum_{\substack{[x_1; k_1; m_1] \in \phi \\ [x_2; k_2; m_2] \in \phi \\ x_1 \neq x_2}} f(x_1, k_1, m_1, x_2, k_2, m_2) P(d\phi) \\ &= \lambda^2 \int_{(\mathbb{R}^d)^2} \int_{\mathbb{K}^2} \int_{\mathbb{M}^2} f(x_1, k_1, m_1, x_2, k_2, m_2) \mathcal{M}_{x_1, k_1, x_2, k_2}(d(m_1, m_2)) \\ & \quad \cdot F(dk_1)F(dk_2) dx_1 dx_2. \end{aligned} \tag{7.8}$$

8 A thinned point process and the mark-correlation function

The goal of this section is to find the mark–correlation function for the pairwise and the global models in the case of spherical grains. With the exceptions of Propositions 8.2 and 8.3 the results are valid for any thinned process subject to the limitations that the marks are independent and that the point pattern is Poissonian before thinning. The mark–correlation is a measure of the mean of the product of two marks at certain locations divided by the mean mark squared. If the mark–correlation is larger than one, calculated at some locations of points, there is an indication that marks of points at those locations, are on average larger than the mean mark, or really the product of the marks at those locations are on average larger than the mean mark squared. If it is below one the marks are on average smaller than the mean mark. Let F_K be the mark distribution, then the mean \mathbb{K} -mark can be written as

$$\bar{k} = \int_{\mathbb{R}} k F_K(dk). \tag{8.1}$$

Let K_1, K_2 be marks of points in x_1 and x_2 respectively. The formal definition of the mark–correlation function for a marked process is

$$k_{mm}(x_1, x_2) = \frac{\mathbb{E}_{x_1, x_2}[K_1 K_2]}{\bar{k}^2}, \tag{8.2}$$

where \mathbb{E}_{x_1, x_2} is the expectation with respect to, \mathcal{K}_{x_1, x_2} , the conditional distribution of two marks given points in x_1 and x_2 , that is

$$\mathbb{E}_{x_1, x_2}[K_1 K_2] = \int_{\mathbb{K}} \int_{\mathbb{K}} k_1 k_2 \mathcal{K}_{x_1, x_2}(d(k_1, k_2)). \quad (8.3)$$

The following description of the thinned processes will be used when deriving their mark–correlation function. Start with a homogeneous Poisson process with intensity λ and marks that can be thought of as radii of spheres. In the thinning procedure each point is given a second type of mark that is one if the point is kept and zero otherwise. With notation as in Section 7 we have $\mathbb{M} = \{0, 1\}$ and $\mathbb{K} = \mathbb{R}^+$. The radii are taken independently and according to distribution F_R independently of the Poisson process. Let $\Phi_{th} = [X_n; K_n]$ be the process with \mathbb{M} –marks all ones and let its distribution be denoted P_{th} . Then depending on how the thinning is performed P_{th} can be either the pairwise process or the global process. We do not need this description yet since the formulas leading up to Lemma 8.1 only uses the fact that we start with a Poisson process, that one type of mark is positive and independent of marks of other points and that the other type of mark is either 0 or 1.

The mark–correlation for the thinned process is defined in terms of the conditional distribution after thinning of the radii of two spheres given their location and the mean radii after thinning as in (8.2). The conditional distribution after thinning of the radii of two points can be identified with the conditional distribution of the radii in the process with two types of marks given the location of the points and that the \mathbb{M} –marks are both one. This results in the mark–correlation for the thinned process as,

$$k_{mmth}(x_1, x_2) = \frac{\iint k_1 k_2 \mathcal{K}_{x_1, 1, x_2, 1}(d(k_1, k_2))}{\bar{k}^2}, \quad (8.4)$$

with $\mathcal{K}_{x_1, m_1, x_2, m_2}$ defined as \mathcal{M} is in (7.5), but with the roles of \mathbb{M} –marks and \mathbb{K} –marks reversed.

By a similar reversion in (7.7),

$$\begin{aligned} & \alpha^{(2)}(d(x_1, k_1, m_1, x_2, k_2, m_2)) \\ &= \mathcal{K}_{x_1, m_1, x_2, m_2}(d(k_1, k_2)) \mathcal{M}_{x_1, x_2}(d(m_1, m_2)) \alpha_p^{(2)}(d(x_1, x_2)). \end{aligned} \quad (8.5)$$

This and (7.7) gives

$$\mathcal{K}_{x_1, m_1, x_2, m_2}(d(k_1, k_2)) = \frac{\mathcal{M}_{x_1, k_1, x_2, k_2}(d(m_1, m_2)) \mathcal{K}_{x_1, x_2}(d(k_1, k_2))}{\mathcal{M}_{x_1, x_2}(d(m_1, m_2))}. \quad (8.6)$$

Since the radii are taken independently with distribution F_R we can make a further simplification and get,

$$\mathcal{K}_{x_1, m_1, x_2, m_2}(d(k_1, k_2)) = \frac{\mathcal{M}_{x_1, k_1, x_2, k_2}(d(m_1, m_2)) F_R(dk_1) F_R(dk_2)}{\mathcal{M}_{x_1, x_2}(d(m_1, m_2))}. \quad (8.7)$$

By using this expression and that $\varrho^{(2)}(x_1, x_2) = \lambda^2 \mathcal{M}_{x_1, x_2}(1, 1)$ from Lemma 3.1, the mark–correlation becomes

$$\begin{aligned} k_{mmth}(x_1, x_2) &= \frac{\iint k_1 k_2 \mathcal{M}_{x_1, k_1, x_2, k_2}(1, 1) F_R(dk_1) F_R(dk_2)}{\mathcal{M}_{x_1, x_2}(1, 1) \bar{k}^2} \\ &= \frac{\lambda^2 \iint k_1 k_2 \mathcal{M}_{x_1, k_1, x_2, k_2}(1, 1) F_R(dk_1) F_R(dk_2)}{\varrho^{(2)}(x_1, x_2) \bar{k}^2}. \end{aligned} \quad (8.8)$$

This is really all we need to compute the mark–correlation for the pairwise and the global processes, but the numerator can be identified with another second–order factorial moment measure giving a nicer looking expression. To be specific everything will be expressed for the thinned process, but the definitions hold for more general situations also. For a process with non–negative marks it is possible to define a mark–sum measure, see [7],

$$\Phi_{Sth}(B) = \sum_{[X;K] \in \Phi_{th}} K 1_B(X), \quad (8.9)$$

that is the sum of all marks of points belonging to the set B . The second–order factorial moment measure for Φ_{Sth} is defined as

$$\alpha_{Sth}^{(2)}(B_1 \times B_2) = \int \sum_{\substack{[x_1; k_1] \in \phi \\ [x_2; k_2] \in \phi \\ x_1 \neq x_2}} k_1 k_2 1_{B_1}(x_1) 1_{B_2}(x_2) P_{th}(d\phi). \quad (8.10)$$

We now express this in terms of the original marked point process Φ with distribution P ,

$$\alpha_{Sth}^{(2)}(B_1 \times B_2) = \int \sum_{\substack{[x_1; k_1; m_1] \in \phi \\ [x_2; k_2; m_2] \in \phi \\ x_1 \neq x_2}} k_1 k_2 1_{B_1}(x_1) 1_{B_2}(x_2) m_1 m_2 P(d\phi). \quad (8.11)$$

Observe that a term in the sum is zero whenever m_1 and m_2 are not both one. With $\alpha_{Sth}^{(2)}$ written in this way we can apply (7.8) with

$$f(x_1, k_1, m_1, x_2, k_2, m_2) = k_1 k_2 1_{B_1}(x_1) 1_{B_2}(x_2) m_1 m_2$$

giving,

$$\begin{aligned} & \alpha_{Sth}^{(2)}(B_1 \times B_2) \\ &= \lambda^2 \int_{(\mathbb{R}^d)^2} \int_{(\mathbb{R}^+)^2} k_1 k_2 1_{B_1}(x_1) 1_{B_2}(x_2) \mathcal{M}_{x_1, k_1, x_2, k_2}(1, 1) \\ & \quad \cdot F_R(dk_1) F_R(dk_2) dx_1 dx_2. \end{aligned} \quad (8.12)$$

Differentiating with respect to the 2–dimensional Lebesgue measure gives the *second–order product density* for the mark–sum measure

$$\varrho_{Sth}^{(2)}(x_1, x_2) = \lambda^2 \int_{\mathbb{R}^+ \times \mathbb{R}^+} k_1 k_2 \mathcal{M}_{x_1, k_1, x_2, k_2}(1, 1) F_R(dk_1) F_R(dk_2). \quad (8.13)$$

By identifying $\varrho_{Sth}^{(2)}(x_1, x_2)$ with the numerator in (8.8) we can state the following Lemma.

Lemma 8.1 *The mark–correlation function for the pairwise or the global model can be expressed as,*

$$k_{mmth}(x_1, x_2) = \frac{\varrho_{Sth}^{(2)}(x_1, x_2)}{\varrho_{th}^{(2)}(x_1, x_2) \bar{k}_{th}^2}. \quad (8.14)$$

In fact Lemma 8.1 holds for any marked process with positive marks, see [7]. If the point process Φ_{th} is stationary and isotropic we adopt the usual (abuse of) notation and write the mark–correlation in terms of a distance r between two points,

$$k_{mmth}(r) = \frac{\varrho_{Sth}^{(2)}(r)}{\varrho_{th}^{(2)}(r)\bar{k}_{th}^2}. \quad (8.15)$$

Now we move on to the specific cases, but choose to state $\varrho_{Sth}^{(2)}$ instead of the mark–correlation itself, since $\varrho_{th}^{(2)}$ is given in Section 5.

Proposition 8.2 *For the pairwise model with spherical grains, general weight and radius distributions and notations as in Theorem 5.1 the product–density for the mark–sum measure is*

$$\begin{aligned} \varrho_{Sth}^{(2)}(r) = & \lambda^2 \int_0^r \int_0^{r-r_o} r_o r_r \exp\left\{-\lambda \int_0^\infty \right. \\ & \left[(\kappa_d(r_o + r_w)^d - \delta_d(r, r_o + r_w, r_r + r_w)) \mathbb{P}(W_1(r_o) \leq W_2(r_w)) \right. \\ & + (\kappa_d(r_r + r_w)^d - \delta_d(r, r_o + r_w, r_r + r_w)) \mathbb{P}(W_3(r_r) \leq W_4(r_w)) \\ & \left. \left. + \delta_d(r, r_o + r_w, r_r + r_w) \mathbb{P}(W_1(r_o) \leq W_2(r_w) \cup W_3(r_r) \leq W_4(r_w)) \right] \right. \\ & \left. F_R(dr_w) \right\} F_R(dr_r) F_R(dr_o). \end{aligned} \quad (8.16)$$

Proof. This expression is very similar to the product density in Theorem 5.1 and the proof follows closely that of Theorem 5.1. By (8.13) we need $\mathcal{M}_{o,r_o,r,r_r}((1, 1))$, that is the probability that both points of a pair are retained if one point located at the origin and the other at distance r from the origin with radii r_o and r_r . This is equal to the probability that no other points will win over those two, provided they are far enough apart so that their spheres do not overlap. That is

$$\mathcal{M}_{o,r_o,r,r_r}((1, 1)) = 1_{\{r > r_o + r_r\}} \mathbb{P}(\{\# \text{ points that win over } [o; r_o] \text{ or } [r; r_r]\} = 0), \quad (8.17)$$

where the right hand side is found in (5.2). An expression for $\mathcal{M}_{o,r_o,r,r_r}((1, 1))$ now follows exactly as in the proof of Theorem 5.1 and inserting in (8.13) concludes the proof. ■

Proposition 8.3 *For the global model with spherical grains, general weight and radius distribution and notations as in Theorem 5.2, the product–density for the mark–sum measure is*

$$\begin{aligned} \varrho_{Sth}^{(2)}(r) = & \lambda^2 \int_0^r \int_0^{r-r_o} r_o r_r \iint \exp\left\{-\lambda \int_0^\infty \right. \\ & \left[\int_{w_o}^\infty (\kappa_d(r_o + r_w)^d - \delta_d(r, r_o + r_w, r_r + r_w)) F_{W|r_w}(dw) \right. \\ & + \int_{w_r}^\infty (\kappa_d(r_r + r_w)^d - \delta_d(r, r_o + r_w, r_r + r_w)) F_{W|r_w}(dw) \\ & \left. \left. + \int_{\min(w_o, w_r)}^\infty \delta_d(r, r_o + r_w, r_r + r_w) F_{W|r_w}(dw) \right] \right. \\ & \left. F_R(dr_w) \right\} F_{W|r_o}(dw_o) F_{W|r_r}(dw_r) F_R(dr_r) F_R(dr_o). \end{aligned} \quad (8.18)$$

Proof. What we need to find is $\mathcal{M}_{o,r_o,r,r_r}(1, 1)$. It can be expressed as in (8.17) but to get anything useful we must condition on the weights and hence

$$\begin{aligned} & \mathcal{M}_{o,r_o,r,r_r}((1, 1)) \\ &= \iint 1_{\{r>r_o+r_r\}} \mathbb{P}(\{\# \text{ of points that win over } [o; r_o; w_o] \text{ or } [r; r_r; w_r]\} = 0) \\ & \quad F_{W|r_o}(dw_o)F_{W|r_r}(dw_r). \end{aligned} \quad (8.19)$$

The result follows from the proof of Theorem 5.2. ■

The proofs of the theorems in Section 6 can be used in a similar manner to find the second-order product density for the mark–sum measure of the pairwise and global models for convex, compact grains.

Finally, we need the mean radius for the pairwise and the global models. For spherical grains, general radius distribution and continuous weight distribution, the mean radius can be found in [4],

$$\bar{k}_{th} = \frac{\lambda}{\lambda_{th}} \int_0^\infty k h(k) F_R(dk), \quad (8.20)$$

with the retaining probability, h , and intensity after thinning, λ_{th} , as in Section 2.

Example 8.4. Continuation of Example 5.1. Starting with spheres of radii 0.1 and 0.2 with equal probability, intensity 10 for the pairwise model and intensity 4.4 for the global model gives the mark–correlation function in Figure 12. It is similar to the pair–correlation function discussed in Example 5.1. At small distances between points, less than 0.4, the pair–correlation is less than 1. This means that those points on average have smaller radii than the mean radius. When the pair–correlation is greater than 1, the points tend to have larger radii than on average. For larger distances than 0.8 there is no dependence between the radii. Two spheres of radius 0.2 have no potential points in common that may win over them in the thinning and hence their radii are independent. For distances below 0.2, the mark–correlation is undefined since there cannot be any points at such distances. □

Example 8.5. Continuation of Example 5.2. In Figure 13 is the mark–correlation of the three versions of thinning procedures when starting with radii that are Rayleigh distributed with parameter 1 and intensities before thinning giving the same intensity after thinning equal to 0.017. The pairwise model with high starting intensity has mark–correlation above one for distances approximately between 2 and 5, meaning the sizes of spheres at those distances are on average larger than the mean size. As with the pair–correlation the mark–correlation is virtually identical for the pairwise model and the global model when both have the same low starting intensity.

In Figure 14 there is a plot of the mark–correlation for the pairwise model with the same radius distribution as above but with maximal intensity after thinning. The global model with intensity 0.5 before thinning giving intensity after thinning 0.0558 has its pair–correlation in Figure 15. □

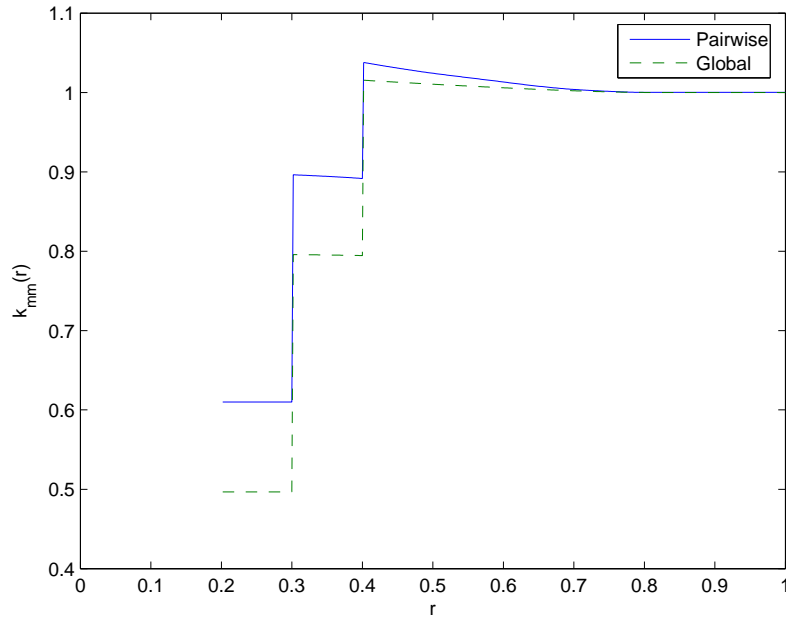


Figure 12: Mark–correlation function for the pairwise and the global model for spheres with radii 0.1 and 0.2 with the same intensity after thinning, $\lambda_{th} = 2.5$. It is undefined for r less than 0.2.

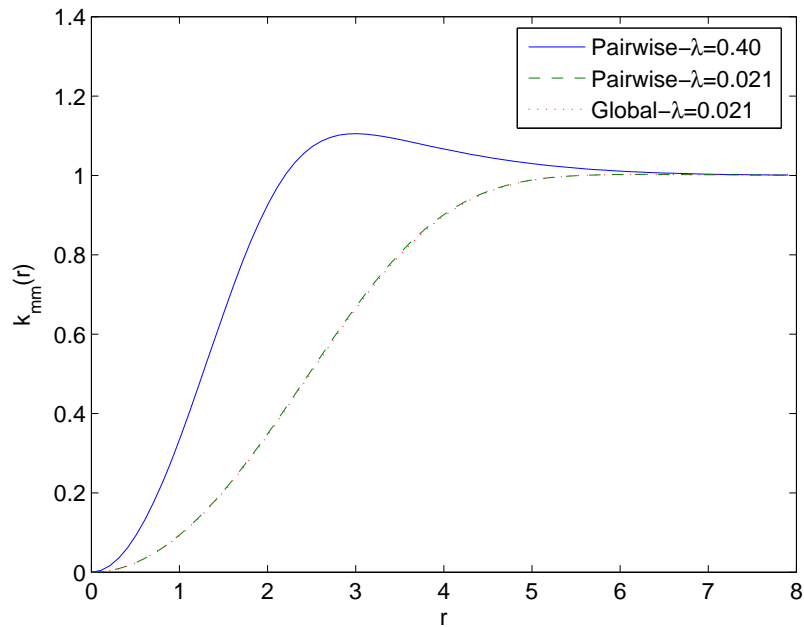


Figure 13: Mark–correlation function for models starting with Rayleigh distributed radii with parameter 1 and weights independent of the radii. See Example 8.5 for further details.

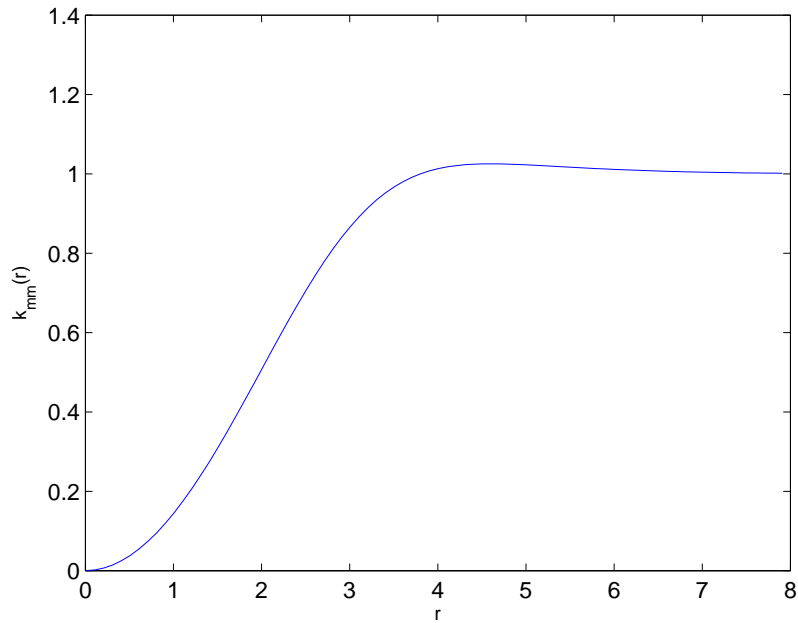


Figure 14: Mark–correlation for the pairwise model with Rayleigh(1) distributed radii and intensity before thinning 0.115. See Example 8.5.

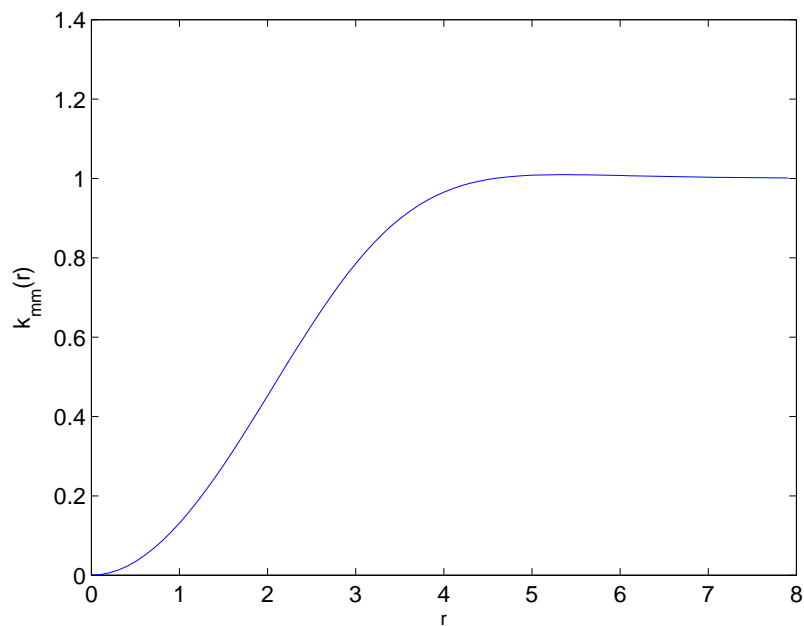


Figure 15: Mark–correlation for the global model with Rayleigh(1) distributed radii and intensity before thinning 0.5. See Example 8.5.

9 Inclusions in cast iron

The models were originally inspired by images of inclusions in cast iron such as the image in Figure 16 by Stefano Beretta (private communication). The fit of the models will be examined by using the estimated intensity after thinning and estimated radius distribution after thinning to find the intensity and radius distribution before thinning in the models and then checking if the pair-correlation looks similar for the images and the models. Inclusions are important in metal fatigue and in particular the metal is weak where several inclusions occur close, therefore it is reasonable to use the pair-correlation or the mark-correlation as a judge of the model fit.

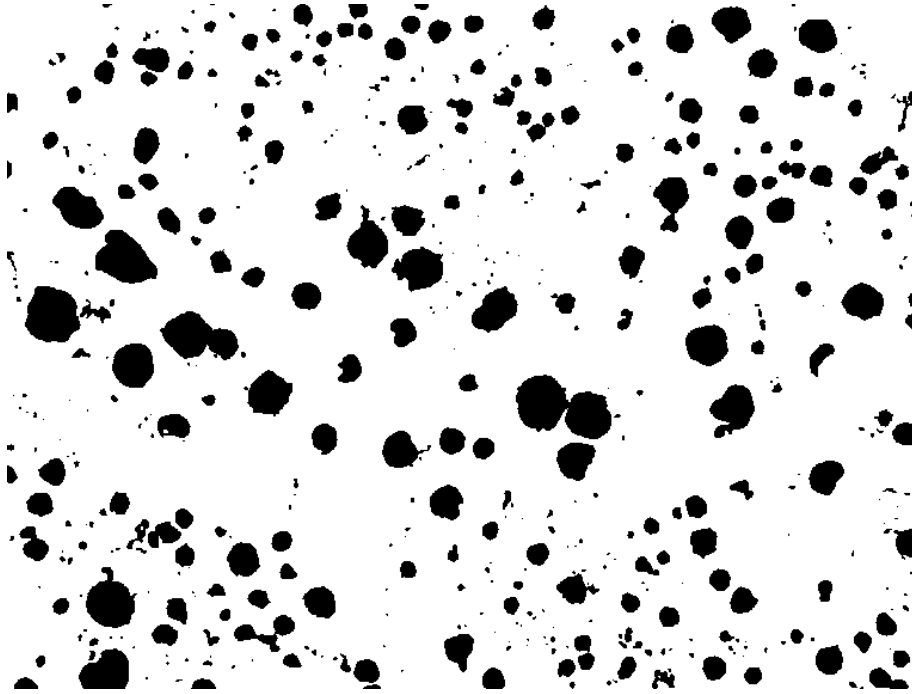


Figure 16: Image of cast iron.

The data set consists of about 1200 images of size approximately 1260 times 950 microns corresponding to 768 times 576 pixels. They are inhomogeneous and it is not realistic to fit one stationary model to them all. Examining Figure 16 there seems to be a region across the image consisting of large inclusions surrounded by smaller inclusions. Furthermore, Figure 17 shows a histogram of the number of points in 61 images of separate areas of the same sample. As a comparison the 5th percentile and 95 percentile of a Poisson process with mean 241, the mean of the histogram, is 216 and 267 respectively, which strengthens the inhomogeneities observed by the eye. Because of the inhomogeneities we only pick two of the images, fit the models to each separately and see if the models are good. The inclusions are assumed to be circular and with this idealisation the two images chosen look as in Figure 18. The estimated pair-correlation is shown in Figure 19. The estimator we used for the pair-correlation, see for example [16] or [6], is

$$\hat{g}(r) = \frac{1}{\pi r \hat{\lambda}^2} \sum_{i=1}^n \sum_{j=i+1}^n \frac{k_b(r - \|x_i - x_j\|)}{|W_{x_i} \cap W_{x_j}|},$$

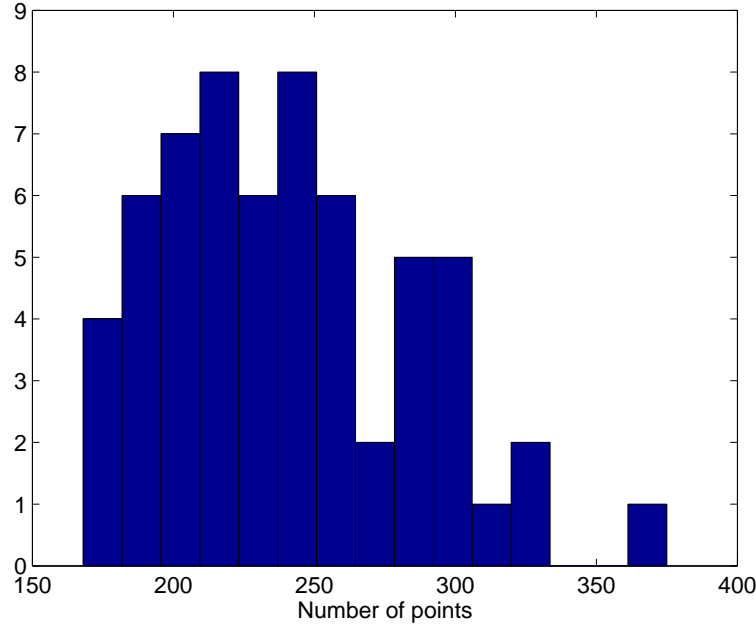


Figure 17: Histogram of the number of points in 61 equally sized images of one sample.

where $\hat{\lambda}$ is the intensity estimate, x_1, \dots, x_n are the centre points of the inclusions, W_{x_i} is the sample window translated by x_i and k_b is the Epanečikov kernel

$$k_b(u) = \begin{cases} \frac{3}{4b} \left(1 - \left(\frac{u}{b}\right)^2\right) & \text{if } u/b \leq 1, \\ 0 & \text{otherwise.} \end{cases}$$

The bandwidth b was 0.2 divided by the intensity. The left sample in Figure 19 seems to have pair-correlation over 1 for quite short distances. We have seen similar behaviour in both the global and the pairwise model, but more pronounced for the pairwise model, suggesting that it will fit better.

From the images the intensity and the radius distribution were estimated. The radius distribution were assumed to be of gamma type since it is a flexible distribution and gave a quite good fit according to a quantile plot with the only reservation that the minimal radius in the images were determined by the resolution. Hence the radius distribution in the images did not start at zero but at 2.95 microns. This problem is not thought to have a large impact on the estimation. Once the radius distribution and intensity were estimated, the intensity before thinning and the radius distribution before thinning were calculated by an iteration procedure described in [4], with the assumption that the weight distribution is independent of the radii. The intensity after thinning in the left image in Figure 18 was $1.61 \cdot 10^{-4}$ and the calculated intensity before thinning was $2.31 \cdot 10^{-4}$ for the pairwise model and $2.15 \cdot 10^{-4}$ for the global model. The intensity after thinning in the right image in Figure 18 was $2.11 \cdot 10^{-4}$ and the calculated intensity before thinning was $3.49 \cdot 10^{-4}$ for the pairwise model and $3.04 \cdot 10^{-4}$ for the global model. Previously we have seen that the pairwise model have two different behaviours for the same starting intensity. It does not seem to be the case that we can get two different behaviours when calculating in the other direction.

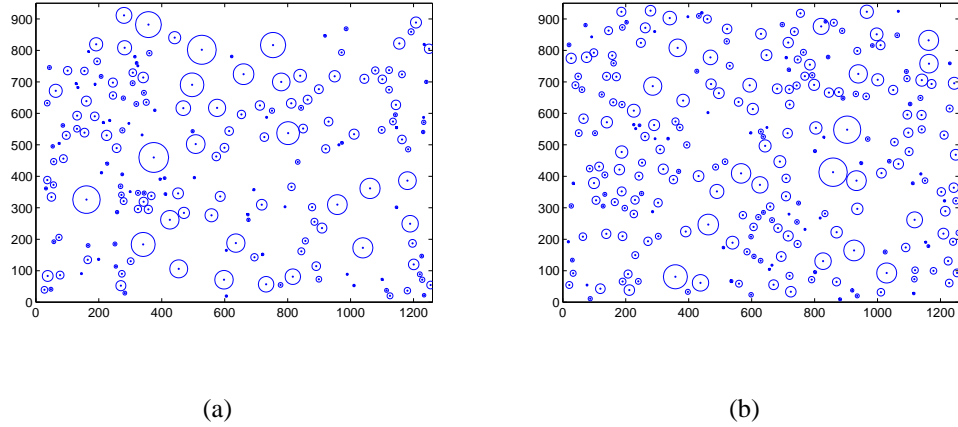


Figure 18: Two examples of inclusions in cast iron when the inclusions are assumed to be circular.

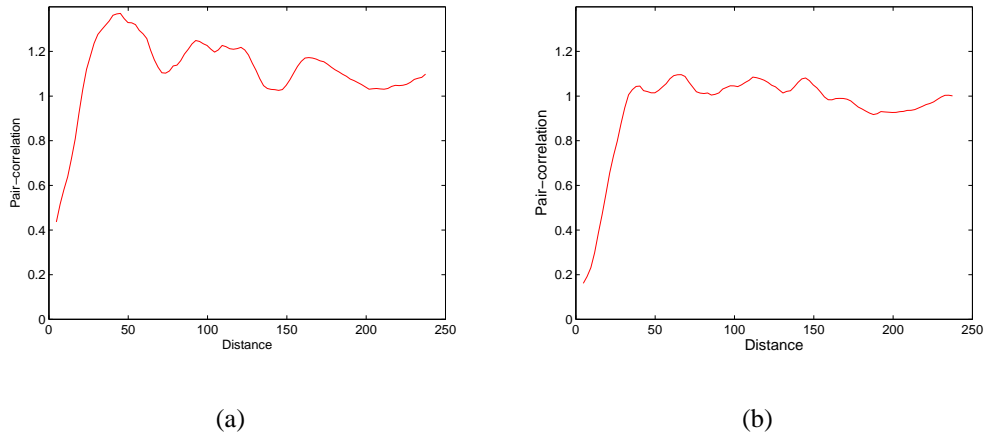


Figure 19: The estimated pair-correlation of the examples in Figure 18.

Now it is possible to numerically compute the theoretical pair-correlations for the fitted models, but due to the fluctuations in the estimated pair-correlation function it might be more informative to simulate and estimate the pair-correlation from simulations. Simulations of both models were made using the estimated intensity and radius distribution before thinning. From each of 1000 simulations the pair-correlation was estimated and for each value of the distance the 97.5 percentile and the 2.5 percentile were estimated. Figure 20 shows the estimated pair-correlation for the image along with a 95% envelope from simulations of the pairwise model. Figure 21 is similar but the envelopes are computed for the global model.

For the left image the pair-correlation is well outside the envelope for both the pairwise and the global model. For the right image the pair-correlation is within the envelopes which might indicate that at least in terms of the pair-correlation function the models are appropriate. Both models seem to behave alike in this context. The possibility for the

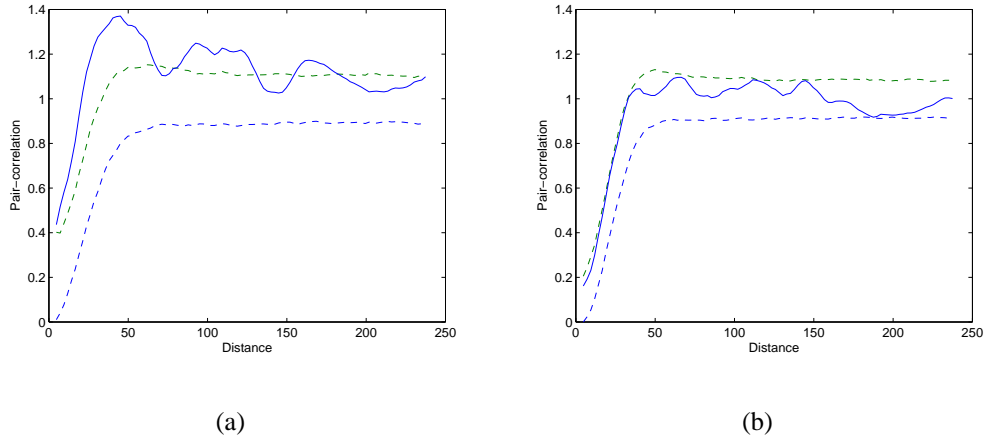


Figure 20: Estimated pair–correlation for the images in Figure 18 with approximate 95% envelopes from 1000 simulations of the pairwise model.

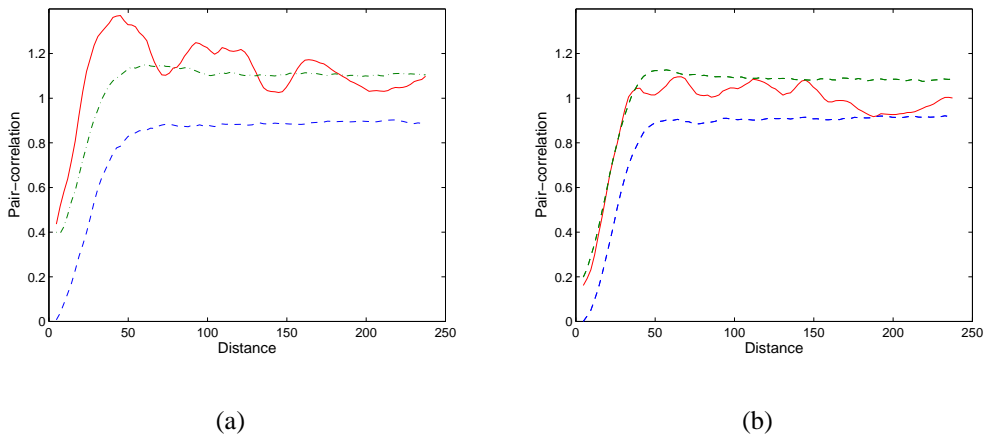


Figure 21: Estimated pair–correlation for the images in Figure 18 with approximate 95% envelopes from 1000 simulations of the global model.

pairwise model to have pair–correlation clearly above one for some distances does not show here, possibly since that phenomenon shows for sparse point patterns. The conclusion is that the two models are not flexible enough to be able to handle all the images of the inclusions. There might be some hope in using the models with weight distribution depending on radius, but it seems hard to choose a reasonable dependence. More promising is probably to use an inhomogeneous Poisson process for the points before thinning since the images are clearly inhomogeneous. The left pair–correlation in Figure 19 have several humps which might be due to inhomogeneities of the kind that inclusions of roughly the same size occur in the same region. One constriction that we applied is the use of the gamma distribution for the radius. Instead a distribution free estimation could be performed, but it would probably not influence the results much. The mark–correlation

could have been an additional tool in assessing the fit, but since the pair-correlation did not show a good fit, it was not used at this point.

10 Concluding remarks

We have considered the second-order product density and the mark–correlation function for two models of non-overlapping grains. In simple cases it is possible to get explicit results and in general we get integrals that need to be calculated numerically. It is an advantage of these models that they allow easy computation of the product density compared to many other models of non-overlapping grains found in literature. Other measures, especially the K–function is commonly used to describe the second order behaviour of point processes. It is possible to calculate the K–function from the pair–correlation function. The mark–correlation and the pair–correlation looks very similar for these two models but that is generally not the case for other marked point processes.

The models are used in an example with inclusion data where it appeared that the data was too inhomogeneous for a good fit. It would be interesting to try using an inhomogeneous Poisson process as the point process before thinning. In that case the results for the pairwise and global models would need to be recalculated. It may also be worthwhile to study the behaviour of the models with different kinds of dependence of the weights on the radii. The most general result in this paper concerns convex grains with the same orientation. It is not hard to generalise further to allow for random orientations.

References

- [1] Daley, D.J., Mallows, C.L., Shepp, L.A. (2000), *A one-dimensional Poisson growth model with non-overlapping intervals*. Stochastic Process. Appl., 90, 223-241.
- [2] Daley, D.J., Vere-Jones, J. (1988), *An Introduction to the Theory of Point Processes*. Springer-Verlag.
- [3] Jeulin, D. (1989), *Morphological modeling of images by sequential random functions*. Signal Processing, 16, 403-431.
- [4] Månsson, M., Rudemo, M. (2002), *Random patterns of nonoverlapping convex grains*. Adv. Appl. Prob., 34, 718-738.
- [5] Matérn, B. (1960), *Spatial Variation*. Meddelanden Statens Skogsforskningsinst. 49. Statens Skogsforskningsinstitut, Stockholm, Second edition: Springer, Berlin, 1986.
- [6] Møller, J., Waagepetersen, R. P. (2004), *Statistical Inference and Simulation for Spatial Point Processes*, Chapman & Hall/CRC.
- [7] Stoyan, D. (1984), *On correlations of marked point processes*. Math. Nachr., 116, 197-207.
- [8] Stoyan, D. (1987), *Statistical analysis of spatial point processes: a soft-core model and cross-correlations of marks*. Biom. J., 29, 971-980.
- [9] Stoyan, D. (1988), *Thinnings of point processes and their use in the statistical analysis of a settlement pattern with deserted villages*. Statistics, 19, 45-56.
- [10] Stoyan, D. (1990), *Stereological formulae for a random system of non-intersecting spheres*. Statistics, 21, 131-136.
- [11] Stoyan, D. (1998), *Models of random systems of non-intersecting spheres*. Prague Stochastics '98, 543-547.
- [12] Stoyan, D., Kendall, S.K., Mecke, J. (1995), *Stochastic Geometry and its Applications*. 2nd edition. Wiley.
- [13] Stoyan, D. Penttinen, A. (2000), *Recent applications of point process methods in forestry statistics*. Statist. Sci., 15, 61-78.
- [14] Stoyan, D. Schlather, M. (2000), *Random sequential adsorption: relationships to dead leaves and characterization of variability*. J. Statist. Phys., 100, 969-979.
- [15] Stoyan, D. Stoyan, H. (1985), *On one of Matérn's hard-core point process models*. Math. Nachr., 122, 205-214.
- [16] Stoyan, D., Stoyan, H. (1994), *Fractals, Random Shapes and Point Fields*. Wiley.
- [17] Talbot, J., Tarjus, G., Van Tassel, P.R., Viot, P. (2000), *From car parking to protein adsorption: an overview of sequential adsorption processes*. Colloids and Surfaces A, 165, 287-324.

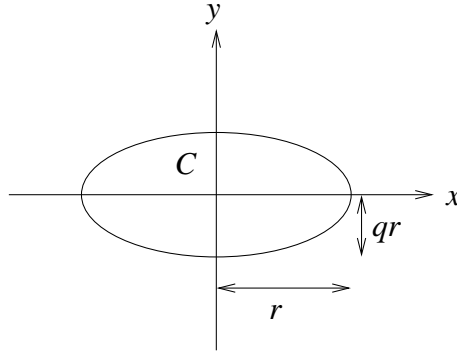
A Areas and volumes for some convex sets

A.1 Sphere

d	$l_d(B_d(x, r))$	$l_d(B_d(x, h) \cap B_d(x + r, h))$
2	πr^2	$2h^2 \arccos \frac{r}{2h} - \frac{r}{2} \sqrt{4h^2 - r^2}$
3	$4/3\pi r^3$	$4/3\pi r^3 \left(1 - \frac{3r}{4h} + \frac{1}{16} \left(\frac{r}{h}\right)^3\right)$

$$\begin{aligned} \delta_2(r, r_1, r_2) &= l_2(B_2(x, r_1) \cap B_2(x + r, r_2)) \\ &= r_1^2 \arccos \left(\frac{r^2 + r_1^2 - r_2^2}{2rr_1} \right) + r_2^2 \arccos \left(\frac{r^2 + r_2^2 - r_1^2}{2rr_2} \right) \\ &\quad - \frac{1}{2} \sqrt{2r^2r_1^2 + 2r^2r_2^2 + 2r_1^2r_2^2 - r^4 - r_1^4 - r_2^4} \end{aligned}$$

A.2 Ellipse



$$C(r) = \left\{ (x, y) : \left(\frac{x}{r}\right)^2 + \left(\frac{y}{qr}\right)^2 \leq 1, 0 < q < 1 \right\}$$

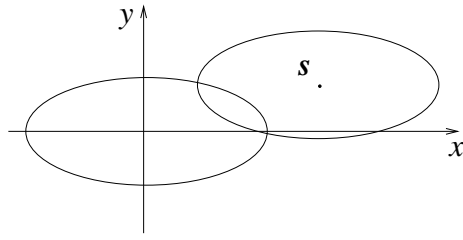
$$l_2(C(r)) = \pi qr^2$$

$$l_2(C(r) \oplus \check{C}(r)) = l_2(C(2r)) = 4\pi qr^2$$

The area of the intersection of two ellipses where the centre of the second ellipse is translated by $s = (x_s, y_s)$ from the centre of the first is

$$l_2(C(r) \cap C(r)_s) = q l_2(B_2(x, r) \cap B_2(x + \sqrt{x_s^2 + (y_s/q)^2}, r)).$$

$$\begin{aligned} &l_2([C(r) \oplus \check{C}(r)] \cap [C(r)_s \oplus \check{C}(r)]) \\ &= q l_2(B_2(x, 2r) \cap B_2(x + \sqrt{x_s^2 + (y_s/q)^2}, 2r)) \end{aligned}$$



A.3 Square

$$C(r) = \{(x, y) : -r/\sqrt{2} \leq x, y \leq r/\sqrt{2}\}.$$

The area of the intersection of two squares where the centre of the second square is translated by $s = (x_s, y_s)$ from the centre of the first is

$$l_2(C(r) \cap C(r)_s) = |\sqrt{2}r - x_s| \cdot |\sqrt{2}r - y_s|.$$

$$l_2([C(r) \oplus \check{C}(r)] \cap [C_s(r) \oplus \check{C}(r)]) = |2\sqrt{2}r - x_s| \cdot |2\sqrt{2}r - y_s|$$

Paper C

The volume fraction of a non–overlapping germ–grain model

Jenny Andersson, Olle Häggström and Marianne Månsson

Abstract

We discuss the volume fraction of a model of non–overlapping convex grains. It is obtained from thinning a Poisson process where each point has a weight and is the centre of a grain, by removing any grain that is overlapped by one of larger or equal weight. In the limit as the intensity of the Poisson process tends to infinity, the model can be identified with the intact grains in the dead leaves model if the weights are independent of the grain sizes. In this case we can show that the volume fraction is at most $1/2^d$ for $d = 1$ or 2 if the shape is fixed, but the size and the orientation are random. The upper bound is achieved for centrally symmetric sets of the same size and orientation. For general d we can show the upper bound, $1/2^d$, for spherical grains with two–point radius distribution. If dependence between weight and size is allowed, it is possible to achieve a volume fraction arbitrarily close to one.

1 Introduction

The model considered in this paper is a non–overlapping germ–grain model, which is a generalisation of one of Matérns hard–core models in [6]. It was proposed by Månsson and Rudemo in [5]. The model is constructed by generating a Poisson process in \mathbb{R}^d and letting each point be the centre of a grain. The sizes and orientations of the grains are random and each grain is given a weight which may depend on its size. The process is thinned by rejecting any grain that intersects with another grain that has equal or higher weight. In [5] the intensity and size distribution of the grains after thinning for this model were given. Furthermore, the asymptotic value of the volume fraction as the intensity before thinning tends to infinity was derived in the case of fixed-sized grains. One result is that centrally symmetric sets of equal size give the volume fraction $1/2^d$.

The aim of the present paper is to study the asymptotic volume fraction, namely if fixed-sized grains give the highest volume fraction in the case where the weights are independent of the grain size and if it is possible to choose weights so that the volume fraction can become arbitrarily close to 1. We believe that $1/2^d$ is an upper limit for the volume fraction in \mathbb{R}^d for any d if the weights are independent of the grain sizes. However we can only show it in general for $d = 1$ or 2 and for spherical grains with two–point distribution for any d . Furthermore, we show that it is possible to achieve a volume fraction arbitrarily close to one by a particular choice of radius distribution and weights depending on the radii.

If the weight distribution is continuous and the intensity tends to infinity, the grains kept in our model are the same as the intact grains in Matheron’s dead leaves model,

[7]. It can be defined as follows. Consider a stationary Poisson process $\{(x_i, t_i)\}$ with unit intensity in $\mathbb{R}^d \times (-\infty, 0]$. Interpret t_i as the arrival time of the point $x_i \in \mathbb{R}^d$. Let d -dimensional, possibly random, compact grains be implanted at the points x_i sequentially in time, so that a new grain deletes portions of the “older” ones. At time $t = 0$ the space \mathbb{R}^d is completely occupied, and the grains which are not completely deleted constitute a tessellation of \mathbb{R}^d .

The grains which are intact, that is not intersected by any later grains, constitute a model of non-intersecting grains. The intact grains can also be considered as the limit of the generalisation of Matérn’s hard-core model under study here. Let the weights be continuously distributed on $(-\infty, 0]$, independent of each other and of the radii. Then the weights can be identified with the time coordinate in the description of the dead leaves model given above. The connection between Matérn’s hard-core model and the dead leaves model in the case of fixed-sized spheres was noted by Stoyan and Schlater [10]. The dead leaves model and generalisations of it, for instance the colour dead leaves, are studied in a number of papers by Jeulin, see e.g. [4]. Results on the intensity and size distribution of the intact grains can be found in [3].

When the intensity of the Poisson process tends to infinity and the grains are spherical an alternative formulation of our model, which is related to the description of the dead leaves model above, can be found in [2]. Consider a $(d + 1)$ -dimensional space $\mathbb{R}^d \times \mathbb{R}^+$ where \mathbb{R}^+ is a time dimension. Each point in a Poisson process in this space is the centre of a sphere in \mathbb{R}^d which is tried to be added to the model and the final coordinate represents the time of the trial. A sphere has radius $R(t)$ at time t . A sphere is not added if it overlaps with any sphere with smaller value of t regardless of whether this sphere was rejected or not. The only difference from the formulation in [5] is that the sizes of the spheres are not random. Large times corresponds to small weights in our model and the function $R(t)$ is similar to weights depending deterministically on the radius.

Obviously volume fraction one is impossible to achieve. However, Gilbert, [2], proves that the volume fraction can be made arbitrarily close to one by choosing the function $R(t)$ carefully. One choice is

$$R(t) = \left(1 + \frac{a(d + a)t}{A}\right)^{1/(d+a)} \quad (1.1)$$

where a and $A > 0$ are constants and $|a| < 1$. Volume fractions close to one are achievable if A and $|a|$ are small. If a is negative, in addition $A/|a|$ needs to be large. Here we will give an alternative proof of the achievability of volume fractions close to one, based on a “separation of size” argument somewhat reminiscent of the construction of Meester, Roy and Sarkar, [8], to demonstrate the nonuniversality of critical volume fractions in the so-called Boolean model of continuum percolation.

The paper is outlined as follows. In Section 2 we give a detailed description of the model with spherical grains and show that it is stochastically increasing in the intensity of the Poisson process if the weight distribution is independent of the radius. In Section 3 we discuss the volume fraction when the intensity of the Poisson process tends to infinity and the weight distribution is independent of the radius. Our alternative proof that the volume fraction can be made arbitrarily close to one if the weight distribution is dependent of the radius is given in Section 4. The use of more general convex sets in place of spheres is considered in Section 5.

2 Model

For simplicity we give the description of the model for spherical grains, but the generalisation to convex grains is obvious. In Section 5 we give the counterpart to (2.2) for convex grains. The model is constructed by thinning a marked Poisson process, also known as a Boolean model, with proposal intensity λ_{pr} in \mathbb{R}^d . Each point in the Poisson process is given two marks. One of the marks is the radius of a sphere centred at the point and the other mark is a weight that is allowed to depend on the radius. Points are assigned radii independently and according to a proposal radius distribution F_{pr} . The radii are independent of the point process. Weights are also assigned independently of the point process but to stress the possible dependence on radius, the weight distribution is denoted $F_{W|r}$. A point is kept in the thinning only if its sphere is not intersected by any other sphere with equal or higher weight. Note that the radii of the spheres are no longer independent after thinning. One way of quantifying the dependence is by the mark–correlation function, see [1]. Some further notation is needed. Let κ_d be the volume of the unit sphere in \mathbb{R}^d and define $\bar{F}(x) = \mathbb{P}(X \geq x)$ for a random variable X with distribution function F .

In Sections 3 and 4 we will need some properties of the model, primarily the volume fraction ρ . For a stationary model with intensity λ and non-overlapping grains of random size it can be written as the intensity times the mean volume of a typical grain \bar{v} , that is

$$\rho = \lambda \bar{v}. \quad (2.1)$$

One useful property is the probability that a randomly chosen point with radius r is kept when thinning, henceforth called the retention probability, which from [5] is

$$g(r) = \int_0^\infty \exp \left\{ -\lambda_{pr} \kappa_d \int_0^\infty \bar{F}_{W|y}(w)(r+y)^d F_{pr}(dy) \right\} F_{W|r}(dw). \quad (2.2)$$

Also from [5] the intensity after thinning is

$$\lambda = \lambda_{pr} \int_0^\infty g(r) F_{pr}(dr) \quad (2.3)$$

and the distribution function of the radius of a randomly chosen sphere after thinning is

$$F(r) = 1 - \frac{\lambda_{pr}}{\lambda} \int_r^\infty g(s) F_{pr}(ds). \quad (2.4)$$

In the following we will mostly be concerned with the case when the intensity of the Poisson process tends to infinity. When the weight distribution is independent of radius, the intensity and the volume fraction after thinning are strictly increasing as functions of the intensity before thinning. In fact the process is increasing in the intensity before thinning as can be seen in the following theorem.

Theorem 2.1 *Consider the model with continuous weight distribution independent of the radii and let $\lambda_1 < \lambda_2$. Let X be the union of the resulting spheres for $\lambda_{pr} = \lambda_1$ and let Y be the union of the resulting spheres for $\lambda_{pr} = \lambda_2$. Then X is stochastically dominated by Y .*

Proof. We prove the theorem by a coupling argument. Take a Poisson process in \mathbb{R}^d with intensity λ_2 and give each point independently a radius with distribution F_{pr} . Furthermore give each point a weight that is uniform $(0, \lambda_2)$. Let \tilde{Y} consist of the spheres that are left when the thinning is performed. This process has the same distribution as Y . In the Poisson process, consider only those spheres that have weights in the interval $(\lambda_2 - \lambda_1, \lambda_2)$. The intensity of this process is λ_1 and the radius distribution is still F_{pr} because the weights are independent of the radii. Carry out the thinning and call the resulting process of spheres \tilde{X} . It has the same distribution as X . A sphere before thinning with weight greater than or equal to $\lambda_2 - \lambda_1$ will belong to \tilde{Y} if and only if it belongs to \tilde{X} . A sphere with weight $\lambda_2 - \lambda_1$ will only be contained in \tilde{Y} . We have shown

$$\tilde{X} \subseteq \tilde{Y}$$

and hence X is stochastically dominated by Y . ■

The condition that the weight distribution is continuous is necessary in the argument above.

Example 2.1. Let the spheres have equal radii, r , and let the weights be constant. Then all spheres will be removed except those that do not intersect with any other sphere. The intensity after thinning is by using (2.2) and (2.3)

$$\lambda_{pr} \exp\{-\lambda_{pr}\kappa_d 2^d r^d\}.$$

The intensity after thinning is at most $1/(\kappa_d 2^d r^d e)$ for $\lambda_{pr} = 1/(\kappa_d 2^d r^d)$ and it tends to zero as λ_{pr} tends to infinity. □

If the weights are continuous but depend on the radii, the process is not necessarily increasing.

Example 2.2. Let the radii take value 1 or a with probabilities p and $q = 1 - p$ respectively. Let the weight distribution be uniform in $(0, 1)$ given radius 1 and let it be uniform in $(1, 2)$ given radius a . Then the intensity, by (2.2) and (2.3), is

$$\frac{1}{\kappa_d 2^d} \left\{ \exp(-\lambda_{pr}\kappa_d(1+a)^d q)(1 - \exp(-\lambda_{pr}\kappa_d 2^d p)) + \frac{1 - \exp(-\lambda_{pr}\kappa_d 2^d a^d q)}{a^d} \right\}.$$

When λ_{pr} tends to infinity λ tends to $1/(\kappa_d 2^d a^d)$. Let $d = 2$, $a = 2$ and $p = q = 1/2$, then numerical inspection shows that the intensity has maximum approximately 0.027 for $\lambda_{pr} \approx 0.088$. The value of λ as λ_{pr} tends to infinity is $1/(16\pi) \approx 0.020$. □

Theorem 2.1 implies that the process exists in the limit as λ_{pr} tends to infinity. If the weights are allowed to depend on the radii, the limit process does not necessarily exist.

Example 2.3. Suppose we have a model with two different radii of the spheres, 1 and 2, with probabilities 1/2 each. Let N be large, $N = 100$ say, and let the weight of a sphere of radius 1 be uniform in

$$\bigcup_{i=0}^{\infty} \left(\frac{N^{2i} - 1}{N^{2i}}, \frac{N^{2i+1} - 1}{N^{2i+1}} \right)$$

and let the weight of a sphere of radius 2 be uniform in

$$\bigcup_{i=0}^{\infty} \left(\frac{N^{2i+1} - 1}{N^{2i+1}}, \frac{N^{2i+2} - 1}{N^{2i+2}} \right).$$

The limit process is not well defined since as $\lambda_{pr} \rightarrow \infty$ the process will fluctuate between consisting mostly of spheres of radius 1 and consisting mostly of spheres of radius 2. \square

3 Volume fraction for the spherical case if the weight distribution is independent of the radius

In this section we will consider the case where the weight distribution is continuous and independent of the radii and $\lambda_{pr} \rightarrow \infty$. As noted earlier the model then coincides with the intact grains of the dead leaves model. We will show that the largest volume fraction achievable is that of the process with all radii being equal. In that case the volume fraction, as shown in [5], is 2^{-d} .

Theorem 3.1 *If the weight distribution is continuous and independent of the radii and $\lambda_{pr} \rightarrow \infty$, then, for \mathbb{R}^d with $d = 1$ or 2 , the volume fraction is at most*

$$\frac{1}{2^d},$$

with equality if and only if the spheres have equal radii.

Proof. First we need to find an expression for the volume fraction. From (2.2) the retention probability for fixed r , when λ_{pr} is the intensity of the Poisson process, is

$$g(r) = \frac{1 - \exp\{-\lambda_{pr}\kappa_d \mathbb{E}[(r + Y)^d]\}}{\lambda_{pr}\kappa_d \mathbb{E}[(r + Y)^d]},$$

where Y has distribution F_{pr} . By (2.4), the expectation of R^d is

$$\mathbb{E}[R^d] = \frac{\lambda_{pr}}{\lambda} \int_0^{\infty} r^d g(r) F_{pr}(dr)$$

and hence the volume fraction is by (2.1),

$$\rho = \int_0^{\infty} r^d \frac{1 - \exp\{-\lambda_{pr}\kappa_d \mathbb{E}[(r + Y)^d]\}}{\mathbb{E}[(r + Y)^d]} F_{pr}(dr).$$

Letting the intensity tend to infinity gives

$$\lim_{\lambda_{pr} \rightarrow \infty} \rho = \int_0^{\infty} \frac{r^d}{\mathbb{E}[(r + Y)^d]} F_{pr}(dr). \quad (3.1)$$

If $d = 1$ the function

$$\frac{r}{r + \mathbb{E}Y}$$

is concave and we can use Jensen's inequality to deduce

$$\int_0^\infty \frac{r}{r + \mathbb{E}Y} F_{pr}(dr) \leq \frac{\mathbb{E}Y}{\mathbb{E}Y + \mathbb{E}Y} = \frac{1}{2}.$$

We have equality above only if the radius is constant, since otherwise the function is strictly convex.

If $d = 2$ the function

$$f(r) = \frac{r^2}{r^2 + 2r\mathbb{E}Y + \mathbb{E}Y^2}$$

is not concave but it can be shown to lie below a tangent passing through the origin. Let $\mu = \mathbb{E}Y$ and $\gamma = \mathbb{E}Y^2$ and the equation for the tangent is

$$t(r) = \frac{r}{2(\mu + \sqrt{\gamma})}.$$

The difference between the tangent and the curve is

$$t(r) - f(r) = \frac{r(r - \sqrt{\gamma})^2}{2(\mu + \sqrt{\gamma})(r^2 + 2r\mu + \gamma)}.$$

Hence $t(r) - f(r) \geq 0$ and

$$\int_0^\infty \frac{r^2}{r^2 + 2\mu r + \gamma} F_{pr}(dr) \leq \int_0^\infty \frac{r}{2(\mu + \sqrt{\gamma})} F_{pr}(dr) = \frac{\mu}{2(\mu + \sqrt{\gamma})} \leq \frac{1}{4},$$

where in the last inequality we used $\gamma \geq \mu^2$. Since equality holds only for fixed radius, the volume fraction is $1/4$ only if that is the case. ■

We cannot prove that the upper bound of the volume fraction is $1/2^d$ for general d . In fact the method used in the proof above gives an upper bound for the volume fraction in $d = 3$ as $4/27$. This can be seen by considering the function

$$f(r) = \frac{r^3}{\mathbb{E}[(r + Y)^3]}.$$

Since $\mathbb{E}Y^3 \geq (\mathbb{E}Y)^3$ for $Y \geq 0$ we have

$$f(r) \leq \frac{r^3}{(r + \mathbb{E}Y)^3}.$$

As before this function lies below a tangent that passes through the origin. The equation of the tangent is

$$\frac{4r}{27\mu}.$$

Proposition 3.2 *For a two point radius distribution and continuous weight distribution independent of the radius in \mathbb{R}^d and $\lambda_{pr} \rightarrow \infty$, the volume fraction is at most $1/2^d$. The upper bound is achieved only if the radius is fixed.*

Proof. Let the radius take value 1 with probability p and value a with probability $q = 1 - p$. From (3.1) the volume fraction as the intensity of the Poisson process tends to infinity is

$$\rho = \frac{p}{2^d p + (1+a)^d q} + \frac{a^d q}{(1+a)^d p + 2^d a^d q}.$$

Rewriting with a common divisor gives,

$$\rho = \frac{(1+a)^d p^2 + 2^{d+1} a^d p q + (1+a)^d q^2}{(2^d p + (1+a)^d q)((1+a)^d p + 2^d a^d q)}.$$

By subtracting the volume fraction from $1/2^d$ we have

$$\frac{1}{2^d} - \rho = \frac{((1+a)^{2d} - 2^{2d} a^d) p q}{(2^d p + (1+a)^d q)((1+a)^d p + 2^d a^d q)}.$$

It is easy to see that $a = 1$ is a root to $(1+a)^{2d} - 2^{2d} a^d = 0$. It is actually a double root and by some tedious manipulation using binomial expansions, we can write

$$\frac{1}{2^d} - \rho = \frac{(a-1)^2 p q \left(\sum_{j=0}^{d-1} \sum_{m=0}^j \sum_{k=0}^m \binom{2d}{k} a^{2d-j-2} + \sum_{j=0}^{d-2} \sum_{m=0}^j \sum_{k=0}^m \binom{2d}{k} a^j \right)}{(2^d p + (1+a)^d q)((1+a)^d p + 2^d a^d q)},$$

which is clearly 0 only for $a = 1$ and positive otherwise. ■

Proposition 3.2 gives an indication that Theorem 3.1 holds for any d . Hence we state the following conjecture.

Conjecture 3.3 *If the weight distribution is continuous and independent of the radii and $\lambda_{pr} \rightarrow \infty$, then in \mathbb{R}^d for any d , the volume fraction is at most*

$$\frac{1}{2^d},$$

attained by spheres of equal radius.

4 Volume fraction if the weight distribution depends on the radius

As can be seen in the Introduction, Gilbert [2], showed that the volume fraction can be made arbitrarily close to one by choosing the right function $R(t)$. This is similar in our view to let the weight distribution depend deterministically on the radius. We will make an alternative proof of this fact. The idea is the same in our setting as in Gilbert's, namely letting the function $R(t)$ decrease in such a way that not much space is wasted. In Gilbert's case $R(t)$, see (1.1), is continuous while we have discrete radii.

Theorem 4.1 *If the weight distribution is independent of the radius, it is possible to achieve a volume fraction arbitrarily close to 1 in \mathbb{R}^d for any d .*

Proof. The theorem will be proved by considering a model with spheres having discrete radius distribution with k possible values. The weight will be proportional to the radius of the sphere. The idea is to let each size of spheres have sufficiently low intensity so that they do not overlap spheres of the same size and to let smaller spheres be so much smaller that not much space is wasted if they overlap partially with a larger sphere.

Fix small $\alpha > 0$ and $\delta > 0$. Below we will show that we can achieve a volume fraction of at least

$$1 - \alpha\kappa_d(3^d - 1) - 2\delta. \quad (4.1)$$

The volume fraction can be made arbitrarily close to one by picking α and δ small. Let the radius of a sphere before thinning take value $r_i = \epsilon^{i-1}$ with probability $p_i = \lambda_i/\lambda_{pr}$, $i = 1, \dots, k$, where λ_{pr} is the intensity of the Poisson process. Think of $\epsilon > 0$ as being small and k large. Let the weight of a sphere with radius r_i be uniform $((r_{i-1} + r_i)/2, (r_i + r_{i+1})/2)$. The intensity of spheres of radius r_i is λ_i before thinning.

The volume fraction after thinning is the same as the probability that the origin is covered after thinning and can be written

$$\begin{aligned} \rho &= 1 - \mathbb{P}(\text{The origin is not covered after thinning}) \\ &= 1 - \mathbb{P}(\text{The origin is not covered before thinning}) \\ &\quad - \mathbb{P}(\text{All spheres covering the origin are deleted}). \end{aligned} \quad (4.2)$$

The number of spheres with radius r_i that covers the origin before thinning is Poisson distributed with expectation $\lambda_i\kappa_d r_i^d$ and hence

$$\mathbb{E}[\# \text{ spheres covering the origin before thinning}] = \sum_i^k \kappa_d r_i^d \lambda_i.$$

Letting $\lambda_i = \alpha/r_i^d$ the expectation becomes $k\kappa_d\alpha$. Pick k large enough so that

$$\mathbb{P}(\text{The origin is not covered before thinning}) = \exp(-k\kappa_d\alpha) \leq \delta. \quad (4.3)$$

To obtain the probability that all spheres covering the origin are deleted we assume that at least one sphere covers the origin before thinning. Let the largest of all such spheres be denoted B . In case several spheres having the same radius cover the origin we let B be the one with highest weight. If B has radius r_i , a centre of a sphere with higher weight than B , having radius $r_j \geq r_i$, that intersects B must be separated by at least a distance of r_j from the origin, otherwise we get a contradiction of the definition of B . On the other hand, the centre of B is at most a distance r_i from the origin and hence the centre of a sphere with radius r_j overlapping B cannot be further away from the origin than $2r_i + r_j$. Now we can get an upper bound for the probability that all spheres covering the origin are deleted by

$$\begin{aligned} &\mathbb{P}(\text{All spheres covering the origin are deleted}) \\ &\leq \mathbb{P}(\text{A sphere with radius larger than or equal to } r_i \text{ overlaps } B) \\ &\leq \mathbb{E}[\# \text{ spheres with radius larger than or equal to } r_i \text{ overlapping } B] \\ &\leq \sum_{j=1}^i \mathbb{E} \left[\# \text{ spheres with radius } r_j \text{ and center at} \right. \\ &\quad \left. \text{distance between } r_j \text{ and } 2r_i + r_j \text{ from the origin} \right]. \end{aligned}$$

The number of spheres with radius r_j is Poisson distributed and

$$\begin{aligned}
& \mathbb{P}(\text{All spheres covering the origin are deleted}) \\
&= \sum_{j=1}^i \lambda_j \kappa_d ((2r_i + r_j)^d - r_j^d) = \sum_{j=1}^i \alpha \kappa_d ((2\epsilon^{i-j} + 1)^d - 1) \\
&= \alpha \kappa_d (3^d - 1) + \alpha \kappa_d \sum_{j=1}^{i-1} ((1 + 2\epsilon^{i-j})^d - 1).
\end{aligned} \tag{4.4}$$

We can choose a small ϵ such that, for all i simultaneously,

$$\alpha \kappa_d \sum_{j=1}^{i-1} ((1 + 2\epsilon^{i-j})^d - 1) < \delta.$$

Insert this estimation of (4.4) together with (4.3) in (4.2) and we have shown (4.1). ■

5 Convex grains

In our model we may replace the spheres with convex sets of different sizes. We introduce a minimum of notation to prove a counterpart to Theorem 3.1 and refer to [5] for a more detailed description.

We begin with some definitions. First, $D(A)$, denotes the diameter of a set A , that is

$$D(A) = \sup_{x, y \in A} \|x - y\|.$$

We let half the diameter be called the size. Let C^d be the set of all convex, compact sets C in \mathbb{R}^d such that the origin belongs to C and $D(C)/2 = 1$. Moreover let $C(x, r)$ be the set C translated by x and with half its diameter equal to r and let $\check{C} = \{-x : x \in C\}$ be the reflection of C in the origin. Finally we denote the Lebesgue measure in d dimensions by l_d .

In the following we will only consider \mathbb{R}^2 and $C \in C^2$. Replacing $\kappa_2(r + y)^2$ in (2.2) with $l_2(\{x : C(o, r) \cap C(x, y) \neq \emptyset\})$ gives the retention probability for convex sets with the same shape and orientation as C . Let $\nu(C, \check{C})$ be the mixed volume of C and \check{C} , then

$$l_2(\{x : C(o, r) \cap C(x, y) \neq \emptyset\}) = (r^2 + y^2)l_2(C) + 2ry\nu(C, \check{C}).$$

If the sets are uniformly rotated about the origin, then $\kappa_2(r + y)^2$ should be replaced by $\mathbb{E}[l_2(\{x : C(o, r) \cap mC(x, y) \neq \emptyset\})]$, where m is a rotation matrix, i.e. orthogonal with determinant 1, and the expectation is taken with respect to an angle of rotation that is uniform $(0, 2\pi)$. Let $S_1(C)$ be the perimeter of C , then by the generalised Steiner formula

$$\mathbb{E}[l_2(\{x : C(o, r) \cap mC(x, y) \neq \emptyset\})] = (r^2 + y^2)l_2(C) + \frac{ryS_1(C)^2}{2\pi}.$$

Just as in the spherical case the maximal volume fraction, at least in \mathbb{R}^2 , is given by grains of equal size.

Proposition 5.1 *Let the grains be convex of the same shape as $C \in \mathcal{C}^2$ and let the weight distribution be continuous and independent of the size. For grains of the same orientation and when $\lambda_{pr} \rightarrow \infty$, the volume fraction is at most*

$$\frac{l_2(C)}{2(l_2(C) + \nu(C, \check{C}))}.$$

For grains of random orientation and when $\lambda_{pr} \rightarrow \infty$, the volume fraction is at most

$$\frac{l_2(C)}{2l_2(C) + S_1(C)^2/(2\pi)}.$$

In both cases the upper bound is attained if and only if all the grains have the same size.

Proof. The volume fraction as $\lambda_{pr} \rightarrow \infty$ is deduced similar to (3.1). For convex sets of the same orientation we have volume fraction

$$\rho = \int_0^\infty \frac{r^2 l_2(C)}{\int_0^\infty (r^2 + y^2) l_2(C) + 2ry\nu(C, \check{C})} F_{pr}(\mathrm{d}r),$$

and for uniformly rotated convex sets we have volume fraction

$$\rho_{rot} = \int_0^\infty \frac{r^2 l_2(C)}{\int_0^\infty \left((r^2 + y^2) l_2(C) + \frac{ry S_1(C)^2}{2\pi} \right)} F_{pr}(\mathrm{d}r).$$

In both cases we take the expectation of a function that can be written as

$$\frac{r^2}{r^2 + ar + b},$$

for some positive constants a and b . The result is shown exactly as for the $d = 2$ case in the proof of Theorem 3.1. ■

In two dimensions it is well-known that for convex C

$$l_2(C) \leq \nu(C, \check{C}) \leq 2l_2(C)$$

with equality to the left if and only if C is centrally symmetric and to the right if and only if C is a triangle. No convex set has a larger perimeter relative to its area than a circle, more precisely $S_1(C)^2 \geq l_2(C)4\pi$. By these bounds and Proposition 5.1 it follows that among all dead leaves models with convex grains of equal shape, fixed or uniformly distributed orientations, and independent random radii, the highest volume fraction results for fixed-sized centrally symmetric sets of equal orientation. In this case the volume fraction is $1/4$ if $d = 2$ and we believe that the bound $1/2^d$ holds in any dimension. Finally, we generalise Conjecture 3.3 to hold among convex grains of fixed or random orientation and the upper bound is achieved for centrally symmetric sets of fixed size.

References

- [1] Andersson, J. (2005), *Product–densities and mark–correlations of two models of non–overlapping grains*. In preparation.
- [2] Gilbert, E.N. (1964), *Randomly packed and solidly packed spheres*. *Canad. J. Math.*, 16, 286-298.
- [3] Jeulin D. (1989), *Morphological Modeling of images by Sequential Random Functions*. *Signal Processing*, 16, pp. 403-431.
- [4] Jeulin D. (1997), *Dead Leaves Models: from space tessellation to random functions*. In *Proc. of the Symposium on the Advances in the Theory and Applications of Random Sets (Fontainebleau, 9-11 October 1996)*, D. Jeulin (ed), World Scientific Publishing Company, pp. 137-156.
- [5] Månsson, M., Rudemo, M. (2002), *Random patterns of nonoverlapping convex grains*. *Adv. Appl. Prob.*, 34, 718-738.
- [6] Matérn, B. (1960), *Spatial Variation*. Meddelanden Statens Skogsforskningsinst. 49. Statens Skogsforskningsinstitut, Stockholm, Second edition: Springer, Berlin, 1986.
- [7] Matheron, G. (1968), *Scéma Booléen séquentiel de partition aléatoire*. Internal Report N-83, C.M.M., Paris School of Mines.
- [8] Meester, R., Roy, R., Sarkar, A. (1994), *Nonuniversality and continuity of the critical covered volume fraction in continuum percolation*. *J. Statist. Phys.*, 75, 123-134.
- [9] Stoyan, D., Kendall, S.K., Mecke, J. (1995), *Stochastic Geometry and its Applications*. 2nd edition. Wiley.
- [10] Stoyan, D. Schlather, M. (2000), *Random sequential adsorption: relationships to dead leaves and characterization of variability*. *J. Statist. Phys.*, 100, 969-979.